Osteology of the wide-hipped titanosaurian sauropod dinosaur *Savannasaurus elliottorum* from the Upper Cretaceous Winton Formation of Queensland, Australia

Journal:	*Journal of Vertebrate Paleontology*
Manuscript ID	JVP-2019-0164.R1
Manuscript Type:	Article
Date Submitted by the Author:	17-Apr-2020
Complete List of Authors:	Poropat, Stephen; Swinburne University of Technology, Faculty of Science, Engineering and Technology; Australian Age of Dinosaurs Natural History Museum, Mannion, Philip; University College London, Earth Sciences Upchurch, Paul; University College London, Earth Sciences; Tischler, Travis; Australian Age of Dinosaurs Natural History Museum, Sloan, Trish; Australian Age of Dinosaurs Natural History Museum, Sinapius, George; Australian Age of Dinosaurs Natural History Museum, Elliott, Judy; Australian Age of Dinosaurs Natural History Museum, Elliott, David; Australian Age of Dinosaurs Museum of Natural History, Palaeontology
Key Words:	Gondwana, Somphospondyli, Titanosauriformes, Macronaria, Eromanga Basin, Mesozoic

Osteology of the wide-hipped titanosaurian sauropod dinosaur *Savannasaurus elliottorum* from the Upper Cretaceous Winton Formation of Queensland, Australia

STEPHEN F. POROPAT,[*,1,2] PHILIP D. MANNION,[3] PAUL UPCHURCH,[3] TRAVIS R. TISCHLER,[2] TRISH SLOAN,[2] GEORGE H. K. SINAPIUS,[2] JUDY A. ELLIOTT,[2] and DAVID A. ELLIOTT[2]

[1]Faculty of Science, Engineering and Technology, Swinburne University of Technology, John Street, Hawthorn, Victoria 3122, Australia; sporopat@swin.edu.au

[2]Australian Age of Dinosaurs Museum of Natural History, The Jump-Up, Winton, Queensland 4735, Australia; stephenfporopat@gmail.com; travisr.tischler@outlook.com; trish.sloan@aaod.com.au; laboratory@aaod.com.au; judy.elliott@aaod.com.au; david.elliott@aaod.com.au

[3]Department of Earth Sciences, University College London, Gower Street, London WC1E 6BT, United Kingdom; philipdmannion@gmail.com; p.upchurch@ucl.ac.uk

*Corresponding author

ABSTRACT—The titanosaurian sauropod dinosaur *Savannasaurus elliottorum* is represented by a partial postcranial skeleton from the lower Upper Cretaceous (Cenomanian–lowermost Turonian) Winton Formation of Queensland, northeast Australia. Here, we present a detailed description of this specimen, as well as an emended diagnosis of *Savannasaurus elliottorum*. *Savannasaurus* displays numerous character states that are generally regarded as plesiomorphic for Titanosauria, as well as several traits that are often regarded as apomorphic of that clade or a less inclusive subset thereof. Several features of *Savannasaurus* support a close relationship with the coeval *Diamantinasaurus matildae*, and this clade appears to occupy an early-branching position within Titanosauria. Relative to body size, the thoracic and abdominal breadth of *Savannasaurus* is greater than that seen in giant titanosaurs such as the contemporaneous South American lognkosaurians; however, this relative breadth is not quite as extreme as that of the small-bodied latest Cretaceous saltasaurines, or *Opisthocoelicaudia skarzynskii*. The possible advantages engendered by the barrel-shaped thorax, robust limbs, wide-gauge gait, and lack of hyposphene–hypantrum articulations are explored, and it is hypothesised that these traits were positively selected by the wet, temperate floodplain environment in which *Savannasaurus* lived. Greater stability and flexibility might have reduced the risk of bogging, and/or facilitated more expedient self-extraction from muddy waterholes. Similar environmental pressures acting upon other titanosaurian taxa or clades elsewhere might have led to the repeated independent development, or accentuation, of the bauplan regarded as ‘typical’ for the clade Titanosauria. This would explain the many observed convergences between *Savannasaurus* and *Diamantinasaurus*, and Saltasauridae.

INTRODUCTION

Cretaceous sedimentary sequences in Australia have mostly provided only limited evidence of sauropod dinosaurs. The Western Australian Cretaceous record is restricted to footprints from the Valanginian–Barremian Broome Sandstone (Thulborn et al., 1994; Thulborn, 2012; Salisbury et al., 2017), whereas the Victorian Cretaceous sauropod record is non-existent: both the upper Strzelecki Group (upper Barremian–lower Aptian) and the Eumeralla Formation (upper Aptian–lower Albian) entirely lack sauropods, despite preserving abundant remains of ornithopods, ankylosaurs, and theropods (Poropat et al., 2018). The upper Albian Toolebuc Formation of Queensland has produced several fragmentary sauropod specimens (Molnar and Salisbury, 2005), whereas the upper Albian Allaru Mudstone has yielded only one: the holotype of the somphospondylan titanosauriform *Austrosaurus mckillopi* (Longman, 1933; Poropat et al., 2017). The Cenomanian Griman Creek Formation in New South Wales has produced sauropod teeth (Molnar and Salisbury, 2005), whereas the same unit in Queensland has yielded only fragmentary postcranial elements (Molnar, 2011b).

By far the most productive Australian Cretaceous stratum in terms of sauropods is the Cenomanian–lowermost Turonian 'upper' Winton Formation of Queensland (Coombs and Molnar, 1981; Molnar, 2001, 2010, 2011a; Molnar and Salisbury, 2005), which is also the stratigraphically youngest sauropod-bearing unit in Australia. To date, three somphospondylan titanosauriforms have been named from this unit: the non-titanosaurian *Wintonotitan wattsi* (Hocknull et al., 2009; Poropat et al., 2015a), and the titanosaurs *Diamantinasaurus matildae* (Hocknull et al., 2009; Poropat et al., 2015b, 2016; Klinkhamer et al., 2018, 2019) and *Savannasaurus elliottorum* (Poropat et al., 2016). The osteology of both *Wintonotitan* and *Diamantinasaurus* has recently been described in detail (Poropat et al., 2015a, b), whereas that of *Savannasaurus* has only been addressed briefly (Poropat et al.,

2016). In this paper, we fully describe the osteology of the holotype and only known specimen of *Savannasaurus elliottorum*.

Institutional Abbreviations—AAOD, Australian Age of Dinosaurs Museum of Natural History (Winton, Queensland, Australia); **AODF**, Australian Age of Dinosaurs Fossil; **41HIII**, Henan Geological Museum, Zhengzhou, Henan Province, China; **MACN**, Museo Argentino de Ciencias Naturales 'Bernardino Rivadavia', Buenos Aires, Argentina; **MAU-PV**, Museo Municipal "Argentino Urquiza" (Rincón de los Sauces, Neuquén, Argentina); **MCT**, Museu de Ciências da Terra, Rio de Janeiro, Brazil; **MPEF**, Museo Paleontológico Egidio Feruglio, Trelew, Argentina; **QM**, Queensland Museum (Brisbane, Queensland, Australia); **UNPSJB-PV**, Universidad Nacional de la Patagonia 'San Juan Bosco' — Paleovertebrados, Comodoro Rivadavia, Argentina.

Anatomical Abbreviations—ACDL, anterior centrodiapophyseal lamina; **ACPL**, anterior centroparapophyseal lamina; **aSPDL**, anterior spinodiapophyseal lamina; **CDF**, centrodiapophyseal fossa; **CPAF**, centroparapophyseal fossa; **CPOF**, centropostzygapophyseal fossa; **CPOL**, centropostzygapophyseal lamina; **CPRF**, centroprezygapophyseal fossa; **CPRL**, centroprezygapophyseal lamina; **dp**, diapophysis; **dPCPL**, dorsal posterior centroparapophyseal lamina; **lCPRL**, lateral centroprezygapophyseal lamina; **mCPRL**, medial centroprezygapophyseal lamina; **PACDF**, parapophyseal centrodiapophyseal fossa; **PACPRF**, parapophyseal centroprezygapophyseal fossa; **PCDL**, posterior centrodiapophyseal lamina; **PCPL**, posterior centroparapophyseal lamina; **POCDF**, postzygapophyseal centrodiapophyseal fossa; **PODL**, postzygodiapophyseal lamina; **POSDF**, postzygapophyseal spinodiapophyseal fossa; **POSL**, postspinal lamina; **poz**, postzygapophysis; **pp**, parapophysis; **PPDL**, parapodiapophyseal

lamina; **PRDL**, prezygodiapophyseal lamina; **PRPADF**, prezygapophyseal parapodiapophyseal fossa; **PRPL**, prezygoparapophyseal lamina; **PRSDF**, prezygapophyseal spinodiapophyseal fossa; **PRSL**, prespinal lamina; **pSPDL**, posterior spinodiapophyseal lamina; **SDF**, spinodiapophyseal fossa; **SPDL**, spinodiapophyseal lamina; **SPDL-F**, spinodiapophyseal lamina fossa; **SPOF**, spinopostzygapophyseal fossa; **SPOL**, spinopostzygapophyseal lamina; **SPRF**, spinoprezygapophyseal fossa; **SPRL**, spinoprezygapophyseal lamina; **TPOL**, interpostzygapophyseal lamina; **TPRL**, interprezygapophyseal lamina; **vPCPL**, ventral posterior centroparapophyseal lamina.

GEOLOGICAL SETTING AND ASSOCIATED PALEOBIOTA

The holotype specimen of *Savannasaurus elliottorum* was preserved in the Cenomanian–lowermost Turonian (Tucker et al., 2013) 'upper' Winton Formation (Fig. 1), the stratigraphically youngest Mesozoic unit in the Eromanga Basin (Dunstan, 1916; Whitehouse, 1954; Vine and Day, 1965; Exon and Senior, 1976). The sedimentology of the Winton Formation is variable, consisting of interbedded mudstones, siltstones, and sandstones, with rare intraformational conglomerates (Exon and Senior, 1976; Senior and Mabbutt, 1979; Gray et al., 2002; Tucker et al., 2017). Mica, pyrite, gypsum, coal, other carbonaceous material, and wood fragments are all present in varying quantities (Gray et al., 2002). On the basis of its geology, flora and fauna, the 'upper' Winton Formation has been interpreted to have been deposited in a freshwater setting, likely a floodplain dominated by meandering river systems (Fletcher et al., 2018). The climate was seasonal, with high annual rainfall (Fletcher et al., 2014b).

In addition to the aforementioned sauropods (Fig. 2), other dinosaurs represented in the 'upper' Winton Formation by body fossils are the megaraptorid theropod *Australovenator wintonensis* (Hocknull et al., 2009; White et al., 2012, 2013, 2015), an indeterminate ankylosaur (Leahey and Salisbury, 2013), and a small, indeterminate ornithopod (Hocknull and Cook, 2008). Fossil footprints from Dinosaur Stampede National Monument at Lark Quarry Conservation Park site have been interpreted as representing both ornithopods and theropods (Thulborn and Wade, 1979, 1984; Thulborn, 2013, 2017), or ornithopods only (Romilio and Salisbury, 2011, 2014; Romilio et al., 2013).

Non-dinosaurian archosaurs from the 'upper' Winton Formation include the ornithocheirid pterosaur *Ferrodraco lentoni* (Pentland et al., 2019) and undescribed pterosaur and crocodyliform specimens (Hocknull et al., 2009), whereas the 'lower' Winton Formation has yielded the neosuchian crocodyliform *Isisfordia duncani* (Salisbury et al., 2006; Turner and Pritchard, 2015; Leite and Fortier, 2018). Although a turtle steinkern has been reported from the Winton Formation (Molnar, 1991; Kear, 2016), this specimen might in fact derive from the underlying Mackunda Formation (B. P. Kear, *pers. comm.*); regardless, turtles are represented in the 'upper' Winton Formation by undescribed skeletal remains that might be referable to Chelidae (Hocknull et al., 2009). A solitary vertebra from the 'upper' Winton Formation, originally tentatively assigned to cf. *Coniasaurus*, within Dolichosauridae (Scanlon and Hocknull, 2008), was more recently regarded as Varanoidea indet. (Kear, 2016). *Metaceratodus wollastoni* and *Metaceratodus ellioti* are the only two dipnoan species known from the 'upper' Winton Formation, and tooth plates from both species have been recovered from multiple localities (Kemp and Molnar, 1981; Kemp, 1997). The actinopterygian *Cladocyclus geddesi* is represented by a single partial skeleton from the 'lower' Winton Formation (Berrell et al., 2014); an actinopterygian skeleton has also been found in the 'upper' Winton Formation, but this remains undescribed (S.F.P., *pers. obs*.).

Invertebrate fossils are relatively rare in the 'upper' Winton Formation, with only the freshwater bivalves *Megalovirgus wintonensis*, *Hyridella macmichaeli* (designated *Prohyria macmichaeli* by Hocknull et al. (2009)), *Hyridella goondiwindiensis*, and *Alathyria jaqueti* represented by large numbers of specimens in Queensland (Hocknull, 1997, 2000). Rare gastropods (*Melanoides* sp.) have also been reported (Cook, 2005). Insect body fossils pertaining to Odonata (dragonflies) and Mecoptera (scorpionflies) have been reported but not described (Jell, 2004), and trace fossils attributed to oribatid mites have been identified in silicified wood (Fletcher and Salisbury, 2014).

The fossil flora of the 'upper' Winton Formation is co-dominated by conifers (Peters and Christophel, 1978; Dettmann et al., 2012) and angiosperms (McLoughlin et al., 1995; Dettmann et al., 2009). Conifers include the cupressacean *Austrosequoia wintonensis* (Peters and Christophel, 1978), the araucariaceans *Araucaria* cf. *mesozoica* (McLoughlin et al., 1995) and *Emwadea microcarpa* (Dettmann et al., 2012), and the podocarpacean *Protophyllocladoxylon owensii* (Fletcher et al., 2014a), whereas the angiosperms comprise *Lovellea wintonensis* (Dettmann et al., 2009) and nine magnoliophyte forms left in open nomenclature (McLoughlin et al., 1995, 2010). Ferns are also abundant and diverse in the Winton Formation (McLoughlin et al., 2010), with *Phyllopteroides macclymontae* (Osmundaceae; McLoughlin et al., 1995) and *Tempskya judithae* (Tempskyaceae; Clifford and Dettmann, 2005) among the most notable. The liverwort *Marchantites marguerita* (Dettmann and Clifford, 2000), the horsetail *Equisetites* sp. (McLoughlin et al., 2010), the cycadalean *Pterostoma hirsutus* (Pole & Douglas 1999), the bennettitaleans *Otozamites* cf. *bengalensis* and *Ptilophyllum* sp. (McLoughlin et al., 2010), and the ginkgoalean *Ginkgo wintonensis* (McLoughlin et al., 1995) round out the Winton Formation flora (Fletcher et al., 2018).

EXCAVATION, POST-HOC SITE RECONSTRUCTION AND TAPHONOMY

The *Savannasaurus elliottorum* type site was discovered by one of the authors (D.A.E.) in March 2005, and excavated in July and September of that year. Most of the specimen was preserved within a large siltstone concretion, which was broken up with jackhammers and chisels along naturally occurring, gypsum-filled fractures. Prior to extraction from the site, each siltstone fragment was assigned a number so that broken specimens could be easily put back together after preparation. Although a third excavation in September 2006 yielded no additional specimens, surface collection of the site in 2013 produced a partial caudal centrum and other fragments.

Mechanical preparation of the *Savannasaurus elliottorum* type specimen (Fig. 3A) was conducted using tungsten carbide-tipped pneumatic air scribes and micro-jacks. Once prepared, joining surfaces between fragments were marked with paint pens, and superglue and araldite were used to piece individual elements back together. The markings made on each specimen were also used to determine their relative positions in the site. Post hoc reconstruction of the site involved physical reassembly of various sections. Photogrammetric models of the upper and lower surfaces of each site section were generated in AgiSoft PhotoScan, and these were stitched together in Rhinoceros 4.0 to form complete three-dimensional models of each site component. These were then arranged (using field notes and known points of inter-specimen contact) to produce a three-dimensional digital site map (Fig. 3B–C).

The dorsal vertebrae of *Savannasaurus* were not articulated, but were in association immediately in front of the pelvic girdle. The posteriormost dorsal vertebrae were situated closer to the pelvic girdle than the more anterior dorsal vertebrae, which expedited

determination of the vertebral sequence. Ribs were present on both sides of the dorsal series, although all were fragmented (mostly post-fossilisation), and those on the left side were crushed prior to fossilisation. The sacrum was situated above, but rotated relative to, the fused pubes and ischia. The sternal plates and coracoid were found in association with the radius, dorsal ribs and the fragmentary (presumed) scapula. Left metacarpals III–V were positioned above dorsal vertebra III, whereas the left humerus was found to the left side of the dorsal series. Other remains were not found in contact, but all were restricted to an area of less than 20 m^2.

Although no bite marks have been identified on the *Savannasaurus elliottorum* holotype, a single tooth (AODF 819) referable to *Australovenator wintonensis* was recovered from the site (White et al., 2015). It is likely, therefore, that the disarticulation of the *Savannasaurus elliottorum* type specimen was partly a result of feeding by megaraptorid theropods. Some elements (e.g. dorsal vertebra V, both humeri) appear to have been trampled post mortem; this implies that other dinosaurs (most likely sauropods) traversed the site after at least partial burial of the carcass (pre-fossilisation), and that they also contributed to the scattering of the bones.

The *Savannasaurus elliottorum* holotype specimen was significantly less scattered than most other dinosaur specimens recovered from the 'upper' Winton Formation, including the type specimens of *Wintonotitan wattsi* (Poropat et al., 2015a: fig. 3), and *Diamantinasaurus matildae* and *Australovenator wintonensis* (Hocknull et al., 2009; Poropat et al., 2015b: fig. 3). The only articulated vertebrate specimens reported from the Winton Formation to date are those of the crocodyliform *Isisfordia duncani* (Salisbury et al., 2006: fig. 2) and the actinopterygian fish *Cladocyclus geddesi* (Berrell et al., 2014: fig. 3), both of which were preserved in *ex situ* sandstone concretions (Syme et al., 2016; Syme and Salisbury, 2018) in the 'lower' Winton Formation (Tucker et al., 2017).

SYSTEMATIC PALEONTOLOGY

SAUROPODA Marsh, 1878

MACRONARIA Wilson and Sereno, 1998

TITANOSAURIFORMES Salgado, Coria and Calvo, 1997

SOMPHOSPONDYLI Wilson and Sereno, 1998

TITANOSAURIA Bonaparte and Coria, 1993

SAVANNASAURUS ELLIOTTORUM Poropat *et al.*, 2016

Holotype—AODF 660—one posterior cervical vertebra; several cervical ribs; dorsal vertebrae III–X; several fragmentary dorsal ribs; at least four coalesced sacral vertebrae with processes; at least five partial caudal vertebrae; fragmentary scapula; left coracoid; left and right sternal plates; incomplete left and right humeri; fragmentary ulna; left radius; left metacarpals I–V; right metacarpal IV; two manual phalanges; iliac fragments; co-ossified left and right pubes and ischia; left astragalus; right metatarsal III; and associated fragments.

Type Locality—AODL 82 (the 'Ho-Hum' Site), Belmont Station, ~60 km northeast of Winton, Queensland, Australia.

Type Stratum—Winton Formation; Cenomanian–lowermost Turonian, Upper Cretaceous.

Diagnosis—The following characters are considered to be autapomorphies of *Savannasaurus elliottorum*: 1) undulating anterior articular surface of anterior caudal vertebral centra (concave dorsally and convex ventrally); 2) anterior-most caudal centra with shallow lateral pneumatic fossae (local autapomorphy within Somphospondyli); 3) sternal plate with straight lateral margin (reversal); 4) sternal plate lacking anteroposteriorly elongate ridge along the anterior portion of the ventral surface (local autapomorphy within Titanosauria); 5) metacarpal IV distal end hourglass-shaped; 6) pubis with ridge extending anteroventrally from ventral margin of obturator foramen on lateral surface; 7) ischium with proximal plate anteroposterior length >40% the overall proximodistal length of the element; 8) astragalus taller proximodistally than wide mediolaterally or long anteroposteriorly; 9) astragalus mediolateral width and anteroposterior length essentially equal.

DESCRIPTION AND COMPARISONS

The terminology used to describe the vertebral laminae largely follows Wilson (1999) and Wilson (2012), whereas the terminology employed for the fossae follows Wilson et al. (2011). The internal texture of all preserved presacral vertebrae is camellate, following Wedel (2003). The fragments identified as pertaining to the scapula, ulna and ilia have been so heavily affected by post mortem distortion and/or fracturing that they are anatomically uninformative; consequently, they are not described herein.

Cervical Vertebra

The only preserved cervical vertebra is represented by the majority of the centrum (excluding the anterior condyle and the right parapophysis) and a minor portion of the firmly coalesced neural arch (Fig. 4; Table S1). It is herein interpreted as a posterior cervical vertebra because of the relatively low average elongation index (aEI) of the centrum (~1.86, based on the preserved portion; it is unlikely to have been higher than 2.0), and the broad transverse width across the parapophyses relative to the anteroposteriorly short length of the centrum. The anterior portion of the non-condylar centrum is not preserved. However, based on the position of the remaining portion of the left parapophysis, which would have occupied the anteroventral corner of the lateral surface of the centrum, and the morphology of the lateral pneumatic fossa and foramen, the vertebra would not have been substantially longer than preserved (Fig. 4A, B). The fact that the posterior articular surface (Fig. 4C) is concave suggests that the vertebra was opisthocoelous, as are the cervical vertebrae of all eusauropods (Upchurch, 1998). The dorsal margin of the posterior articular surface is shallowly concave, in line with the posterior neural canal opening (Fig. 4C). Although incompletely preserved, the posterior cotyle was clearly wider transversely than dorsoventrally tall (ratio ~1.25); this distinguishes *Savannasaurus* from several Asian somphospondylans (Mannion et al., 2013, 2019a), including the euhelopodids *Euhelopus* (Wiman, 1929; Wilson and Upchurch, 2009) and *Erketu* (Ksepka and Norell, 2006, 2010), and the possible titanosaur *Daxiatitan* (You et al., 2008). The anterior portion of the ventral surface of the centrum is concave transversely and, to a lesser degree, concave anteroposteriorly (Fig. 4D). This concavity is exaggerated by (or might simply be a consequence of) the slight ventral projection of the parapophyses. There are no sharp-lipped excavations on the ventral surface, contrasting with the paired fossae that characterise the anterior portion of the middle–posterior cervical centra of some titanosaurs, including *Muyelensaurus* (MAU-PV-LL-391: P.D.M. pers. obs. 2014), *Overosaurus* (Coria et al., 2013), and *Rukwatitan* (Gorscak et al., 2014). A subtle, slightly

off-centre, anteroposteriorly-oriented, and rather weak ventral keel is present (Fig. 4D). Whereas the presence of a ventral keel is plesiomorphic for sauropod cervical vertebrae (Upchurch, 1998), and also characterises some somphospondylans (e.g. *Euhelopus*; Wilson and Upchurch, 2009), most titanosaurs lack ventral keels (Mannion et al., 2013). However, a midline crest is present in at least one posterior cervical vertebra of *Mendozasaurus* (González Riga, 2005; González Riga et al., 2018), *Overosaurus* (Coria et al., 2013), and probably *Austroposeidon* (Bandeira et al., 2016), and is present throughout the cervical series in *Rapetosaurus* (Curry Rogers, 2009). Towards the posterior cotyle, the ventral surface of the centrum becomes transversely convex. The lateral surface of the centrum is dominated by an anteroposteriorly elongate pneumatic foramen, which is divided by several bony struts. This is set within the anterior half of an anteroposteriorly elongate, posteriorly acuminate, pneumatic fossa, which extends almost the full length of the centrum (Fig. 4A). The presence of a well-developed lateral excavation contrasts with the cervical centra of many somphospondylans, especially titanosaurs (e.g. *Futalognkosaurus*, *Rapetosaurus*), which are often characterised by a shallow fossa, or lack an excavation altogether (Upchurch, 1998; Wilson, 2002; Curry Rogers, 2005). The ventral margin of the pneumatic fossa is defined by a thickened PCPL which, when viewed dorsally (Fig. 4B) or ventrally (Fig. 4D), runs parallel to the long axis of the centrum before sweeping laterally towards the parapophysis. The PCPL becomes thicker dorsoventrally towards the parapophysis and is well defined along its length, almost to the margin of the posterior cotyle. The posterior portion of the lateral pneumatic fossa is bounded dorsally by the PCDL, which runs anterodorsally–posteroventrally. A horizontal lamina, extending from the posterior end of the PCDL to the anteriormost preserved portion of the vertebra, constitutes the rest of the dorsal margin of the lateral pneumatic fossa. The robust parapophysis projects laterally and slightly ventrally from the anteroventral corner of the centrum, lacking the strong ventral deflection that

characterises the middle–posterior cervical vertebrae of several somphospondylans (D'Emic, 2012; Mannion et al., 2013), including the titanosaurs *Isisaurus* (Jain and Bandyopadhyay, 1997) and *Overosaurus* (Coria et al., 2013), as well as some members of Lognkosauria (González Riga et al., 2018). Unlike the elongate parapophyses of the middle–posterior cervical vertebrae of several derived titanosaurs (e.g. saltasaurids; D'Emic, 2012), those of *Savannasaurus* are restricted to the anterior half of the centrum. The dorsal surface of the parapophysis is convex along its length, lacking any pneumatic excavation or extension of the lateral pneumatic fossa, whereas its ventral surface is flat. The articular surface of the parapophysis was firmly sutured to the cervical rib, but breakage of this specimen during excavation has resulted in their separation (the connection point is labelled in Fig. 4A and E). At the anterior margin of the dorsal surface of the parapophysis, an anteroposteriorly thin ridge is present, separating anterior and posterior fossae on the internal surface of the mediolaterally thin plate connecting the capitular and tubercular heads of the cervical rib. The anterior fossa continues onto the anterior margin of the parapophysis as a dorsoventrally and somewhat mediolaterally concave surface, whereas the posterior surface of the base of the parapophysis is dorsoventrally convex. The cervical rib is poorly preserved and incomplete; nevertheless, there are indications that both anterior and posterior projections were present (Fig. 4A–B, D). Immediately below the ventral margin of the cervical rib, portions of the distal shafts of two additional parallel cervical ribs are present (Fig. 4E–G). This suggests that at least some of the cervical ribs of *Savannasaurus* were elongate, extending along the length of at least three centra (including the one to which they were adhered).

Dorsal Vertebrae

A total of eight dorsal vertebrae from *Savannasaurus* have been recovered (Figs. 5–12; Table S1). Assuming that the entire dorsal series comprised ten vertebrae, as in most other titanosaurs with complete sequences (e.g. *Trigonosaurus* (Campos et al., 2005), *Futalognkosaurus* (Calvo et al., 2007), *Overosaurus* (Coria et al., 2013), *Rapetosaurus* (Curry Rogers, 2009)), and based on the position of the parapophysis on the preserved vertebrae, we infer that the anterior two dorsal vertebrae are missing. Therefore, we describe the preserved elements as dorsal vertebrae III–X.

All of the dorsal centra are strongly opisthocoelous, as in most macronarians (Salgado et al., 1997; Wilson and Sereno, 1998), with no decrease in the degree of development of the anterior condyle along the series. Virtually all preserved centrum articular surfaces are notably shorter dorsoventrally than they are wide transversely, which is consistent with the condition in titanosaurs (Mannion et al., 2013, 2019b), especially in the anterior part of the dorsal series. The anterior condyles of dorsal vertebrae IV (Fig. 6A), VII (Fig. 9A), and VIII (Fig. 10A) each bear a dorsoventrally elongate groove, which is less than half the height of the condyle and located approximately centrally. The lateral and ventral margins of the anterior condyles and posterior cotyles are convex. By contrast, the dorsal margin of each anterior condyle is flat, whereas that of each posterior cotyle is concave. All preserved dorsal centra are transversely constricted at their mid-lengths and flared both anteriorly and posteriorly. The ventral surfaces of the centra are (generally) transversely and anteroposteriorly concave, and lack midline ridges. Thus, the midline keel that is present in the middle–posterior dorsal vertebrae of a small number of titanosaurs, including *Diamantinasaurus* (Poropat et al., 2015b), *Futalognkosaurus* (Calvo et al., 2007), and *Opisthocoelicaudia* (Borsuk-Białynicka, 1977), is absent in *Savannasaurus*. Weakly developed ventrolateral ridges are present on some of the dorsal centra of *Savannasaurus*. Similar, albeit better-developed, ridges characterise the middle–posterior dorsal centra of

Diamantinasaurus (Poropat et al., 2015b) and *Opisthocoelicaudia* (Borsuk-Białynicka, 1977). All dorsal centra have dorsoventrally short, posteriorly acuminate pneumatic foramina set within fossae on their lateral surfaces, as in most somphospondylans (Upchurch et al., 2004). Ventral to the pneumatic fossa, the lateral surface of each centrum is dorsoventrally convex and anteroposteriorly concave.

In each dorsal vertebra, the prezygapophysis is supported ventrally by a CPRL; two left CPRLs (designated the mCPRL and lCPRL) are present in dorsal vertebrae III–IV and VIII (Fig. 5A, 6A, 10A). The TPRL, CPRLs, and the dorsal margin of the anterior condyle define the CPRF, within which the anterior neural canal opening lies. This contrasts with the middle–posterior dorsal vertebrae of several titanosaurs (e.g. *Tapuiasaurus*, *Epachthosaurus*, *Rapetosaurus*, *Alamosaurus*, and saltasaurines), in which the anterior neural canal opening is entirely surrounded by the neural arch (Carballido et al., 2012; Poropat et al., 2016). In dorsal vertebrae III–IV and VI–VIII, the CPRF is bisected by a vertical lamina running from the centre of the TPRL to the dorsal margin of the anterior neural canal opening (Fig. 5A, 6A, 8A, 9A, 10A). The CPRL (lCPRL when two left CPRLs are present) shares its base with the ACPL, and a PACPRF is delineated by these laminae and the stout PRPL in dorsal vertebrae III–IV and VI–IX at least (its presence in dorsal vertebrae V and X cannot be determined). The PACPRF is visible only in anterior view in dorsal vertebrae III–IV and VI–VII (Fig. 5A, 6A, 8A, 9A), whereas it is visible in lateral view in dorsal vertebrae VIII–IX (Fig. 10B, 11B).

A hyposphene and hypantrum structure is absent in all dorsal vertebrae, as is the case in nearly all derived titanosaurs (Salgado et al., 1997; Apesteguía, 2005). The prezygapophyseal facets tend to be wider mediolaterally than they are long anteroposteriorly, and are connected to each other via a TPRL in all preserved dorsal vertebrae. In the anteriormost preserved dorsal vertebrae, the prezygapophyses are widely spaced and are strongly dorsomedially oriented (>40°); consequently, the TPRL in these vertebrae is V-shaped, as is the case in most

titanosaurs (Carballido et al., 2012). Further along the dorsal series, the prezygapophyses successively face more dorsally than medially, such that by dorsal X the articular facets and the associated TPRL are essentially horizontal (Fig. 12C). This differs from nearly all other titanosaurs, in which the zygapophyseal table remains strongly tilted in posterior dorsal vertebrae (Carballido et al., 2012; Poropat et al., 2016).

As in all other sauropods, the positions of the parapophyses and diapophyses in *Savannasaurus* shift relative to one another, and to the centrum, along the sequence. This leads to changes in the orientation of their associated laminae, and affects which laminae are present along the sequence. All preserved parapophyseal articular facets are oval, taller dorsoventrally than long anteroposteriorly, and often concave. In all preserved dorsal vertebrae, the parapophysis is situated anteroventral to the diapophysis. The parapophysis is supported ventrally by a sub-vertical ACPL, and at least one PCPL; however, as is common in many titanosauriforms (D'Emic, 2012), including *Austrosaurus* (Poropat et al., 2017) and *Diamantinasaurus* (Poropat et al., 2015b, 2016), two parallel PCPLs are present on several dorsal vertebrae — especially on the left side. In dorsal III, wherein the parapophysis is located near the dorsal margin of the centrum (Fig. 5B), the vPCPL is sub-horizontal and forms the dorsal margin of the lateral pneumatic fossa, whereas the dPCPL is weakly developed and crosscut by the ACDL. In dorsal vertebrae IV and VI–X, where the parapophysis is situated further dorsally, both the vPCPL and dPCPL are anterodorsally–posteroventrally inclined. The vPCPL tends to brace the ACPL, rather than reaching the parapophysis, and often forms the dorsal margin of the pneumatic fossa. The ACPL, dPCPL and the dorsal margin of the centrum invariably define a CPAF; in instances where two PCPLs are present on the same side, the CPAF is split by the vPCPL, and in several cases (e.g. dorsal vertebrae IV and IX) a truncated ACDL also interrupts the CPAF. The PCPL (dPCPL, where relevant) and the PCDL invariably project from the same point as each other

on the centrum. In more anterior dorsal vertebrae (IV, VI, VIII), the dPCPL generally merges smoothly with the base of the PCDL (or coalesced ACDL+PCDL), whereas in more posterior dorsal vertebrae (VII, IX, X) the dPCPL simply projects from the same point on the centrum as the PCDL. In dorsal vertebrae IV–X, a slightly posterodorsally–anteroventrally inclined PPDL connects the parapophysis with the diapophysis. The PPDL bifurcates at its parapophyseal end in dorsal vertebra IV (Fig. 6C). This is an unusual feature but, given its presence on only one dorsal vertebra, we do not include it as an autapomorphy of *Savannasaurus*.

When complete, the diapophyseal facets are invariably longer anteroposteriorly than they are tall dorsoventrally, have a smoothly convex dorsal margin and an undulating ventral one, and are often convex, lacking a distinct distal end surface. Although there is a subtle shift in the orientation of the diapophyses relative to the centra along the series, they are never strongly deflected dorsally: they project mostly laterally and somewhat dorsally in the anteriormost preserved dorsal vertebrae, and more strongly dorsally but still mostly laterally in more posterior dorsal vertebrae. In all dorsal vertebrae, the diapophysis is supported from below by a single, ventrally unexpanded PCDL that projects dorsolaterally and tends to be the most robust lamina on each vertebra. Although an ACDL can be tentatively identified on most of the preserved dorsal vertebrae, this structure is more often than not truncated by the PCPL (or vPCPL where present; e.g. dorsal IV (Fig. 6C), VIII (Fig. 10B)). In dorsal vertebra VII, the ACDL appears to brace the shared base of the PCPL and PCDL (Fig. 9B). A PACDF is present in all preserved dorsal vertebrae. In dorsal vertebra III, the PACDF is bordered by the PRDL, PRPL, PCPL and PCDL, and interrupted by a weak ACDL (Fig. 5B). By contrast, in dorsal vertebrae IV–X — which lack a PRDL — the PACDF is bordered by the PPDL, PCPL (dPCPL, where relevant) and PCDL (coalesced ACDL+PCDL, where relevant). In

dorsal vertebra VIII, accessory laminae are present within the PACDF, dorsal to the junction of the dPCPL and the PCDL (Fig. 10B).

The postzygapophyseal articular facets are generally wider mediolaterally than they are long anteroposteriorly. In the anteriormost preserved dorsal vertebrae they face ventrolaterally, whereas further posteriorly in the sequence they face progressively less laterally and more ventrally; in dorsal vertebrae IX and X, they face almost entirely ventrally (Fig. 11C, 12A). Each postzygapophysis is supported ventrally by a CPOL, at or near its medial margin. This lamina extends dorsally from approximately the same point on the centrum as the PCDL. The ventral end of the left CPOL is bifurcated in dorsal vertebra III, whereas the right one is undivided (Fig. 5D). In all dorsal vertebrae, the paired CPOLs form the lateral margins of the CPOF, the ventral half of which is penetrated by the posterior neural canal opening. The dorsal margin of the CPOF is formed by the TPOL in dorsal vertebrae III–IV (Fig. 5D, 6D), but no TPOL is present in subsequent dorsal vertebrae; thus, the CPOF and SPOF are effectively confluent. A confluent SPOF+CPOF is also seen in an anterior dorsal vertebra of *Choconsaurus* (Simón et al., 2018), in middle dorsal vertebrae of both *Yongjinglong* (Li et al., 2014) and *Sonidosaurus* (Xu et al., 2006), in dorsal vertebra VI of *Epachthosaurus* (UNPSJB-PV 920; S.F.P., pers. obs. 2013), in a posterior dorsal vertebra of *Mnyamawamtuka* (Gorscak and O'Connor, 2019), and in at least some dorsal vertebrae of *Ampelosaurus* (Le Loeuff, 2005) and *Isisaurus* (Jain and Bandyopadhyay, 1997). Similarly, some middle–posterior dorsal vertebrae of saltasaurines have either extremely reduced TPOLs or appear to lack them altogether (Zurriaguz and Powell, 2015). Although the SPOF and CPOF appeared to be confluent in one dorsal vertebra of *Dreadnoughtus*, the presence of a TPOL in most other exemplars suggests that it was present throughout the dorsal series, and that the SPOF and CPOF were separate (Voegele et al., 2017). In dorsal vertebrae IX–X, the postzygapophyses of *Savannasaurus* almost meet on the midline (Fig. 11C, 12A). This is also

evident in some dorsal vertebrae of *Chubutisaurus* (Carballido et al., 2011), *Patagotitan* (Carballido et al., 2017), and *Opisthocoelicaudia* (Borsuk-Białynicka, 1977). The CPOL and PCDL form the ventrolateral corner of a posterolaterally-facing fossa. In dorsal vertebrae III–VI, in which no PODL is present, this fossa is bordered dorsally by the SPDL (pSPDL, where relevant; see below), making it a POCDF+POSDF. In dorsal vertebrae VII–X, which do possess a PODL, this fossa is a POCDF. The left POCDF+POSDF is interrupted by a vertical accessory lamina in dorsal vertebrae IV and VI, as is the left POCDF of dorsal vertebrae VII and VIII, and the right POCDF of dorsal vertebra VII and IX.

As preserved, dorsal neural spine height increases posteriorly along the sequence. This is consistent with the condition in most sauropods, but the reverse is true in some titanosaurs (Mannion et al., 2013), including *Opisthocoelicaudia* (Borsuk-Białynicka, 1977), *Rapetosaurus* (Curry Rogers, 2009), and some members of Lognkosauria (Carballido et al., 2017). We caveat this with the possibility that the unpreserved anteriormost dorsal vertebrae of *Savannasaurus* might be unusually dorsoventrally tall, but consider this unlikely. In general, the dorsal neural spines have a consistent anteroposterior thickness along their length. As is the case in most sauropods (Upchurch, 1995), the neural spines of the posterior dorsal vertebrae are taller than the posterior articular surfaces of their respective centra. However, this is not the case in a small number of derived somphospondylans, with taxa such as *Dongyangosaurus* and *Opisthocoelicaudia* characterised by dorsoventrally short posterior dorsal neural spines (Mannion et al., 2013).

None of the preserved dorsal neural spines of *Savannasaurus* are bifurcated, which contrasts with *Opisthocoelicaudia* (Borsuk-Białynicka, 1977), as well as the putative titanosaurs *Daxiatitan* (You et al., 2008) and *Dongyangosaurus* (Lü et al., 2008). In the anteriormost preserved dorsal vertebrae of *Savannasaurus*, the neural spine is strongly inclined posterodorsally. Further posteriorly, the inclination of the neural spine decreases,

such that in dorsal X it is sub-vertical. These shifts in the orientation of the neural spines result in serial changes in lamina configuration (see below). A similar transition from posterodorsally-inclined to sub-vertical neural spines is observed in the dorsal series of several titanosaurs, including *Epachthosaurus* (Martínez et al., 2004), *Trigonosaurus* (Campos et al., 2005), *Overosaurus* (Coria et al., 2013), *Rapetosaurus* (Curry Rogers, 2009), *Alamosaurus* (Lehman and Coulson, 2002), and *Neuquensaurus* (Salgado et al., 2005); by contrast, the neural spines appear to be vertical throughout the dorsal series in *Isisaurus* (Jain and Bandyopadhyay, 1997). On the lateral sides of each neural spine of *Savannasaurus*, an aliform process is present; in the anteriormost preserved dorsal vertebrae, these processes are small, whereas they are more prominent further along the sequence.

The PRSL fails to reach the apex of the neural spine in all preserved dorsal vertebrae of *Savannasaurus*. It is most extensive in dorsal vertebrae IX–X, wherein it runs for two-thirds of the neural spine height; by contrast, in dorsal vertebrae III–VIII, it fades out before the spine mid-height. In dorsal vertebrae III–IV, there is a weak SPRL that extends from each prezygapophysis to a point where it terminates one-quarter of the way along the neural spine. The SPRL is more strongly developed in dorsal vertebrae VI and VII, reaching one-third and two-thirds of the height of the neural spine, respectively. In dorsal vertebra VIII, the SPRL reaches even further up the neural spine, but not as far as the SPDL. In dorsal vertebra IX, an mSPRL and a lSPRL are present on the right side, whereas the left SPRL is undivided and seemingly equivalent to the right mSPRL. The right lSPRL is prevented from ascending more than one-quarter the height of the neural spine by the mSPRL, which appears to reach the same height as the SPDL. In dorsal X, the SPRLs fade out at the point that the SPDL reaches the neural spine. A shallow SPRF separates each SPRL (mSPRL, where relevant) from the PRSL, whereas a small PRSDF separates the SPRL (lSPRL, where relevant) from the SPDL (mSPDL, where relevant).

In dorsal vertebrae III and IV, the posterodorsal corner of the diapophysis is connected to the neural spine by a near-horizontal, sheet-like SPDL. Two SPDLs are present on each side in dorsal vertebrae VI–VII: an aSPDL, which runs medially across the face of the neural spine towards the midline; and a pSPDL, which forms the lateral margin of the neural spine. In dorsal VII, the pSPDL reaches the level of the aliform process. Where present, the aSPDL and pSPDL are invariably separated by a fossa. Only one SPDL, equivalent to the pSPDL, is present in dorsal vertebrae VIII–IX: in dorsal vertebra VIII, it diminishes at the level of the aliform process, whereas in dorsal vertebra IX it connects to the neural spine anterior to the aliform process. In dorsal vertebra X, the SPDL bifurcates as it approaches the apex of the neural spine, with the posterior projection of the SPDL extending to the aliform process and the anterior one projecting towards the midline. The bifurcated SPDL and aliform process define a small, yet deep, dorsally facing fossa. A small number of titanosaurs also have two SPDLs on either side, as well as a bifid pSPDL, in their middle–posterior dorsal vertebrae, including *Epachthosaurus*, *Rapetosaurus*, and *Saltasaurus* (Poropat et al., 2016), although in those taxa these laminae tend to be more consistently present along the sequence.

The orientation of the neural spine directly impacts upon the SPOLs, which connect the postzygapophyses to the posteroventral surface of the neural spine. In the anterior dorsal vertebrae, each postzygapophysis is connected to the posterodorsally inclined neural spine by a short, stout SPOL, and no PODL is present. As the posterior inclination of the neural spine decreases, the length of the SPOL increases. Evidently, the postzygapophyses and SPOLs in the posterior dorsal vertebrae required additional bracing: in dorsal vertebrae VII–X, a PODL provides such support. A PODL is present only in the posteriormost two dorsal vertebrae of *Trigonosaurus* (Campos et al., 2005; MCT 1488-R: PDM pers. obs. 2019), *contra* Salgado et al. (2006) and Salgado and Powell (2010). By contrast, a PODL is absent in all of the posterior dorsal vertebrae of *Alamosaurus* and *Opisthocoelicaudia* (Salgado et al., 1997). In

dorsal vertebra VI, horizontal accessory laminae connect each SPOL to the POSL; these might have accommodated some of the stresses borne by the PODL in the more posterior dorsal vertebrae. In dorsal vertebrae VII–X, a dorsolaterally facing POSDF is present, separated from the POCDF by the PODL, and otherwise bounded by the SPDL (pSPDL, where relevant) and SPOL. A POSL is present in all preserved dorsal vertebrae, separated from each SPOL by a SPOF. In dorsal vertebrae V–VIII, the wide spacing of the postzygapophyses and the absence of a TPOL means that the POSL enters the CPOF and approaches the dorsal margin of the posterior neural canal opening. This morphology is otherwise known only in *Diamantinasaurus* (Poropat et al., 2016). The POSL is less pronounced in dorsal vertebrae VIII–X than in dorsal vertebrae III–VII.

A notable feature of the dorsal series of the *Savannasaurus elliottorum* type specimen is the bilateral directional asymmetry in the lamina system of the dorsal vertebrae. This is by no means novel to the vertebrae of *Savannasaurus*: Osborn (1899) identified asymmetry in a specimen of *Diplodocus*; Gilmore (1936) in the holotype of *Apatosaurus louisae* and in other diplodocid specimens; Santucci and Bertini (2006) in several titanosaur vertebrae from the Bauru Group of Brazil; Csiki et al. (2010) in the holotype of the titanosaur *Paludititan nalatzensis*; and Wilson (2012) and Wedel and Taylor (2013) in numerous sauropod specimens. In *Savannasaurus* specifically, the left side of each dorsal vertebra appears to have been more strongly reinforced by split and/or accessory laminae than the right. Although the asymmetry in the dorsal vertebral lamina system is most likely a consequence of the independent pneumatisation of each side of the vertebral column (Hogg, 1984; Wedel, 2003), it is also possible that the spinal column of the *Savannasaurus elliottorum* type individual was subjected to asymmetric loading, and that the extra laminae on the left side developed in response to this.

Dorsal Ribs

Several portions of dorsal ribs of *Savannasaurus* are preserved, although the majority were fragmented post mortem, such that in most cases the rib heads are poorly preserved or missing. One exception is a left dorsal rib (Fig. 13), in which the tuberculum and capitulum are well preserved. The incomplete capitular articular surface is taller dorsoventrally (58 mm) than it is long anteroposteriorly (41 mm). By contrast, the complete tubercular articular surface is longer anteroposteriorly (70 mm) than it is tall dorsoventrally (35 mm). The rib heads are separated by 80 mm. A thin (and incompletely preserved) lip of bone is present between the tuberculum and capitulum; on both its external and internal surfaces, an opening is present which would have facilitated the intrusion of pneumatic diverticula. All dorsal ribs in titanosauriforms tend to show pneumatisation (Wilson and Sereno, 1998); however, some non-titanosauriforms preserve rare evidence for pneumatised dorsal ribs as well (e.g. *Apatosaurus* (Gilmore, 1936; Mannion et al., 2012)). The shaft of the rib is teardrop-shaped in cross-section, with the anterior surface broadly convex and the posterior end tapered. The lateral surface is anteroposteriorly convex; by contrast, the medial surface varies from slightly concave at the proximal end to flat further distally, and concave again at the distalmost preserved portion. At the distal end, the cross-section through this rib is triangular.

The remaining dorsal ribs are incompletely preserved. The longest preserved exemplar, which is lacking the proximal end but appears to derive from the right side, is 1680 mm long (measured along the outside surface using a cloth tape measure); when complete it probably exceeded 1800 mm in overall length. The proximalmost preserved portion of this rib is bell-shaped in cross-section: the lateral surface is essentially flat, the medial surface is strongly convex, and the junction between these two surfaces (which occurs in line with the lateral margin) is slightly concave both anteriorly and posteriorly. The anterior surface remains tapered along its length, whereas the flange that runs along the posterior surface varies in

extent. On the posterior surface, a prominent flange is present along the proximalmost preserved 400 mm of the rib; along the same length of rib, the expression of the medial bulge decreases towards the distal end. At the proximal end, the junction between these two features was shallowly mediolaterally concave; 400 mm further distally, the concavity between these two features is a deep trench. The rib is triangular in cross-section at this point, with a concave posterior face. This concavity shallows over the succeeding 300 mm, disappearing slightly proximal to the mid-length of the preserved rib. At the distal end, this rib is clearly 'plank'-like (49 mm long anteroposteriorly; 12 mm wide mediolaterally).

One other dorsal rib (130 mm long proximodistally, missing the proximal end) is bell-shaped in cross-section at its proximalmost preserved point but becomes strongly 'plank'-like along its distal half (91 mm long anteroposteriorly; 13 mm wide mediolaterally). This rib also preserves a complete distal end, with an undulating texture typical of a surface covered with cartilage in life.

Sacrum

The entire dorsal surface of the sacrum of *Savannasaurus*, including the neural spines and the upper row of sacral processes, has been obliterated, as has the anteriormost centrum (or centra). Thus, all that remains are the ventral portions of four sacral vertebrae (anterior to which at least one additional sacral would have been sutured), and six of the eight ventral sacral processes (only five of which are shown in Fig. 14) that would have projected from these centra. As is the case with the pubes and ischia (see below), the preserved portion of the sacrum is extremely broad (1070 mm transversely) although, based on the preserved length of the sacral centra (720 mm anteroposteriorly), it is probable that the complete sacrum was as long or longer anteroposteriorly than it was wide transversely at the acetabulum. The

sacricostal yoke is preserved on both sides of the sacrum, although neither ilium is present; presuming that, as in other titanosauriforms, the ilia flared anterolaterally, the pelvis of *Savannasaurus* would have been even wider at its anterior margin than the preserved sacrum suggests. It appears unlikely that the middle sacral centra of *Savannasaurus* were notably narrower than the anteriormost and posteriormost ones, contrasting with derived titanosaurs (Salgado et al., 2005; D'Emic and Wilson, 2011; Poropat et al., 2016). The lateral surfaces of the centra lack openings. The sutures between the sacral centra are generally indistinct. However, the suture between the ultimate and penultimate preserved sacral vertebrae is pronounced as a consequence of the flared nature of the articular surfaces. This suture might have occurred relatively late in the life of the holotype individual of *Savannasaurus*. The only articular surface observable, the posterior surface of the posteriormost preserved sacral vertebra, is slightly concave.

Caudal Vertebrae

Portions of at least five caudal vertebrae are preserved, although only four of these are sufficiently complete to provide anatomical information (Fig. 15; Table S2). All preserved caudal centra are amphicoelous, distinguishing *Savannasaurus* from most titanosaurs (Salgado et al., 1997). However, other titanosauriforms that are sometimes classified within Titanosauria, such as *Traukutitan* (Salgado and Calvo, 1993; Juárez Valieri and Calvo, 2011) and *Malarguesaurus* (González Riga et al., 2009), also have at least some anterior caudal centra that are non-procoelous (i.e. that lack a posterior condyle). The only preserved caudal vertebrae in the putative titanosaurs *Baotianmansaurus* and *Dongyangosaurus*, which are from the anteriormost section of the tail, have shallowly amphicoelous centra (Lü et al., 2008; Zhang et al., 2009; Mannion et al., 2019a). Nevertheless, perhaps the most relevant taxa for

comparison with *Savannasaurus* are the approximately coeval Gondwanan taxa *Andesaurus*, in which only the anteriormost caudal centra are gently procoelous (Calvo and Bonaparte, 1991; Mannion and Calvo, 2011), *Mnyamawamtuka*, in which the anteriormost caudal centra are either mildly procoelous or lack a posterior condyle entirely (Gorscak and O'Connor, 2019), and *Chubutisaurus*, in which the anterior caudal centra have shallowly concave anterior articular surfaces and flat posterior articular surfaces (Del Corro, 1975; Salgado, 1993; Carballido et al., 2011).

All of the preserved caudal centra are anteroposteriorly short relative to the dimensions of their articular surfaces. In all exemplars, the anterior margin of the centrum is perpendicular to the anteroposterior axis of the centrum, differentiating *Savannasaurus* from aeolosaurines (Santucci and Arruda-Campos, 2011). All caudal vertebrae of *Savannasaurus* lack hyposphene–hypantrum articulations. This distinguishes *Savannasaurus* from brachiosaurids and euhelopodids, in which these articulations are usually present in the anteriormost caudal vertebrae, but unites it with most other titanosauriforms (Upchurch, 1998; Mannion et al., 2013).

Proximal–Middle Anterior Caudal Vertebrae—Two proximal–middle anterior caudal vertebrae are preserved in *Savannasaurus* (Fig. 15A–J); herein, these are designated caudal vertebra A and B. Caudal vertebra A is represented by most of the centrum, the left transverse process, the bases of the prezygapophyses, and a fragmentary neural spine that includes the postzygapophyses; the right lateral surface is poorly preserved, and the ventral surface is mostly missing. The preserved portion of caudal vertebra B comprises an incomplete centrum (missing most of the ventral half), the left transverse process, all four zygapophyses and a complete neural spine. Caudal vertebra A was presumably situated more anteriorly in the tail than caudal vertebra B, based on its larger size and more developed transverse processes. However, it was probably not one of the anteriormost vertebrae in the tail.

The internal bone of caudal vertebra B can only be observed on the broken centrum and postzygapophyses, and in both cases it is cancellous (fine and spongy), with only very small coels present. In the centrum, these become anteroposteriorly elongate near the lateral margin. By contrast, in caudal vertebra A the internal texture can be observed on many broken surfaces (Fig. 15C, E). Along the rim of the posterior articular surface of the centrum, the internal texture is cancellous, with only minuscule spaces (< 5 mm across) present. For the most part, the internal texture of the broken transverse process is similarly cancellous; however, along the posterior margin, the coels become dorsoventrally elongate (thereby paralleling the posterior margin of the transverse process) and increase in size such that they are almost 10 mm tall dorsoventrally, yet only 2 mm long anteroposteriorly. Further dorsally, the portion of the transverse process situated upon the neural arch is filled with larger spaces, ~30 mm across, separated by relatively thin (~5 mm) bony struts; thus, the internal texture is camellate. The internal structure of the left prezygapophysis comprises a single large coel with a thickened ventral rim; otherwise, the internal texture is similar to that of the neural arch portion of the transverse process. The restriction of pneumaticity in the caudal vertebrae of *Savannasaurus* to the neural arch is similar to that seen in an unnamed Early Cretaceous titanosaur from China (PMU 24709 [formerly PMU R 263]; Whitlock et al., 2011; Poropat, 2013), *Xianshanosaurus* (Lü et al., 2009; although it is possible that the pneumaticity in this taxon might extend into the centra as well), *Malawisaurus* (Wedel, 2009), and *Alamosaurus* (Fronimos, 2011). By contrast, the centrum (and possibly the neural arch) in *Volgatitan* is pneumatic (Averianov and Efimov, 2018), whereas in saltasaurine titanosaurs the pneumaticity in the anterior (and middle) caudal vertebrae extends into the centrum as well (Cerda et al., 2012).

The preserved portion of the anterior articular surface of the centrum of caudal vertebra A shows a distinct undulation, with the dorsal half concave and the ventral half flat (Fig. 15C).

This unusual morphology might represent an autapomorphy of *Savannasaurus*. Only the dorsal half of the anterior articular surface of the centrum of caudal vertebra B is preserved, and it too is concave (Fig. 15F); however, the depth of this concavity has been exaggerated by post mortem crushing based on the fractured left lateral margin. The posterior articular surface of caudal vertebra A is more strongly concave than the anterior articular surface (Fig. 15D). This morphology is otherwise primarily known in the anterior–middle caudal centra of a number of East Asian somphospondylans, including euhelopodids and *Huabeisaurus* (D'Emic et al., 2013; Poropat et al., 2016), although it is also variably present in *Wintonotitan* (Poropat et al., 2015a). The posterior articular surface of the centrum of caudal vertebra B is more shallowly concave than the anterior articular surface; however, the aforementioned post mortem crushing to which this centrum was subjected might have impacted this. The lateral margins of the anterior and posterior articular surfaces of both anterior caudal vertebrae are broadly convex. In both anterior caudal vertebrae, the dorsal margin of the anterior articular surface is flat, whereas that of the posterior articular surface is broadly convex. When complete, the anterior and posterior articular surfaces of both anterior caudal vertebrae would have been wider transversely than they were tall dorsoventrally.

The preserved left lateral surfaces each bear a transverse process. In caudal vertebra A, only the base of the transverse process is present (Fig. 15C); although broken, it clearly extended from the base of the neural arch (immediately posteroventral to the prezygapophysis) to the dorsal one-third of the centrum. The anterior surface of the transverse process is concave, whereas the posterior one is convex. The base of the transverse process tapers ventrally, and when complete it presumably would have projected posterolaterally. In caudal vertebra B, the left transverse process is complete, and projects laterally before sweeping posteriorly (Fig. 15G). The ventral surface of the base of the transverse process is mediolaterally concave and anteroposteriorly convex, and tapers to a

ridge both anteriorly (possibly representing a vestigial ACPL or ACDL) and posteriorly (possibly representing a vestigial PCPL or PCDL). Another ridge separates the ventral surface of the transverse process from the ventrolateral surface, which is mediolaterally concave and forms a somewhat compressed parallelogram; the acute corners are located anteroventrally and posterodorsally, whereas the obtuse corners are positioned anterodorsally and posteroventrally (Fig. 15H). A thin ridge separates the ventrolateral surface from the dorsal surface, which is mostly anteroposteriorly convex but slightly flattened laterally and slightly concave anteriorly. A mild bulge on the anterodorsal margin of the transverse process (Fig. 15I), nearer the centrum than the lateral tip, is similar to that observed in an array of eusauropods (Kellner et al., 2005; D'Emic et al., 2013; Poropat et al., 2016; Mannion et al., 2019b). It is usually only prominent in the anteriormost caudal vertebrae. Although the transverse process curves strongly posterolaterally, it does not extend beyond the posterior margin of the centrum (Fig. 15G).

Immediately ventral to the base of the transverse process in each anterior caudal centrum, the lateral surface is strongly concave, with the maximum depth of this pneumatic concavity in line with the posterolateral projection of the transverse process and the margin gradational with the rest of the centrum, rather than being sharp-lipped. The presence of lateral pneumatic fossae distinguishes the anterior caudal centra of *Savannasaurus* from those of most somphospondylans, which tend to lack them (Mannion et al., 2013), although the non-titanosaurian somphospondylan *Padillasaurus* possesses similar blind fossae (Carballido et al., 2015). In both anterior caudal vertebrae, a small foramen is set within the pneumatic fossa (Fig. 15C, H). Similar structures are present in the non-titanosaurian somphospondylan *Chubutisaurus* (MACN 18222: S.F.P., pers. obs. 2018); by contrast, titanosaurs tend to possess foramina only, *Gobititan* has small, shallow excavations, and brachiosaurids lack foramina but possess fossae (D'Emic, 2012; Mannion et al., 2013).

The prezygapophyses of caudal vertebra B are almost complete, whereas those of caudal vertebra A are represented only by their ventral bases. The lateral margin of the prezygapophysis in each anterior caudal vertebra is contiguous with the dorsal margin of the transverse process. In caudal vertebra B, the prezygapophyses project 62 mm anterodorsally from the dorsal margin of the articular surface (Fig. 15H, J), and their posteromedial margins are 32 mm apart. The flattened articular surfaces face dorsomedially and are anteroposteriorly longer (61 mm) than they are mediolaterally broad (39 mm). The ventral surfaces of the prezygapophyses are strongly and smoothly mediolaterally convex.

Both postzygapophyseal articular facets are preserved in each anterior caudal vertebra, and their concave surfaces face mostly laterally and slightly ventrally. CPOLs are not present. In caudal vertebra A, the ventromedial margins of the postzygapophyses meet on the midline; by contrast, in caudal vertebra B they are connected by a TPOL (17 mm wide transversely × 50 mm long anteroposteriorly; Fig. 15I). In both caudal vertebrae, a narrow yet deep SPOF is present between the postzygapophyses. In caudal vertebra A, the postzygapophyses project posteriorly beyond the level of the posterior articular surface of the centrum, whereas in caudal vertebra B the posterior margins of the postzygapophyses and the centrum are approximately level. There is no gap between the junction of the bases of the postzygapophyses and the dorsal margin of the neural spine. As is the case in the anterior caudal vertebrae of most derived somphospondylans (Mannion et al., 2013), there is no hyposphene.

The neural spine of caudal vertebra A is incomplete and poorly preserved; all that can be stated about it with certainty is that its base was transversely wider than anteroposteriorly long (Fig. 15B). By contrast, the neural spine of caudal vertebra B is complete, and forms the basis for the following description. The neural spine projects mostly vertically and slightly posteriorly (Fig. 15H, J), and becomes slightly thickened transversely towards its apex (Fig.

15F, I). A thick PRSL is present on the anterior surface, flanked on either side by what appears to be a rudimentary SPRL. The posterior surface shows a similar morphology to the anterior one, with a thickened POSL projecting dorsally from near the floor of the SPOF, flanked on either side by a poorly developed SPOL. The lateral surfaces are essentially flat, and the dorsal surface is smoothly convex anteroposteriorly and transversely.

Distal Anterior Caudal Vertebrae—The two preserved distal anterior caudal vertebrae are herein designated caudal vertebra C and D (Fig. 15K–S). Each is represented by an incomplete centrum, solidly sutured with the ventralmost vestige of the neural arch. The internal texture of both centra is cancellous. The centrum of caudal vertebra C is amphicoelous, with the posterior articular surface more deeply concave than the anterior one. Within both concavities (Fig. 15K, N), a small bulge is present centrally, slightly above the mid-height; a similar feature has also been described in *Tastavinsaurus sanzi* (Canudo et al., 2008). The posterior articular surface of the centrum is not preserved in caudal vertebra D; however, the anterior articular surface is shallowly concave. Both caudal vertebrae C and D are approximately the same length as caudal vertebra B, implying that the anteroposterior length of the distal anterior caudal vertebrae did not vary greatly along the series. This is further implied by differences in the proportions of the centra: in caudal vertebra C, both articular surfaces are transversely broader than they are dorsoventrally tall, whereas in caudal vertebra D the anterior articular surface is substantially taller dorsoventrally than it is wider transversely. This proportional disparity indicates that these two vertebrae were situated some distance from one another in the caudal series (with caudal vertebra C situated more anteriorly), and that the relative proportions of the caudal centra changed along the length of the tail.

The posterior end of the ventral surface of caudal vertebra C bears chevron facets. Otherwise, this surface is smooth, shallowly concave anteroposteriorly (Fig. 15O), and

separated from each lateral surface by a ventrolateral ridge. This ridge is well preserved on the left side of the centrum (Fig. 15L), but is not evident on the right side (Fig. 15P), which is more heavily eroded despite being otherwise more complete. The right lateral surface of caudal vertebra C potentially preserves evidence of a pneumatic fossa, although erosion appears to have exaggerated the depth and size of this feature (Fig. 15P). The right lateral surface of the centrum of caudal vertebra D is almost complete (Fig. 15R), and preserves a very small fossa immediately dorsal to an anteroposteriorly oriented lateral ridge, which sits two-thirds of the way up from the ventral margin. Dorsal and ventral to this ridge, the lateral surface of the centrum of caudal vertebra D is shallowly concave. No indication of the transverse process has been identified on either side of caudal vertebra C, although this is probably because of non-preservation rather than genuine absence. By contrast, a very subtle bulge is present at the base of the right neural arch on caudal vertebra D, which possibly represents a reduced transverse process; if correct, then it is likely that a better developed transverse process was present in caudal vertebra C as well.

Part of the neural canal is preserved on the dorsal surface of caudal vertebrae C (Fig. 15M) and D (Fig. 15Q), flanked on either side by the base of the neural arch. In both vertebrae, these neural arch pedicels are two-thirds the length of the centrum and are positioned anterior to the mid-length of the centrum, as in all members of Titanosauriformes (Salgado et al., 1997).

Coracoid

The coracoid of *Savannasaurus* (Fig. 16; Table S3) is described as if the long axis of the scapulocoracoid were held horizontally. The coracoid is taller dorsoventrally than long anteroposteriorly, and is ovate in lateral (Fig. 16A) and medial (Fig. 16D) views, with a

broadly curved ventral margin and a more acutely curved dorsal margin. Thus, *Savannasaurus* lacks the quadrangular coracoid characteristic of saltasaurids (Salgado et al., 1997; Upchurch, 1998). Of all the margins of the coracoid, the dorsal one is mediolaterally thinnest (Fig. 16C). The anterior margin of the coracoid varies greatly in mediolateral thickness (Fig. 16F), from ~10 mm dorsally to 65 mm ventrally, whereas the glenoid region is the mediolaterally broadest part (Fig. 16E). The glenoid fossa is surrounded by a subtle ridge. Its articular surface is slightly bevelled, such that it is visible in lateral view. In this regard, *Savannasaurus* differs from several derived titanosaurs (Poropat et al., 2016), such as *Lirainosaurus* (Díez Díaz et al., 2013), saltasaurines (Powell, 1992, 2003; Otero, 2010), and some members of Colossosauria (González Riga et al., 2018, 2019), in which there is little lateral expansion of the glenoid. The glenoid fossa is significantly broader in both anteroposterior and transverse dimensions (Table S3) than that of *Diamantinasaurus* (Poropat et al., 2015b). There is a notch anterior to the glenoid in *Savannasaurus*, but whether or not an infraglenoid lip was present is unclear. Despite the fact that the articulation point for the sternal plate is incompletely preserved, it is presumed that very little of it is missing based on its curvature.

In posterior view (Fig. 16B), the scapular articulation is sub-triangular (narrowing dorsally), whereas it is essentially straight in lateral (Fig. 16A) and medial (Fig. 16D) views. The scapular articular surface is slightly taller dorsoventrally than the coracoid as a whole is long anteroposteriorly; this is uncommon among titanosauriforms (Wilson, 2002; Mannion et al., 2013), but is observed in the early-diverging somphospondylans *Daxiatitan* (You et al., 2008), *Ligabuesaurus* (Bonaparte et al., 2006), and *Sauroposeidon* (Rose, 2007). Immediately anterior to the scapular articular surface lies the oval-shaped coracoid foramen, the long axis of which runs anteroposteriorly. The posterior third of the coracoid, which hosts

the coracoid foramen, is medially convex and correspondingly laterally concave; by contrast, the anterior two-thirds are medially concave and laterally convex (Fig. 16C).

Sternal Plate

The sternal plates were found adjacent to one another, and were associated with the left coracoid. The left element is the more complete and better preserved of the pair (Fig. 17; Table S4), and the description herein is based exclusively on it. It was incorrectly labelled as the right sternal plate in Poropat et al. (2016: fig. 4j). The transverse width of the paired sternal plates would have been approximately 850 mm; this corresponds well with the dimensions of the sacrum and pelvis of *Savannasaurus*, and supports a wide-gauge stance for this sauropod. The ratio of the maximum length of the sternal plate to proximodistal length of the (incompletely preserved) humerus was somewhat less than 0.71 in *Savannasaurus*, but almost certainly exceeded 0.65, as in most other titanosaurs (McIntosh, 1990; Upchurch, 1998; Mannion et al., 2013). The sternal plate is D-shaped in ventral view (Fig. 17A), with the lateral margin straight and all others convex. This distinguishes the sternal plate of *Savannasaurus* from those of most titanosauriforms, which have concave lateral margins (such that the overall morphology is kidney-shaped in most titanosaurs (McIntosh, 1990; Upchurch, 1998)), and constitutes a local autapomorphy of *Savannasaurus*. The medial two-thirds of the ventral surface are mediolaterally convex, whereas the lateral third (marked with a dashed line in Fig. 17A) is concave. The coracoid articulation forms a thickened process at the anterolateral margin of the sternal plate. The dorsoventral thickness of the anterior margin decreases medially. Much of the coracoid articulation surface is roughened by grooves and pits that would have supported a cartilaginous cap. However, the ventral surface of the sternal plate lacks similar furrows or ridges, both medially and posteriorly. There is also no

anteroposteriorly elongate ridge along the anterior portion of the ventral surface, contrasting with most neosauropods (Sanz et al., 1999; Upchurch et al., 2004), and representing a local autapomorphy of *Savannasaurus* within Neosauropoda (Mannion et al., 2019b). The coracoid articulation merges smoothly with the external surface both medially and ventrally, although the intersection of these two surfaces forms a ventromedially–dorsolaterally oriented ridge. Although the lateral margin of the sternal plate is exceptionally thin, the posterolateral corner is thickened — presumably to accommodate cartilaginous extensions from the anterior dorsal/sternal ribs or to provide support to the bony gastralia (if they were present; Tschopp and Mateus, 2013). Further evidence for cartilaginous attachment can be seen in the grooves and ridges that occur along the posterior half of the lateral margin and the posterior margin (even medially, where it is extremely thin). In dorsal and ventral views, the posterior margin is convex, differing from the straight margin that characterises some titanosaurs, including *Alamosaurus*, *Malawisaurus*, and *Mendozasaurus* (González Riga, 2003; González Riga et al., 2009). The medial margin appears to have been thicker than the lateral margin (presumably for articulation with the other sternal plate), and was clearly convex, despite having sustained some damage. The dorsal surface is almost entirely shallowly convex, with the exception of the anterolateral and posterolateral regions, which are shallowly concave (Fig. 17B). Based on the lack of correspondence between the undulations of the ventral and dorsal surfaces, it is clear that the sternal plate thickened towards its centre.

Humerus

Both humeri are incomplete; the description herein is based primarily on the more complete right humerus (Fig. 18; Table S5). Although neither the proximal nor distal end is preserved (Fig. 18A), it is clear that the humerus of *Savannasaurus* was robust (*sensu* Wilson

& Upchurch, 2003), as in *Diamantinasaurus* (Hocknull et al., 2009; Poropat et al., 2015b), *Opisthocoelicaudia* (Borsuk-Białynicka, 1977), and saltasaurines (Powell, 1992, 2003; Salgado et al., 2005; Otero, 2010). Based only on the preserved portions of the proximal and distal ends, the Robusticity Index (Wilson and Upchurch, 2003) of this element was 0.31. Evidently, the base of the deltopectoral crest did not extend as far as the mid-length of the shaft (Fig. 18B–C); this differentiates *Savannasaurus* from some titanosaurs (Curry Rogers, 2005), such as *Neuquensaurus* (Salgado et al., 2005; Otero, 2010). The proximal half of the posterior surface is shallowly convex mediolaterally, with the apex of this convexity running approximately centrally down the shaft until it merges with a similarly subtle convexity much nearer the medial margin than the lateral one (Fig. 18A). Although the posterior surface is too poorly preserved to enable the identification of the attachment points of the triceps, towards the proximal end it becomes distinctly roughened. A similarly distinct rugose patch on the posterolateral surface, at about the same level as the distal extent of the deltopectoral crest, represents the point of attachment of the M. latissimus dorsi. Unlike several derived titanosaurs, including saltasaurids (Borsuk-Białynicka, 1977; Otero, 2010), this does not form a prominent process. In anterior view, the lateral margin of the shaft is straight. The posterior and anterior surfaces of the humerus are separated by subtle ridges at the mid-shaft: the lateral ridge is more sharply defined than the medial one. On the posterior surface, the mid-shaft is smoothly convex mediolaterally; further distally, the dorsal margin of what was clearly a deep supracondylar fossa is present between the preserved portions of the distal condyles. As preserved, the medial condyle is angular, with a distinct corner between a posteriorly facing, shallowly concave surface and a posteromedially facing, shallowly convex–flat surface. By contrast, the preserved base of the lateral condyle is smoothly convex. Evidently, the distal end was trampled prior to fossilisation; extensive disintegration of the internal bone is evident.

Radius

The left radius (Fig. 19; Table S5) was found with its anterior surface contacting the ventral surface of the left sternal plate. Although it is essentially complete, only the posterior surface and the proximal and distal ends are well preserved. The radius of *Savannasaurus* is 0.75 times the length of the incomplete humerus, but whether or not the ratio was 0.65 or less when the humerus was complete (as in most titanosauriforms (Mannion et al., 2013)) cannot be ascertained. The anteroposterior lengths of the proximal and distal ends are almost equal. The long axes of the proximal and distal ends are not oriented in the same plane; thus, the radius shows a distinct axial twist, as in *Huabeisaurus* (D'Emic et al., 2013) and a small number of titanosaurs, including *Epachthosaurus* and *Rapetosaurus* (Mannion et al., 2013; Poropat et al., 2016). The proximal surface of the radius (Fig. 19B) is broadly wedge-shaped, as in most titanosauriforms (Upchurch et al., 2015). It is also essentially flat, and covered with grooves and ridges that would have supported a cartilaginous cap. The maximum diameter of the proximal end of the radius is 0.33 times the overall proximodistal length of the radius, similar to most titanosaurs (Upchurch et al., 2004). The anteromedial surface is convex and forms the external surface of the wedge, whereas the concave posteromedial surface and straight posterolateral surface meet at the posterior apex of the wedge. The preserved portion of the medial surface is strongly convex anteroposteriorly, but is incomplete in the region in which the ridge for the insertion of the tendon from the combined M. biceps brachii and M. brachialis inferior would be expected (Upchurch et al., 2015). The preserved proximal portion of the lateral surface of the shaft is anteroposteriorly concave between two ridges that parallel the long axis of the shaft. This concave surface appears to have become convex at the mid-shaft and continues to the distal end; it is separated from the posterior surface by a strong interosseous ridge, which extends almost three-quarters of the

way down the shaft, as in most titanosaurs (Curry Rogers, 2005). The posterior surface of the radius is essentially flat at the proximal end, but becomes proximodistally concave from one-fifth the length of the shaft to the distal end (Fig. 19A). A marked extension of this concavity is present at the distal end, forming the articulation point for the ulna. Medial to this concavity, a slight protuberance is present that extends towards the medial margin. Little else can be ascertained about the morphology of the radial shaft because of its poor preservation. The distal end of the radius (Fig. 19C) has an essentially straight anterior margin, a broadly convex medial surface, a more acutely convex lateral margin, and an undulating posterior surface. Only the lateral half of the distal end is bevelled proximolaterally relative to the long axis of the shaft (distinguishing *Savannasaurus* from saltasaurines, wherein the entire distal end is bevelled (Poropat et al., 2016)); although the angle of bevelling appears to be relatively low (10°), the true degree of bevelling might have been affected by deformation of the element. The transverse diameter of the distal end is ~1.7 times that of the radius at the mid-shaft; this differs from many somphospondylans, in which this ratio is closer to 2.0 (Wilson and Sereno, 1998; Mannion et al., 2013). The lateral half of the posterior margin is strongly concave, whereas the medial half is strongly convex. Consequently, the medial half of the distal end is almost twice as wide anteroposteriorly as the lateral half.

Metacarpals

Poropat et al. (2016: p. 3) reported that right metacarpals I–V and left metacarpal IV were present in the holotype specimen of *Savannasaurus*; however, the preserved metacarpals are in fact left I–V (Fig. 20A–AF) and right IV (Fig. 20AG–AK). The described metacarpals and phalanges of *Diamantinasaurus*, although correctly placed within the manus by Hocknull et al. (2009) and Poropat et al. (2015b), are all from the left side as well; this was revealed when

the associated right manus of the *Diamantinasaurus* type individual was prepared. The metacarpals of *Savannasaurus* were arranged in a horseshoe shape when observed in proximal (Fig. 20A) and distal views (Fig. 20B), as in all neosauropods (Upchurch, 1998; Wilson and Sereno, 1998). Description of the elements *in vivo* (i.e. in articulation) has the potential to cause confusion (see Mannion and Otero, 2012); consequently, here they are all described with their internal (palmar) surfaces facing posteriorly. In life, the external surfaces of the metacarpals would have faced in the following directions: I, posteromedially; II, anteromedially; III, anteriorly; IV, anterolaterally; and V, posterolaterally.

The proximodistal lengths of the metacarpals of *Savannasaurus* vary (Table S6). From longest to shortest, the metacarpals of *Savannasaurus* are III-II-I-IV-V, as in both *Diamantinasaurus* (Poropat et al., 2015b) and *Wintonotitan* (Poropat et al., 2015a). Given that metacarpal I is incomplete, it is probable that its proximodistal length has been underestimated. However, it is clear that it was shorter than metacarpal II, differentiating *Savannasaurus* from those titanosaurs in which metacarpal I is longest (e.g. *Epachthosaurus* (Martínez et al., 2004), *Alamosaurus* (Gilmore, 1946), and *Opisthocoelicaudia* (Borsuk-Białynicka, 1977)). Although metacarpal IV is shorter than I in most titanosaurs (including *Savannasaurus*), *Aeolosaurus* (Powell, 2003) and *Rapetosaurus* (Curry Rogers, 2009) are exceptions. The variation in length of the metacarpals in *Savannasaurus* implies that they would have been tightly bound proximally and splayed distally, such that each was inclined relative to the vertical. The flattened proximal surface produced by the articulated metacarpus suggests that no ossified carpal elements were present, as in nearly all titanosaurs (e.g. *Epachthosaurus* (Martínez et al., 2004), *Diamantinasaurus* (Poropat et al., 2015b), *Alamosaurus* (Gilmore, 1946), *Opisthocoelicaudia* (Borsuk-Białynicka, 1977; D'Emic, 2012)). The proximodistal length of the longest metacarpal (III) is 0.49 times that of the radius; thus, this ratio exceeds 0.45, as in most macronarians (McIntosh, 1990; Upchurch,

1998; Wilson and Sereno, 1998; Upchurch et al., 2004), although this is at the low end of the spectrum amongst titanosaurs, with ratios exceeding 0.6 in some taxa (Mannion and Otero, 2012; Poropat et al., 2015a). The distal articular surfaces of the metacarpals do not extend on to the anterior surfaces, as is also the case in most titanosaurs (Salgado et al., 1997; D'Emic, 2012), other than *Alamosaurus* (Gilmore, 1946) and *Diamantinasaurus* (Poropat et al., 2015b). This is unusual, given that at least some manual digits possessed phalanges in *Savannasaurus* (see below).

Metacarpal I—The left metacarpal I is almost complete (Fig. 20C–H), missing only a section of the lateral margin of the shaft and a portion of the proximal end. However, it appears to have suffered from significant post mortem distortion, such that the mid-shaft is significantly shorter anteroposteriorly than it would have been in life. The distal end of metacarpal I was found in contact with the proximal end of left metacarpal II. The incompletely preserved proximal surface is horseshoe-shaped (Fig. 20F) and, when viewed posteriorly (Fig. 20G), it is distinctly stepped, with the medial half slightly taller than the lateral. As in both *Wintonotitan* (Poropat et al., 2015a) and *Diamantinasaurus* (Poropat et al., 2015b), the proximal end is longer anteroposteriorly than it is wide mediolaterally; however, this feature might have been exaggerated by deformation, and is in any case highly variable among neosauropods (Apesteguía, 2005; Mannion and Calvo, 2011). The posterolateral surface of the proximal end of metacarpal I is distinctly concave, whereas the other margins are all convex; this gives the proximal end its distinctive horseshoe-shape. The proximal articular surface for metacarpal II is located posterolaterally, whereas the distal one is situated laterally. The anterior surface of the shaft is strongly convex mediolaterally at the proximal end, and weakly so at the distal end, terminating as a distal lip (Fig. 20C). A strong lateral ridge marks the junction of the anterior and posterior surfaces, and is most prominent at mid-shaft (Fig. 20E). Proximal to the mid-shaft, the posterior surface is strongly concave between

the prominently expressed lateral ridge and the less developed medial ridge (Fig. 20G). This concavity might have been exaggerated by post mortem deformation, but appears to be a genuine morphological feature. Distal to mid-shaft, the posterior surface is essentially flat, but becomes slightly concave again at the distal end. The posterior surface forms a distal lip, albeit less prominently expressed than the anterior distal lip. The medial surface of metacarpal I is incompletely preserved (Fig. 20H), although it was clearly less strongly convex than the lateral surface. The distal end of metacarpal I is blocky, massive, and broadly parallelogram-shaped (Fig. 20D). The grooves and bulges on the distal end would have supported a cartilaginous cap. The distal articular surface is undivided and slopes relative to the shaft, such that it is visible in anterior view and forms a pronounced rim. It is likely that this feature has been exaggerated by post mortem deformation, since in most titanosauriforms the distal end of metacarpal I lies perpendicular to the long axis of the shaft (Wilson, 2002). In *Savannasaurus*, the surface area of the distal end of metacarpal I is greater than that of any of the other metacarpals (Fig. 20B); although this was almost certainly the case in life, the degree to which this has been exaggerated by post mortem deformation is unclear.

Metacarpal II—Like metacarpal I, the left metacarpal II (Fig. 20I–N) was subjected to significant post mortem deformation — the proximal and distal ends have become flattened and expanded anteroposteriorly and mediolaterally, and the medial and lateral flare of the proximal end has been exaggerated (see Fig. 20K, N). The proximal end is wedge-shaped, with a flattened anterior margin, a shallowly convex medial margin, and a gently concave lateral margin (Fig. 20L). Posteriorly, the junction between the medial and lateral surfaces is rounded. The distal end is mediolaterally broader than the proximal end. The medial margin is effectively straight, whereas the lateral one is shallowly concave. The anterior surface is more or less flat along its length, although it becomes shallowly convex mediolaterally towards the distal end. The proximal articular surfaces for metacarpals I (on the medial

surface) and III (on the lateral surface) are shallowly convex, whereas the distal articular surfaces are shallowly concave. In both anterior and posterior views, the distal end is strongly concave (Fig. 20I, M); however, this might have been caused (or at least exaggerated) by post mortem deformation. In distal view, the metacarpal is weakly arched (Fig. 20J), with a convex anterior margin, a concave posterior margin, and generally straight medial and lateral margins.

Metacarpal III—The left metacarpal III of *Savannasaurus* (Fig. 20O–T), the longest of the metacarpals, is effectively complete, missing only a small portion of the proximal end. This metacarpal appears to have suffered relatively little post mortem deformation, except at the poorly preserved proximal end. In overall morphology, it is similar to the corresponding element in *Diamantinasaurus* (Poropat et al., 2015b). In proximal view (Fig. 20R), metacarpal III is triangular, with the margins facing anteriorly, posteromedially and posterolaterally and the corners pointing anteromedially, anterolaterally and posteriorly. The proximal end is not expanded mediolaterally relative to its anteroposterior length, distinguishing *Savannasaurus* from brachiosaurids (Mannion et al., 2017). In anterior view (Fig. 20O), the lateral margin is distinctly concave and bowed inwards, whereas the medial margin is only slightly concave; the same is true of metacarpal III in *Diamantinasaurus* (Poropat et al., 2015b). The anterior surface of metacarpal III is relatively flat at the proximal end, but very shallowly mediolaterally concave along the midline at the mid-shaft. This shallow depression is bound by lateral and medial ridges that extend distally towards the articular surface for the manual phalanx. The medial condyle is more strongly developed than its lateral counterpart, and the same is true of the ridges on each condyle. In lateral view (Fig. 20Q), the dorsal margin is dominated by a pronounced ridge that marks the union between the anterior and posterolateral surfaces. The posterolateral surface is markedly concave, with a slight bulge at three-quarters the length of the shaft; below this, the surface again becomes

shallowly concave. Both proximally and distally, articulation points for metacarpal IV are present. The proximal articulation is poorly preserved, but would have been convex; the distal articulation for metacarpal IV is far better preserved. In posterior view (Fig. 20S), metacarpal III is dominated by a ridge that is somewhat closer to the medial margin than the lateral one. This ridge extends from the proximal end to three-quarters of the length of the shaft, merging smoothly with the posterior surface of the medial condyle at the distal end. The posterior ridge is broadest at its proximal end, narrowing as it descends the shaft, and is flanked on both sides by concave surfaces. The posteromedial surface is incompletely preserved along the proximal third, although the more distal two-thirds demonstrate that this surface was less concave than the posterolateral one. In medial view, the anterior margin is defined by a medial ridge (Fig. 20T); like the posterior ridge, this medial ridge is strongly pronounced proximally and tapered distally. The medial surface of the distal condyle is essentially flat. In distal view (Fig. 20P), the metacarpal is wedge-shaped, as a result of the medial condyle being notably anteroposteriorly longer than the lateral one. Roughened pits and grooves again indicate the presence of a cartilaginous cap and, presumably, a manual phalanx on this digit.

Metacarpal IV—The left metacarpal IV is essentially complete, missing only a small section of the medial margin (Fig. 20U–Z). By contrast, only the proximal half of the right metacarpal IV is preserved (Fig. 20AG–AK); despite this, it is slightly less distorted than left metacarpal IV. In proximal view, the left (Fig. 20X) and right (Fig. 20AI) fourth metacarpals are virtually mirror images of one another, despite the distortion suffered by left metacarpal IV; however, the proximal surface of the right is much flatter than that of the left. Because it is more complete, left metacarpal IV will serve as the basis for much of the following description. Its proximal end is broad on its anterior margin but tapers to a point posteriorly (Fig. 20X). The medial and lateral margins are concave for articulation with metacarpals III

and V respectively. The concavity for metacarpal III is shallower but slightly more extensive than that for metacarpal V: the latter is exacerbated by an anterolateral projection that would have wrapped around the dorsal face of metacarpal V (Fig. 20A), similar to that present in the fourth metacarpals of brachiosaurids (D'Emic, 2012) and some somphospondylans (Mannion et al., 2013). The proximal two-thirds of metacarpal IV can be divided into three surfaces: anterior, posteromedial, and posterolateral. A true posterior surface is only present along the distal third of the shaft (see below). The anterior surface of metacarpal IV is shallowly proximodistally concave at the proximal end, and very shallowly mediolaterally convex along the distal three-quarters of the shaft (Fig. 20U). At the distal end, a concavity separates the paired, evenly developed distal condyles. In posterior view (Fig. 20Y), a ridge extends down the midline along the proximal three-quarters of the shaft. This ridge is strongly bulbous at the proximal end but decreases slightly in thickness as it descends the shaft. At its base, the posterior surface of the metacarpal is shallowly concave between the paired distal condyles. In posterior view, the lateral condyle is more strongly developed than the medial one. The posterolateral surface is incompletely preserved (Fig. 20W), although it is clear that the anterolateral ridge was more robust than the anteromedial one. The proximal portion of the posterolateral surface is concave to accommodate metacarpal V, although this concavity extends along the proximalmost three quarters of the shaft. The surface of the distal lateral condyle is incomplete, although a distinct posterolateral concavity is present for the articulation of metacarpal V. The posteromedial surface is proximally concave to accommodate metacarpal III (Fig. 20Z). This concavity, which is bordered by thin medial and posterior ridges, extends approximately two-thirds of the way down the shaft; distal to this, a second, shallower concavity is present, which is separated from the proximal concavity by a slightly convex region. This convex region occurs at the same level as that of the disappearance of the posterior ridge. In distal view, metacarpal IV is hourglass-shaped, with

the long axis of the hourglass running transversely (Fig. 20V), unlike the trapezoidal or hexagonal fourth metacarpal distal ends seen in most titanosaurs (Poropat et al., 2016); this feature is autapomorphic for *Savannasaurus*. The discrepancy between the medial and lateral condyles is most marked in this view: the lateral condyle is broader mediolaterally and longer anteroposteriorly than the medial one. The morphology of the distal end implies that a manual phalanx articulated with metacarpal IV. The distal surface is covered in roughened pits and bulges that presumably supported a cartilaginous pad.

Metacarpal V—The left metacarpal V is almost complete, missing only a small portion of the posterior ridge (Fig. 20AA–AF). The proximal end is roughly wedge-shaped, being broadly convex on its anterior margin, slightly concave on its medial margin, and gently convex on its lateral margin. Posteriorly, it tapers to a rounded point (Fig. 20AD). The anterior surface is slightly convex proximally, flattened at the mid-shaft, and slightly concave distally (Fig. 20AA). This distal concavity is flanked by medial and lateral ridges, which extend approximately three-quarters of the length of the shaft, but might have been exaggerated by post mortem distortion. The undulating proximal portion of the medial surface is convex near the posterior ridge but concave towards the medial one (Fig. 20AF). The medial ridge extends along the anterior margin and remains narrow for much of its length, becoming less strongly pronounced towards the distal end as it expands to form the surface of the distal medial condyle. Thus, *Savannasaurus* lacks the ridge present in this region in *Mendozasaurus*, *Muyelensaurus* and *Petrobrasaurus* (González Riga et al., 2018). In posterior view, metacarpal V is transversely narrow at the proximal end and expanded distally (Fig. 20AE). A strong ridge extends along the posterior surface from the proximal margin for approximately two-thirds the length of the shaft. The distal third of the posterior surface is convex towards the lateral margin and slightly concave towards the medial one; this undulation is caused by the lateral bulge, which is more strongly pronounced than the

medial one. In lateral view, metacarpal V bears a ridge: at the proximal end this structure is confluent with the anterior margin, whereas further distally it becomes more centrally placed (Fig. 20AC). Posterior to this ridge, the proximal half is slightly concave, becoming markedly convex distal to the mid-length as it merges with the posterior surface. In lateral view, the narrowest point of the metacarpal occurs just proximal to the distal end. In distal view, metacarpal V is essentially rectangular (Fig. 20AB), although it is slightly constricted along the midline because of the subtle division of the medial and lateral condyles. The grooves and ridges at the distal end (to which a cartilaginous cap would have adhered), and the presence of a slight midline concavity on the anterior margin, support the interpretation that this metacarpal would have articulated with a manual phalanx.

Manual Phalanges

At least two manual phalanges of *Savannasaurus* have been identified, although only one is sufficiently complete and well preserved to warrant description (Fig. 20AL–AQ; Table S7). That manual phalanges were present at all is significant, since titanosaurs were thought to have lacked them (Wilson, 2002; Upchurch et al., 2004); *Savannasaurus* and *Diamantinasaurus* are exceptions (Poropat et al., 2015b, 2016). Based on the morphology of the better-preserved element, the dimensions of its proximal end, and attempted articulations with the various preserved metacarpals, it is probably left manual phalanx II-1. In dorsal view (Fig. 20AL), the manual phalanx is semicircular, the proximal margin being only slightly convex. The dorsal surface of the phalanx is transversely convex and proximodistally slightly concave, rising towards the proximal margin. In medial (Fig. 20AM) and lateral (Fig. 20AP) views, the proximodistally concave nature of the dorsal margin is clear. The ventral surface (Fig. 20AN) is convex in lateral view (Fig. 20AP), and expands below the level of the

boundary between the dorsal and ventral surfaces. In proximal view (Fig. 20AQ), the phalanx tapers to lateral and medial points but is broadly oval in the mid-section. The dorsal margin of the proximal end is characterised by a bony rim, which would have abutted the ventral margin of metacarpal II; this suggests that the curved dorsal surface faced anterodorsally.

Pelvic Girdle

The paired pubes and ischia of *Savannasaurus* (Fig. 21; Table S8–9) have a combined transverse width in excess of 1.1 metres. Taken together, these four elements form an undulating sheet that attests to the transversely broad and dorsoventrally compressed lower pelvic region of *Savannasaurus*. The curvature of the lateral surfaces of the pubis and ischium (Fig. 21D) mirrors those of the medial surfaces (Fig. 21B). In most somphospondylans, the ischium is much shorter than the pubis (Calvo and Salgado, 1995; Salgado et al., 1997; Upchurch, 1998), with a proximodistal length ratio of less than 0.8 (Mannion et al., 2013). This ratio is very low (0.63) in *Savannasaurus* (one ischium of which is slightly more complete than shown in Fig. 21C), with most other taxa characterised by ratios exceeding 0.7 (Table S10); exceptions include *Rapetosaurus* (0.54: Curry Rogers, 2009) and *Opisthocoelicaudia* (0.64: Borsuk-Białynicka, 1977). The combined pubic and ischiadic acetabular rim in *Savannasaurus* is 520 mm long, measured along the curve (Fig. 21C).

Pubis—The paired pubes are almost completely fused along the midline, with the pubic symphysis manifesting as an irregular, dorsally raised ridge (Fig. 21E); however, a small, posteriorly situated triangular section (80 mm anteroposteriorly × 100 mm transversely) evidently remained unfused (Fig. 21B). Each pubis is also firmly fused with its corresponding ischium (Fig. 21B–D). The dorsoventral height of the ischiadic articulation is 0.56 times that

of the proximodistal length of the pubis — higher than in *Diamantinasaurus* (0.46) and most other titanosaurs (Salgado et al., 1997; Wilson and Sereno, 1998; Upchurch et al., 2004; Mannion et al., 2013; Poropat et al., 2015b). The proximal portions of both pubes are slightly incomplete, although based on the preserved margin of the acetabulum, very little of the right pubis is missing (Fig. 21E). As preserved, the incomplete iliac peduncle is almost three times longer anteroposteriorly than it is wide mediolaterally, although there is no guarantee that it was similarly proportioned at its summit. The iliac peduncle and the proximal portion of each pubis is oriented vertically. However, both pubes curve abruptly towards the midline, such that the long axes of their distal plates are parallel with each other. Consequently, the lateral surface of the distal plate of each pubis faces posteroventrally (Fig. 21D), whereas the medial surface faces anterodorsally (Fig. 21A). The lateral surface of each pubis is broadly divisible into three sections: the posterodorsal portion, including the obturator foramen (Fig. 21C); the anterodorsal portion, comprising the anterior margin; and the distal plate. The posterodorsal portion is dominated by the oval-shaped obturator foramen, which projects ventrolaterally–dorsomedially and is completely encircled by bone. The long axis of the lateral margin of the obturator foramen extends parallel to the long axis of the pubis. Laterally, the dorsal margin of the obturator foramen forms a thin, transversely compressed, dorsoventrally elongate lip; the same is true medially of its ventral margin. Anterior to the obturator foramen, the medial surface of the base of the iliac peduncle is anteroposteriorly convex; however, posteriorly — and immediately ventral to the obturator foramen — it becomes mediolaterally and anteroposteriorly concave. The anterior and posterior margins of the obturator foramen are mediolaterally narrow. Ventral to the obturator foramen, a single anteroventrally–posterodorsally inclined ridge is present, somewhat similar to the multiple grooves and ridges seen in *Diamantinasaurus* (Poropat et al., 2015b). The incompletely preserved anterodorsal portion of the lateral surface of the pubis is essentially flat anterior to the obturator foramen,

and is the mediolaterally broadest portion of the pubis. No ambiens process is present (based on a portion of the right pubis not included in Fig. 21). The lateral surface of the pubis lacks the anteriorly positioned ridge and groove seen in several advanced titanosaurs (Powell, 2003; Salgado and Carvalho, 2008; Otero, 2010; Poropat et al., 2016), including *Epachthosaurus* (Martínez et al., 2004). However, the anterodorsal portion of the pubis is separated from the distal plate by a subtle ventrolateral ridge (the external surface of which faces ventrally), which is an autapomorphy of *Savannasaurus* (Poropat et al., 2016). This ridge is approximately aligned with the ridge beneath the obturator foramen, and fades out before reaching the distal end of the pubis. Medial to this feature, the pubis is broadly dorsoventrally convex on its medial surface, becoming concave again towards the pubic symphysis. With the pubes oriented in vivo, the distal plate of each is markedly expanded mediolaterally and extremely compressed dorsoventrally (less than 20 mm thick on average, such that it is laminar as in most somphospondylans (Curry Rogers, 2005; Poropat et al., 2016). The anterior margin of the distal plate is strongly concave in lateral view, such that it forms a pubic 'boot' (Fig. 21C). The ventral surfaces of the distal plates are convex towards their lateral margins and shallowly mediolaterally concave towards the pubic symphysis; this concavity becomes increasingly pronounced towards the posteromedial margin. By contrast, the medial (anterodorsally-facing) surface of the distal plate is very slightly concave mediolaterally.

Ischium—The paired ischia were evidently fused along almost their entire length, as in most other titanosaurs (McIntosh, 1990; Upchurch, 1998; Wilson, 2002), with only a slight separation at the distal end (Fig. 21A–B). The pubic articulation is dorsoventrally taller than the proximal plate is anteroposteriorly long, as in most titanosauriforms (Salgado et al., 1997; Carballido et al., 2012; Mannion et al., 2019b). The long axis of the ischiadic shaft is approximately 60° to the horizontal in lateral view, as in most sauropods (Upchurch, 1995,

1998; Wilson and Sereno, 1998), and is inclined at approximately 90° relative to the acetabular line, as in most macronarians (Carballido et al., 2012; Mannion et al., 2019b), other than *Opisthocoelicaudia* (Borsuk-Białynicka, 1977) and *Isisaurus* (Jain and Bandyopadhyay, 1997). The iliac peduncle of each ischium is essentially complete and is convex on all faces except for the acetabular and medial margins. The mediolateral width of the iliac articular surface is less than half the anteroposterior length of the same (ratio = 0.47), contrasting with *Wintonotitan* (1.43: Poropat et al., 2015a) and *Diamantinasaurus* (0.80: Poropat et al., 2015b). In lateral view, the iliac peduncle is essentially straight. The ratio of the anteroposterior length of the iliac peduncle to that of the proximal plate is 0.32, significantly lower than that of most other sauropods (Wilson, 2002; D'Emic, 2012; Mannion et al., 2013), including *Wintonotitan* (0.63: Poropat et al., 2015a) and *Diamantinasaurus* (0.53: Poropat et al., 2015b), and indicating that the ischium in *Savannasaurus* contributed significantly to the acetabulum. The acetabular margin is well preserved in both ischia. It has an essentially uniform mediolateral thickness along its length, and is strongly concave in lateral view (as in titanosaurs generally (D'Emic, 2012)), tapering to a very thin, medially-projecting lip. Ventral to the acetabulum, the ischium is dorsoventrally convex on its lateral surface, and correspondingly dorsoventrally concave on its medial surface. The ratio of the anteroposterior length of the proximal plate to the proximodistal length of the ischium is 0.42, higher than in any other sauropod (Mannion et al., 2013), including *Wintonotitan* (0.36: Poropat et al., 2015a) and *Diamantinasaurus* (0.31: Poropat et al., 2015b); this possibly represents an autapomorphy of *Savannasaurus* (Table S10). The distinct ridge at the posterior margin of the ischium is thickest at mid-height, forming the point of attachment for *M. flexor tibialis internus 3* (Fig. 21C). This ridge projects further laterally than that of *Diamantinasaurus* (Poropat et al., 2015b), and less so than that of *Wintonotitan* (Poropat et al., 2015a), but is more robust anteroposteriorly in *Savannasaurus* than in either. As in most

titanosauriforms, there is no groove associated with this ridge in *Savannasaurus* (D'Emic, 2012; Poropat et al., 2016). Distally, the lateral surface of the ischium becomes anteroposteriorly (and somewhat dorsoventrally) concave between three landmarks: the proximal ventral convexity, the posterior ridge, and the anteromedialmost portion of the distal plate. The medial portion of each ischium is twisted such that the medial surface faces posterodorsally, and the lateral one faces anteroventrally. Consequently, the distal ends of the ischia are nearly coplanar, as in most macronarians (Upchurch, 1998; Wilson and Sereno, 1998). The mediolateral width of the distal end of the ischium is equal to almost exactly half the proximodistal length of the entire element (0.49); the only other sauropod with a similarly high value for this ratio (0.51) is *Diamantinasaurus* (Mannion et al., 2013; Poropat et al., 2015b). By contrast, the mediolateral width of the distal end of the ischium is only 1.26 times the minimum mediolateral width of the ischium as a whole, as in many titanosauriforms (1.1–1.7; Mannion et al., 2013), but not *Diamantinasaurus* (1.95: Poropat et al., 2015b).

Astragalus

The left astragalus of *Savannasaurus* is virtually complete (Fig. 22A–F; Table S11). It is unusual inasmuch as its proximodistal height is greater than either the mediolateral or anteroposterior diameters, as a result of the reduction of the medial process and the accentuation of the ascending process. Presuming that the astragalus has not suffered significant post mortem distortion, the extremely low mediolateral width to proximodistal height ratio (0.87) and the low mediolateral width to anteroposterior length ratio (0.98) are both autapomorphic for *Savannasaurus* (Poropat et al., 2016), since these values are substantially lower than those of all other titanosauriforms (Mannion et al., 2013). In proximal view (Fig. 22A), the astragalus is wedge-shaped, as in all neosauropods (Upchurch,

1998; Wilson and Sereno, 1998). The apex of the ascending process is positioned nearer to the posterior margin than the anterior one (Fig. 22C), which is typical of neosauropods (Wilson and Sereno, 1998; Wilson, 2002), and is closer to the lateral margin than the medial one (Fig. 22B, E). The tibial articular surface of the ascending process can be divided into three regions: a flat anterior surface; a concave medial surface; and a flat posterior surface. The anterior surface (Fig. 22E) is steeply inclined anterodistally and is reasonably smooth near its apex, whereas further distally it develops a series of ridges and grooves that are more elongate and shallower than those elsewhere. The concave medial surface (Fig. 22C) is separated from the anterior surface by a subtle anteromedial shelf. Although no paired foramina are visible on the medial surface, it is likely that they are present but are infilled with matrix. Both medial and posterior surfaces of the astragalus are covered in subtle ridges and shallow grooves, and they are separated from one another by a posteromedial ridge. In this regard, the astragalus of *Savannasaurus* differs from those of some derived titanosaurs (e.g. *Neuquensaurus*, *Opisthocoelicaudia*), in which the posterior fossa is undivided (Wilson, 2002). The posterior surface of the ascending process is essentially flat (Fig. 22B). The fibular articular facet, which is situated on the lateral side of the ascending process (Fig. 22F), is shallow and has its long axis oriented posteroventrally–anterodorsally. Unlike the other surfaces of the astragalus, the bone forming the fibular articular facet is smoothly concave. The laterally-directed ventral shelf that underlies the fibula in many neosauropods is absent (Wilson and Upchurch, 2009; Mannion et al., 2013), contrasting with *Diamantinasaurus* (Poropat et al., 2015b). In distal view (Fig. 22D), the astragalus is broadly rhomboidal. The distal surface is shallowly convex mediolaterally, and the medial margin is more tapered than the lateral one; both of these features are typical of neosauropods (Upchurch, 1998). The posterodistal process that is present in *Diamantinasaurus* (Poropat et al., 2015b) and many

other titanosauriforms (D'Emic, 2012; Mannion et al., 2013) could not be identified in *Savannasaurus*, although the position it would have occupied (if present) is damaged.

Metatarsal III

The right metatarsal III is essentially complete, missing only a small portion of bone along its dorsal surface (Fig. 22G–L; Table S12). In proximal view, it is wedge-shaped (Fig. 22G), with the convex medial and ventromedial margins merging smoothly into one another. The medial and ventromedial margins meet the straight dorsal and ventrolateral margins respectively at sharp angles, whereas the latter unite to form a dorsolateral point. The ventrolateral margin would have articulated with metatarsal IV, whereas the convex medial margin would have abutted against metatarsal II. The proximal surface is covered in ridges separated by deep grooves, implying the presence of a cartilaginous cap in life. The dorsal surface (Fig. 22H) is broadly concave proximodistally. This surface is transversely convex at the proximal end and along the distal third, but is flat in between. The lateral margin (Fig. 22I) is expressed as a twisted ridge that is thick at the proximal end (extending from the dorsolateral corner), narrows slightly towards the mid-shaft, and thickens again as it merges with the lateral condyle at the distal end. Ventral to this ridge, the proximal end is deeply concave. This concavity fades out at approximately the mid-length of the shaft, distal to which the ventral surface becomes flat to slightly convex as it approaches the distal condyles. The distalmost section of the ventral surface (Fig. 22K) is concave between the weakly developed (and slightly incomplete) medial condyle and the more strongly developed lateral condyle. The medial surface (Fig. 22L) is relatively well preserved, and is proximodistally concave when viewed dorsally or ventrally. A small, worn, triangular facet at the proximal end was presumably the articulation site for metatarsal II; distal to this, the proximal half of

the shaft is essentially flat and meets the dorsal and ventral surfaces at a 90° angle. The corner separating the dorsal and medial margins projects distoventrally–proximodorsally because of the distal expansion of the dorsal surface. The external bone at the mid-shaft of the medial surface is missing, although it is clear that the medial surface became dorsoventrally convex at or just distal to this point; it remains dorsoventrally convex along the entire distal half. The distal end is reniform (Fig. 22J), with the dorsal margin broadly convex and the ventral one shallowly concave between the distal condyles. The medial surface of the distal end is nearly flat, whereas the lateral surface tapers ventrolaterally to a rounded point.

DISCUSSION

The Phylogenetic Affinities of *Savannasaurus elliottorum*

Although *Savannasaurus* has been included in several phylogenetic analyses since its initial description (Poropat et al., 2016), all of which ultimately derive from that of Mannion et al. (2013), its precise position within Somphospondyli remains uncertain. In several analyses it has been resolved as a non-lithostrotian titanosaur, specifically as the sister taxon to the clade comprising the *Diamantinasaurus matildae* holotype (AODF 603) and referred (AODF 836) specimens (Royo-Torres et al., 2017; Averianov and Efimov, 2018; González Riga et al., 2018; Mocho et al., 2019a, b); note that in Mannion et al. (2017), the resolved topology was the same, but incorrectly depicted as *Diamantinasaurus* + (*Savannasaurus* +AODF 836). However, in one of these analyses (Royo-Torres et al., 2017), the exclusion of three taxa changed the topology such that *Savannasaurus* was situated at the base of a grade

comprising *Diamantinasaurus*, AODF 836, and *Baotianmansaurus* + *Dongyangosaurus*. Although *Savannasaurus* and *Baotianmansaurus* do share several features (e.g., absence of PRSL throughout dorsal vertebral series; presence of aSPDL and pSPDL in some middle dorsal vertebrae; absence of TPOL in middle dorsal vertebrae; amphicoelous caudal centra), there are other features that separate them (Zhang et al., 2009; 41H III-0200: PDM and PU pers. obs. 2012). These include the morphology of the anterior dorsal neural spines (bifid in *Baotianmansaurus*, undivided in *Savannasaurus*), number of PCPLs per side on the dorsal vertebrae (one in *Baotianmansaurus*, one or two in *Savannasaurus*), the inclination of the dorsal transverse processes (inclined dorsolaterally in *Baotianmansaurus*, essentially horizontal in *Savannasaurus*), and the presence/absence of hyposphene–hypantrum articulations in the dorsal vertebrae (present in anterior–middle dorsal vertebrae but not in the middle–posterior dorsal vertebrae of *Baotianmansaurus*, absent throughout the dorsal series in *Savannasaurus*). Similarly, there are several features that are shared between *Dongyangosaurus* and *Savannasaurus* (e.g. lack of ridges or excavations on ventral surfaces of dorsal centra; amphicoelous caudal centra; no ridge on lateral surface of pubic shaft). However, there are many other features that distinguish them: PODLs are present throughout the dorsal series of *Dongyangosaurus* but are only present in dorsal vertebrae VII–X of *Savannasaurus*; the dorsal neural spines of *Dongyangosaurus* are bifid, whereas those of *Savannasaurus* are not; and the anterior caudal centra of *Dongyangosaurus* lack the lateral excavations seen in (Lü et al., 2008; Mannion et al., 2019a).

In another analysis (González Riga et al., 2019), the removal of eleven taxa (including AODF 836) and the addition of three characters caused *Savannasaurus* to fall out in a polytomy with *Dongyangosaurus*, *Baotianmansaurus*, and all titanosaurs more derived than *Andesaurus* + *Ruyangosaurus*, whereas *Diamantinasaurus* was resolved as the sister taxon to Lithostrotia. Another recent analysis (Silva Junior et al., 2019), which was based on that of

González Riga et al. (2018) but excluded all non-titanosauriform taxa, resolved *Savannasaurus* as a non-titanosaurian somphospondylan, whereas *Diamantinasaurus* was placed within Saltasauridae, as the sister taxon to AODF 836 + *Baotianmansaurus*. However, it is worth noting that this analysis also produced some unusual results that have not been recovered before, including the placement of *Epachthosaurus* and Colossosauria outside Titanosauria. Finally, in recent analyses of two slightly different, updated versions of the same matrix, *Savannasaurus* has been resolved within Saltasauridae as the sister taxon to AODF 836 + *Diamantinasaurus* when equal weights were used (Mannion et al., 2019a, b). However, when the analysis was run under extended implied weights, *Savannasaurus* was resolved outside Lithostrotia (Mannion et al., 2019a).

As outlined above, *Savannasaurus* presents several anatomical features that argue against a placement within Saltasaurinae or Saltasauridae: cervical vertebrae with anteroposteriorly short parapophyses; dorsal vertebrae with deep pneumatic foramina; caudal vertebral centra not pneumatised; coracoid rounded; humerus lacks strong tuberosity for *M. latissimus dorsi*; radius distal end partially bevelled. Similarly, numerous features seem to set *Savannasaurus* apart from Lithostrotia, and from 'classic' members of Titanosauria as a whole: posterior dorsal vertebrae with horizontal TPRLs; middle sacral vertebral centra not constricted; caudal centra amphicoelous; anterior caudal vertebrae with pneumatic fossae; sternal plate D-shaped; manual phalanges present; pubis without lateral ridge. Nevertheless, in some respects *Savannasaurus* is similar to saltasaurids (e.g. humerus robust; ischium very short relative to pubis) and titanosaurs more generally (e.g. sternal plate elongate relative to humerus; ossified carpals absent; metacarpal distal articular surfaces non-extensive).

One feature shared by *Savannasaurus* and *Diamantinasaurus*, that links them with 'classic' titanosaurs and some basal somphospondylans, while simultaneously distinguishing them from brachiosaurids, euhelopodids and other basal somphospondylans, is the absence of

hyposphene–hypantrum articulations throughout the dorsal and caudal vertebral series. Most basal titanosauriforms, including brachiosaurids, euhelopodids, and some basal somphospondylans, possess hyposphene–hypantrum articulations in their middle–posterior dorsal vertebrae (Apesteguía, 2005). However, they are absent in the early-branching somphospondylan *Jiangshanosaurus* (Mannion et al., 2019a), and in many, but not all, titanosaurs (Salgado et al., 1997; Apesteguía, 2005). Some of the few titanosaurs that possess hyposphene–hypantrum articulations in (at least some of) their middle–posterior dorsal vertebrae are *Andesaurus* (Mannion and Calvo, 2011) — the sister taxon to all other titanosaurs by definition — and *Epachthosaurus* (Martínez et al., 2004). The lognkosaurian titanosaur *Patagotitan* has a hyposphene on dorsal vertebra III (and is presumed to have had a corresponding hypantrum on dorsal vertebra IV), and might have had a hyposphene on dorsal vertebra VI (MPEF-PV 3400: S.F.P., pers. obs. 2018); however, it lacks hyposphenes–hypantra throughout the rest of its dorsal series (Carballido et al., 2017). Although the prezygapophyses of at least one dorsal vertebra of *Argentinosaurus* appear to have hypantral articular facets (Bonaparte and Coria, 1993), there is no corresponding hyposphene on any of them, suggesting that this 'hypantrum' is an independently derived structure (Salgado et al., 1997; Apesteguía, 2005). Given that hyposphene–hypantrum articulations are present in brachiosaurids, euhelopodids, many (but not all) non-titanosaurian somphospondylans, some early-branching titanosaurs, and at least one lognkosaurian, the absence of these structures in *Savannasaurus* and *Diamantinasaurus* could be used to support a relatively derived position within Titanosauria. However, it is also possible that hyposphene–hypantrum articulations were independently lost or acquired multiple times within Titanosauria, since (for example) *Epachthosaurus*, which has prominent hyposphene–hypantrum articulations, shows more features aligned with 'classic' members of Titanosauria (e.g. strongly procoelous caudal vertebrae) than *Savannasaurus* and *Diamantinasaurus*. The absence of hyposphene–

hypantrum articulations in *Savannasaurus* and *Diamantinasaurus*, in tandem with numerous characters that are plesiomorphic for Titanosauria, might support the notion that they occupy an earlier-branching position within Titanosauria than *Epachthosaurus*, as resolved in many, but not all, recent phylogenetic analyses (Mannion et al., 2017, 2019a, 2019b; González Riga et al., 2018).

The anterior caudal vertebrae of *Savannasaurus* also lack hyposphene–hypantrum articulations. This feature distinguishes *Savannasaurus* from brachiosaurids and euhelopodids, which tend to have narrow hyposphenal ridges on their caudal vertebrae (Mannion et al., 2013), and from *Astrophocaudia* (D'Emic, 2013), which has prominent, triangular hyposphenes on its caudal vertebrae. Among titanosaurs, hyposphenes are present in at least some caudal vertebrae of very few taxa; these include *Volgatitan* (Averianov and Efimov, 2018), *Epachthosaurus* (Martínez et al., 2004), *Malawisaurus* (Gomani, 2005) and *Opisthocoelicaudia* (Borsuk-Białynicka, 1977). Thus, the absence of hyposphene–hypantrum articulations in the caudal vertebrae of *Savannasaurus* aligns it with most, but not all, titanosaurs (Mannion et al., 2013). Caudal vertebral hyposphene–hypantrum articulations might also have been independently gained or lost multiple times within Titanosauria.

Based on numerous similarities between *Savannasaurus* and *Diamantinasaurus*, we hypothesise that they form a clade (as resolved in many previous analyses (e.g., Poropat et al., 2016)) which occupies an early-branching position within Titanosauria. The anatomy of *Savannasaurus* (and *Diamantinasaurus*), as well as that of other taxa resolved in close phylogenetic proximity to them, suggests that 'classic' titanosaurs developed several features that the earliest diverging members of the clade lacked, such as procoelous (or opisthocoelous) anterior caudal vertebrae, loss of manual phalanges, and (in some cases) osteoderms. Several of the anatomical features that have led *Savannasaurus* (and *Diamantinasaurus*) to be resolved within Lithostrotia or Saltasauridae presumably represent

convergences (e.g., a robust humerus that is not much longer than the sternal plate); consequently, it is plausible that these features were linked to the wide-gauge gait adopted by *Savannasaurus* (and, to a lesser extent, *Diamantinasaurus*), which might in turn have developed (or been exaggerated) in response to the unique palaeoenvironment in which these titanosaurs lived.

***Savannasaurus* as a 'Wide-Gauge' Sauropod: A Response to Paleoenvironmental Pressures?**

Even among titanosaurs, which are especially wide-bodied among sauropods, *Savannasaurus elliottorum* was extremely transversely broad across the thorax and pelvis relative to its body size. Given that dorsal vertebra III is ~560 mm wide transversely across the diapophyses, that the most complete dorsal rib is 1680 mm long proximodistally, and that each sternal plate is 425 mm wide mediolaterally (total sternal breadth = 850 mm), the circumference of the thorax of *Savannasaurus* would have exceeded 5 metres (including cartilage). Moreover, given that the sacrum is 934 mm across the posteriormost sacral processes, and the pelvis is 1140 mm wide transversely across the iliac peduncles of the pubes (and would have been broader still across the ilia, were they preserved), it was also clearly wide-hipped.

Several truly gigantic sauropods appear to be less transversely broad relative to body size than *Savannasaurus*. The total sternal transverse breadth (1090 mm) of *Patagotitan* is 1.28 times that of *Savannasaurus*, whereas the pubis (1400 mm) of *Patagotitan* is 1.49 times as long (Carballido et al., 2017). Similarly, the total sternal transverse breadth (at least 1160 mm) of *Dreadnoughtus* is 1.36 times that of *Savannasaurus*, and the transverse breadth of the sacrum (1160 mm wide across the posteriormost sacral processes, sans ilia) is 1.24 times that

of *Savannasaurus*, despite the fact that the pubis (1400 mm) of *Dreadnoughtus* is 1.49 times as long. The sacrum of *Futalognkosaurus* (1170 mm wide transversely across the posteriormost sacral processes, sans ilia) is 1.25 times as broad as that of *Savannasaurus*, despite the pubis (1370 mm) of *Futalognkosaurus* being 1.46 times as long. By these metrics, these titanosaurs, which were substantially larger than *Savannasaurus*, were not as wide-bodied relative to body size.

By contrast, *Opisthocoelicaudia* appears to exceed *Savannasaurus* in terms of transverse breadth relative to body size (Borsuk-Białynicka, 1977). Each appendicular element preserved in *Savannasaurus* is proximodistally longer than its counterpart in *Opisthocoelicaudia* (even the humerus, which is incomplete in *Savannasaurus*). Despite this, in *Opisthocoelicaudia* the left and right sternal plates have mediolateral widths of 480 mm and 500 mm respectively (giving a total sternal breadth of at least 980 mm, 1.15 times that of *Savannasaurus*), whereas the sacrum measures approximately 1060 mm across the posteriormost sacral processes (1.13 times that of *Savannasaurus*; approximated from published figures). Saltasaurines also appear to have been broader relative to body size than *Savannasaurus.* The transverse breadth of the sacrum in *Neuquensaurus* (~580 mm across the posteriormost sacral processes) is 0.62 times that of *Savannasaurus*, despite the fact that the humerus (520 mm long proximodistally) is less than half as long (Salgado et al., 2005).

There is little doubt that *Savannasaurus* would have habitually had a wide-gauge stance (Fig. 23) and, presumably, a wide-gauge gait, as has been hypothesised for titanosaurs generally (Wilson and Carrano, 1999; Carrano, 2005). The increased robusticity of the humerus might have developed in response to this, whereas the marked distal expansion of metacarpal I implies that more weight was supported by it than the more lateral metacarpals. The unique morphology of the astragalus of *Savannasaurus* might also have developed in

response to increased weight-bearing, although the absence of the femur, tibia and fibula makes this difficult to discern.

The vertebral column of *Savannasaurus* shows several features that appear to be linked to increased flexibility. Prominent among these is the lack of a hyposphene–hypantrum system throughout the vertebral column. Instead, dorsal vertebrae VI–X of *Savannasaurus* lack TPOLs (resulting in the confluence of the CPOF+SPOF), and the CPOLs and postzygapophyses are separated on the midline. This is unusual among sauropods generally, but is also observed in *Diamantinasaurus* (Poropat et al., 2016). In addition, all preserved dorsal vertebrae of *Savannasaurus* have a prominent CPRF ventral to the TPRL, an unusual feature among titanosaurs, but again seen in *Diamantinasaurus* (S.F.P., P.D.M & P.U., unpublished data).

Savannasaurus and *Diamantinasaurus* inhabited a floodplain environment, characterised by clay-rich soils and probably dominated by extensive meandering river systems (Fletcher et al., 2018). Average annual rainfall is thought to have been relatively high (Fletcher et al., 2014b), which implies that the volcanogenic soils surrounding the watercourses on the floodplain might have been treacherous for multi-tonne sauropods to traverse at certain times of year. Although it is tempting to suggest that this environmental pressure would have selected for sauropods with more elongate necks, which would have been able to access water sources while standing several metres back from the edge, the preserved cervical vertebrae of both *Diamantinasaurus* and *Savannasaurus* suggest that their necks were relatively short and unspecialised for such a purpose (that said, the elongate cervical ribs of *Savannasaurus* [at least] might have improved the stability of the neck when it was held horizontally). In light of this, it is possible that the environmental pressures to which sauropods in northeast Australia were subjected might have selected for individuals that were better able to enter, traverse and exit muddy watercourses. In this scenario, more flexible

dorsal and caudal vertebral series, barrel-like bodies (more akin to those of hippopotamus than to the slab-sided thoraces of other sauropods), and robust forelimbs might have been favoured. If other titanosaurian taxa or lineages were independently subjected to similar environmental pressures elsewhere, then it is possible that the bauplan regarded as 'typical' for this clade might in fact have developed, or at least been accentuated, multiple times. This might also serve to explain the many convergences between *Savannasaurus* and saltasaurids.

CONCLUSION

The postcranial skeleton of *Savannasaurus elliottorum* shows a mosaic of anatomical features. Some of these are generally regarded as plesiomorphic for Titanosauria, whereas others are often regarded as apomorphies of Titanosauria or a less inclusive clade thereof. This blend of putative titanosaurian plesiomorphies and apomorphies is also seen in a contemporary of *Savannasaurus*, *Diamantinasaurus matildae*, and it is likely that they form a clade. Based on the absence of hyposphene–hypantrum articulations, the pneumatic nature of the caudal vertebral neural arches, the proportions of the appendicular elements, and other features, this clade would appear to occupy a position within Titanosauria, probably outside Lithostrotia. The non-reniform sternal plate presumably represents a reversal within Titanosauriformes, whereas the presence of manual phalanges supports an early-branching position for *Savannasaurus* (and *Diamantinasaurus*) within Titanosauria.

The anatomical specialisations seen in the axial and appendicular skeleton of *Savannasaurus* suggest that it was well adapted to the wet, temperate floodplain environment it inhabited. The barrel-shaped thorax, reminiscent of that of the hippopotamus, might

indicate that *Savannasaurus* spent more time in or near shallow water (or at least waterlogged sediments) than other sauropods. The increased flexibility of the spinal column potentially enabled *Savannasaurus* to more expediently extricate itself from wallows and bogs. By contrast, the capacity that *Savannasaurus* clearly possessed to distribute its body weight over a greater area through its wide-gauge stance might have reduced its risk of becoming bogged in the first place when traversing the muddy floodplains of northeast Australia during times of high rainfall or flood.

ACKNOWLEDGMENTS

The authors would like to thank: additional members of the Elliott family for facilitating the excavation of 'Wade' on Belmont Station in 2005; the volunteers who participated in the 'Wade' digs in 2005 and who prepared the specimen over the course of the next decade; the staff at the Australian Age of Dinosaurs Museum of Natural History; A. Kramarz and M. Ezcurra (Museo Argentino de Ciencias Naturales 'Bernardino Rivadavia'), A. Otero (Museo de La Plata), J. Powell (Universidad Nacional de Tucuman), B. González Riga and L. Ortíz David (Universidad Nacional de Cuyo), J. Calvo and J. Mansilla (Museo de Geología y Paleontología de la Universidad Nacional del Comahue), V. Zurriaguz and I. Cerda (Universidad Nacional de Río Negro; Museo Provincial de Cipolletti "Carlos Ameghino"), D. Pol and J. Carballido (Museo Paleontológico Egidio Feruglio), R. Martínez and M. Luna (Universidad Nacional de la Patagonia San Juan Bosco), L. Ibiricu (Instituto Patagónico de Geología y Paleontología) and others for allowing S.F.P., P.D.M. and P.U. to make firsthand observations of Argentinean sauropod specimens in their care; and reviewers J. Whitlock (Mount Aloysius College) and J. Carballido (Museo Paleontológico Egidio Feruglio), and

editor M. D'Emic (Adelphi University) for their constructive comments that greatly improved this manuscript. S.F.P.'s early work on this project was funded by an Australian Research Council Linkage Grant (LP100100339, awarded to B. Kear) and hosted at Uppsala University (Sweden). S.F.P. would also like to thank the Winston Churchill Memorial Trust for a Churchill Fellowship (awarded in 2017) that enabled him to make firsthand observation of several Argentinian sauropod specimens, and The Paleontological Society for an Arthur James Boucot Research Grant (awarded in 2017) that funded a trip to Winton to study *Savannasaurus* firsthand. P.D.M.'s research is supported by a Royal Society University Research Fellowship (UF160216). P.U.'s contribution was facilitated by a Leverhulme Trust Research Grant (RPG-129).

REFERENCES

Apesteguía, S. 2005. Evolution of the hyposphene-hypantrum complex within Sauropoda; pp. 248–267 *in* V. Tidwell, and K. Carpenter (eds.), Thunder-lizards: The Sauropodomorph Dinosaurs. Indiana University Press, Bloomington & Indianapolis, IA.

Averianov, A., and V. Efimov. 2018. The oldest titanosaurian sauropod of the Northern Hemisphere. Biological Communications 63:145–162.

Bandeira, K. L. N., F. Medeiros Simbras, E. B. Machado, D. d. A. Campos, G. R. Oliveira, and A. W. A. Kellner. 2016. A new giant Titanosauria (Dinosauria: Sauropoda) from the Late Cretaceous Bauru Group, Brazil. PLOS One 11:e0163373.

Berrell, R. W., J. Alvarado-Ortega, Y. Yabumoto, and S. W. Salisbury. 2014. The first record of the ichthyodectiform fish *Cladocylcus*[*sic*: *Cladocyclus*] from eastern Gondwana: a

new species from the Lower Cretaceous of Queensland, Australia. Acta Palaeontologica Polonica 59:903–920.

Bonaparte, J. F. 1986. Les Dinosaures (Carnosaures, Allosauridés, Sauropodes, Cétiosauridés) du Jurassique Moyen de Cerro Cóndor (Chubut, Argentine) (2e partie et fin). Annales de Paléontologie (Vert.-Invert.) 72:325–386.

Bonaparte, J. F., and R. A. Coria. 1993. Un nuevo y gigantesco saurópodo titanosaurio de la Formación Rio Limay (Albiano-Cenomaniano) de la Provincia del Neuquén, Argentina. Ameghiniana 30:271–282.

Bonaparte, J. F., B. J. González Riga, and S. Apesteguía. 2006. *Ligabuesaurus leanzai* gen. et sp. nov. (Dinosauria, Sauropoda), a new titanosaur from the Lohan Cura Formation (Aptian, Lower Cretaceous) of Neuquén, Patagonia, Argentina. Cretaceous Research 27:364–376.

Borsuk-Białynicka, M. 1977. A new camarasaurid sauropod *Opisthocoelicaudia skarzynskii* gen. n., sp. n. from the Upper Cretaceous of Mongolia. Palaeontologia Polonica 37:5–64.

Calvo, J. O., and J. F. Bonaparte. 1991. *Andesaurus delgadoi* gen. et sp. nov. (Saurischia–Sauropoda), dinosaurio Titanosauridae de la Formación Río Limay (Albiano–Cenomaniano), Neuquén, Argentina. Ameghiniana 28:303–310.

Calvo, J. O., J. D. Porfiri, B. J. González Riga, and A. W. A. Kellner. 2007. Anatomy of *Futalognkosaurus dukei* Calvo, Porfiri, González Riga & Kellner, 2007 (Dinosauria, Titanosauridae) from the Neuquén Group (Late Cretaceous), Patagonia, Argentina. Arquivos do Museu Nacional, Rio de Janeiro 65:511–526.

Calvo, J. O., and L. Salgado. 1995. *Rebbachisaurus tessonei* sp. nov. a new Sauropoda from the Albian–Cenomanian of Argentina: new evidence on the origin of the Diplodocidae. Gaia 11:13–33.

Campos, D. d. A., A. W. A. Kellner, R. J. Bertini, and R. M. Santucci. 2005. On a titanosaurid (Dinosauria, Sauropoda) vertebral column from the Bauru Group, Late Cretaceous of Brazil. Arquivos do Museu Nacional, Rio de Janeiro 63:565–593.

Canudo, J. I., R. Royo-Torres, and G. Cuenca-Bescós. 2008. A new sauropod: *Tastavinsaurus sanzi* gen. et sp. nov. from the Early Cretaceous (Aptian) of Spain. Journal of Vertebrate Paleontology 28:712–731.

Carballido, J. L., D. Pol, I. Cerda, and L. Salgado. 2011. The osteology of *Chubutisaurus insignis* Del Corro, 1975 (Dinosauria: Neosauropoda) from the 'Middle' Cretaceous of Central Patagonia, Argentina. Journal of Vertebrate Paleontology 31:93–110.

Carballido, J. L., D. Pol, A. Otero, I. A. Cerda, L. Salgado, A. C. Garrido, J. Ramezzani, N. R. Cúneo, and M. J. Krause. 2017. A new giant titanosaur sheds light on body mass evolution among sauropod dinosaurs. Proceedings of the Royal Society B 284:20171219.

Carballido, J. L., D. Pol, M. L. Parra Ruge, S. Padilla Bernal, M. E. Páramo-Fonseca, and F. Etayo-Serna. 2015. A new Early Cretaceous brachiosaurid (Dinosauria, Neosauropoda) from northwestern Gondwana (Villa de Leiva, Colombia). Journal of Vertebrate Paleontology 35:e980505.

Carballido, J. L., L. Salgado, D. Pol, J. I. Canudo, and A. Garrido. 2012. A new basal rebbachisaurid (Sauropoda, Diplodocoidea) from the Early Cretaceous of the Neuquén Basin; evolution and biogeography of the group. Historical Biology 24:631–654.

Carrano, M. T. 2005. The evolution of sauropod locomotion: morphological diversity of a secondary quadrupedal rotation; pp. 229–251 *in* K. A. Curry Rogers, and J. A. Wilson (eds.), The Sauropods: Evolution and Paleobiology. University of California Press, Berkeley.

Cerda, I. A., L. Salgado, and J. E. Powell. 2012. Extreme postcranial pneumaticity in sauropod dinosaurs from South America. Paläontologische Zeitschrift 86:441–449.

Clifford, H. T., and M. E. Dettmann. 2005. First record from Australia of the Cretaceous fern genus *Tempskya* and the description of a new species, *T. judithae*. Review of Palaeobotany and Palynology 134:71–84.

Cook, A. G. 2005. First record of fossil freshwater gastropods within the Winton Formation. Memoirs of the Queensland Museum 51:406.

Coombs, W. P., Jr., and R. E. Molnar. 1981. Sauropoda (Reptilia, Saurischia) from the Cretaceous of Queensland. Memoirs of the Queensland Museum 20:351–373.

Coria, R. A., L. S. Filippi, L. M. Chiappe, R. García, and A. B. Arcucci. 2013. *Overosaurus paradasorum* gen. et sp. nov., a new sauropod dinosaur (Titanosauria: Lithostrotia) from the Late Cretaceous of Neuquén, Patagonia, Argentina. Zootaxa 3683:357–376.

Csiki, Z., V. Codrea, C. Jipa-Murzea, and P. Godefroit. 2010. A partial titanosaur (Sauropoda, Dinosauria) skeleton from the Maastrichtian of Nălaţ-Vad, Haţeg Basin, Romania. Neues Jahrbuch für Geologie und Paläontologie, Abhandlungen 258:297–324.

Curry Rogers, K. 2009. The postcranial osteology of *Rapetosaurus krausei* (Sauropoda: Titanosauria) from the Late Cretaceous of Madagascar. Journal of Vertebrate Paleontology 29:1046–1086.

Curry Rogers, K. A. 2005. Titanosauria: a phylogenetic overview; pp. 50–103 *in* K. A. Curry Rogers, and J. A. Wilson (eds.), The Sauropods: Evolution and Paleobiology. University of California Press, Berkeley.

D'Emic, M. D. 2012. Early evolution of titanosauriform sauropod dinosaurs. Zoological Journal of the Linnean Society 166:624–671.

D'Emic, M. D. 2013. Revision of the sauropod dinosaurs of the Lower Cretaceous Trinity Group, southern USA, with the description of a new genus. Journal of Systematic Palaeontology 11:707–726.

D'Emic, M. D., P. D. Mannion, P. Upchurch, R. B. J. Benson, Q. Pang, and Z. Cheng. 2013. Osteology of *Huabeisaurus allocotus* (Sauropoda: Titanosauriformes) from the Upper Cretaceous of China. PLOS One 8:e69375.

D'Emic, M. D., and J. A. Wilson. 2011. New remains attributable to the holotype of the sauropod dinosaur *Neuquensaurus australis*, with implications for saltasaurine systematics. Acta Palaeontologica Polonica 56:61–73.

Del Corro, G. 1975. Un nuevo saurópodo del Cretácico Superior, *Chubutisaurus insignis* gen. et sp. nov. (Saurischia, Chubutisauridae nov.) del Cretácico Superior (Chubutiano), Chubut, Argentina. Actas I Congreso Argentino de Paleontología y Biostratigrafía:229–240.

Dettmann, M. E., and H. T. Clifford. 2000. Gemmae of the marchantiales from the Winton Formation (mid-Cretaceous), Eromanga Basin, Queensland. Memoirs of the Queensland Museum 45:285–292.

Dettmann, M. E., H. T. Clifford, and M. Peters. 2009. *Lovellea wintonensis* gen. et sp. nov. – Early Cretaceous (late Albian), anatomically preserved, angiospermous flowers and fruits from the Winton Formation, western Queensland, Australia. Cretaceous Research 30:339–355.

Dettmann, M. E., H. T. Clifford, and M. Peters. 2012. *Emwadea microcarpa* gen. et sp. nov.—anatomically preserved araucarian seed cones from the Winton Formation (late Albian), western Queensland, Australia. Alcheringa 36:217–237.

Díez Díaz, V., X. Pereda Suberbiola, and J. L. Sanz. 2013. Appendicular skeleton and dermal armour of the Late Cretaceous titanosaur *Lirainosaurus astibiae* (Dinosauria: Sauropoda) from Spain. Palaeontologia Electronica 16.2.19A:1–18.

Dunstan, B. 1916. Queensland geological formations; pp. *in* G. Harrap (ed.), A School Geography of Queensland. Department of Public Instruction, Brisbane, Australia.

Exon, N. F., and B. R. Senior. 1976. The Cretaceous of the Eromanga and Surat Basins. Bureau of Mineral Resources, Geology and Geophysics Bulletin 1:33–50.

Fletcher, T. L., D. J. Cantrill, P. T. Moss, and S. W. Salisbury. 2014a. A new species of *Protophyllocladoxylon* from the Upper Cretaceous (Cenomanian–Turonian) portion of the Winton Formation, central-western Queensland, Australia. Review of Palaeobotany and Palynology 208:43–49.

Fletcher, T. L., D. R. Greenwood, P. T. Moss, and S. W. Salisbury. 2014b. Paleoclimate of the Late Cretaceous (Cenomanian–Turonian) portion of the Winton Formation, central-western Queensland, Australia: new observations based on CLAMP and bioclimatic analysis. PALAIOS 29:121–128.

Fletcher, T. L., P. T. Moss, and S. W. Salisbury. 2018. The palaeoenvironment of the Upper Cretaceous (Cenomanian–Turonian) portion of the Winton Formation, Queensland, Australia. PeerJ 6:e5513.

Fletcher, T. L., and S. W. Salisbury. 2014. Probable oribatid mite (Acari: Oribatida) tunnels and faecal pellets in silicified conifer wood from the Upper Cretaceous (Cenomanian–Turonian) portion of the Winton Formation, central-western Queensland, Australia. Alcheringa 38:541–545.

Fronimos, J. 2011. Patterns of postcranial pneumaticity in the Late Cretaceous titanosaur *Alamosaurus sanjuanensis*. Journal of Vertebrate Paleontology 31:112A–113A.

Gilmore, C. W. 1936. Osteology of *Apatosaurus* with special reference to specimens in the Carnegie Museum. Memoirs of the Carnegie Museum 11:175–300.

Gilmore, C. W. 1946. Reptilian fauna of the North Horn Formation of central Utah. United States Geological Survey Professional Paper 210-C:29–53.

Gomani, E. M. 2005. Sauropod dinosaurs from the Early Cretaceous of Malawi, Africa. Palaeontologia Electronica 8:27A.

González Riga, B. J. 2003. A new titanosaur (Dinosauria, Sauropoda) from the Upper Cretaceous of Mendoza Province, Argentina. Ameghiniana 40:155–172.

González Riga, B. J. 2005. Nuevos restos fósiles de *Mendozasaurus neguyelap* (Sauropoda, Titanosauria) del Cretácico Tardío de Mendoza, Argentina. Ameghiniana 42:535–548.

González Riga, B. J., M. C. Lamanna, A. Otero, L. D. Ortíz David, A. W. A. Kellner, and L. M. Ibiricu. 2019. An overview of the appendicular skeletal anatomy of South American titanosaurian sauropods, with definition of a newly recognized clade. Anais da Academia Brasileira de Ciências 91:e20180374.

González Riga, B. J., P. D. Mannion, S. F. Poropat, L. D. Ortíz David, and J. P. Coria. 2018. Osteology of the Late Cretaceous Argentinean sauropod dinosaur *Mendozasaurus neguyelap*: implications for basal titanosaur relationships. Zoological Journal of the Linnean Society 184:136–181.

González Riga, B. J., E. Previtera, and C. A. Pirrone. 2009. *Malarguesaurus florenciae* gen. et sp. nov., a new titanosauriform (Dinosauria, Sauropoda) from the Upper Cretaceous of Mendoza, Argentina. Cretaceous Research 30:135–148.

Gorscak, E., and P. M. O'Connor. 2019. A new African titanosaurian sauropod dinosaur from the middle Cretaceous Galula Formation (Mtuka Member), Rukwa Rift Basin, southwestern Tanzania. PLOS One 14:e0211412.

Gorscak, E., P. M. O'Connor, N. J. Stevens, and E. M. Roberts. 2014. The basal titanosaurian *Rukwatitan bisepultus* (Dinosauria, Sauropoda) from the middle Cretaceous Galula Formation, Rukwa Rift Basin, southwestern Tanzania. Journal of Vertebrate Paleontology 34:1133–1154.

Gray, A. R. G., M. McKillop, and J. L. McKellar. 2002. Eromanga Basin Stratigraphy; pp. 30–56 *in* J. J. Draper (ed.), Geology of the Cooper and Eromanga Basins, Queensland. Department of Natural Resources and Mines, Brisbane.

Hocknull, S. A. 1997. Cretaceous freshwater bivalves from Queensland. Memoirs of the Queensland Museum 42:223–226.

Hocknull, S. A. 2000. Mesozoic freshwater and estuarine bivalves from Australia. Memoirs of the Queensland Museum 45:405–426.

Hocknull, S. A., and A. G. Cook. 2008. Hypsilophodontid (Dinosauria, Ornithischia) from latest Albian, Winton Formation, central Queensland. Memoirs of the Queensland Museum 52:212.

Hocknull, S. A., M. A. White, T. R. Tischler, A. G. Cook, N. D. Calleja, T. Sloan, and D. A. Elliott. 2009. New mid-Cretaceous (latest Albian) dinosaurs from Winton, Queensland, Australia. PLOS One 4:e6190.

Hogg, D. A. 1984. The distribution of pneumatisation in the skeleton of the adult domestic fowl. Journal of Anatomy 138:617–629.

Jain, S. L., and S. Bandyopadhyay. 1997. New titanosaurid (Dinosauria: Sauropoda) from the Late Cretaceous of central India. Journal of Vertebrate Paleontology 17:114–136.

Jell, P. A. 2004. Fossil insects of Australia. Memoirs of the Queensland Museum 50:1–123.

Juárez Valieri, R. D., and J. O. Calvo. 2011. Revision of MUCPv 204, a Senonian basal titanosaur from northern Patagonia; pp. 143–152 *in* J. Calvo, J. Porfiri, B. González Riga, and D. Dos Santos (eds.), Paleontología y Dinosaurios desde América Latina. Editorial de la Universidad Nacional de Cuyo, Mendoza.

Kear, B. P. 2016. Cretaceous marine amniotes of Australia: perspectives on a decade of new research. Memoirs of Museum Victoria 74:17–28.

Kellner, A. W. A., D. d. A. Campos, and M. N. F. Trotta. 2005. Description of a titanosaurid caudal series from the Bauru Group, Late Cretaceous of Brazil. Arquivos do Museu Nacional, Rio de Janeiro 63:529–564.

Kemp, A. 1997. Four species of *Metaceratodus* (Osteichthyes: Dipnoi, family Ceratodontidae) from Australian Mesozoic and Cainozoic deposits. Journal of Vertebrate Paleontology 17:26–33.

Kemp, A., and R. E. Molnar. 1981. *Neoceratodus forsteri* from the Lower Cretaceous of New South Wales, Australia. Journal of Paleontology 55:211–217.

Klinkhamer, A. J., H. Mallison, S. F. Poropat, G. H. K. Sinapius, and S. Wroe. 2018. Three-dimensional musculoskeletal modelling of the sauropodomorph hind limb: the effect of postural change on muscle leverage. Anatomical Record 301:2145–2163.

Klinkhamer, A. J., H. Mallison, S. F. Poropat, T. Sloan, and S. Wroe. 2019. Comparative three-dimensional moment arm analysis of the sauropod forelimb: implications for the transition to a wide-gauge stance in titanosaurs. Anatomical Record 302:794–817.

Ksepka, D. T., and M. A. Norell. 2006. *Erketu ellisoni*, a long-necked sauropod from Bor Guvé (Dornogov Aimag, Mongolia). American Museum Novitates 3508:1–16.

Ksepka, D. T., and M. A. Norell. 2010. The illusory evidence for Asian Brachiosauridae: new material of *Erketu ellisoni* and a phylogenetic reappraisal of basal Titanosauriformes. American Museum Novitates 3700:1–27.

Le Loeuff, J. 2005. Osteology of *Ampelosaurus atacis* (Titanosauria) from southern France; pp. 115–137 *in* V. Tidwell, and K. Carpenter (eds.), Thunder-lizards: The

Sauropodomorph Dinosaurs. Indiana University Press, Bloomington & Indianapolis, IA.

Leahey, L. G., and S. W. Salisbury. 2013. First evidence of ankylosaurian dinosaurs (Ornithischia: Thyreophora) from the mid-Cretaceous (late Albian–Cenomanian) Winton Formation of Queensland, Australia. Alcheringa 37:249–257.

Lehman, T. M., and A. B. Coulson. 2002. A juvenile specimen of the sauropod dinosaur *Alamosaurus sanjuanensis* from the Upper Cretaceous of Big Bend National Park, Texas. Journal of Paleontology 76:156–172.

Leite, K. J., and D. C. Fortier. 2018. The palate and choanae structure of the *Susisuchus anatoceps* (Crocodyliformes, Eusuchia): phylogenetic implications. PeerJ 6:e5372.

Li, L.-G., D.-Q. Li, H.-L. You, and P. Dodson. 2014. A new titanosaurian sauropod from the Hekou Group (Lower Cretaceous) of the Lanzhou-Minhe Basin, Gansu Province, China. PLOS One 9:e85979.

Longman, H. A. 1933. A new dinosaur from the Queensland Cretaceous. Memoirs of the Queensland Museum 10:131–144.

Lü, J., Y. Azuma, R. Chen, W. Zheng, and X. Jin. 2008. A new titanosauriform sauropod from the early Late Cretaceous of Dongyang, Zhejiang Province. Acta Geologica Sinica 82:225–235.

Lü, J., L. Xu, X. Jiang, S. Jia, M. Li, C. Yuan, X. Zhang, and Q. Ji. 2009. A preliminary report on the new dinosaurian fauna from the Cretaceous of the Ruyang Basin, Henan Province of central China. Journal of the Paleontological Society of Korea 25:43–56.

Mannion, P. D., R. Allain, and O. Moine. 2017. The earliest known titanosauriform sauropod dinosaur and the evolution of Brachiosauridae. PeerJ 5:e3217.

Mannion, P. D., and J. O. Calvo. 2011. Anatomy of the basal titanosaur (Dinosauria, Sauropoda) *Andesaurus delgadoi* from the mid-Cretaceous (Albian–early Cenomanian) Río Limay Formation, Neuquén Province, Argentina: implications for titanosaur systematics. Zoological Journal of the Linnean Society 163:155–181.

Mannion, P. D., and A. Otero. 2012. A reappraisal of the Late Cretaceous Argentinean sauropod dinosaur *Argyrosaurus superbus*, with a description of a new titanosaur genus. Journal of Vertebrate Paleontology 32:614–638.

Mannion, P. D., P. Upchurch, R. N. Barnes, and O. Mateus. 2013. Osteology of the Late Jurassic Portuguese sauropod dinosaur *Lusotitan atalaiensis* (Macronaria) and the evolutionary history of basal titanosauriforms. Zoological Journal of the Linnean Society 168:98–206.

Mannion, P. D., P. Upchurch, X. Jin, and W. Zheng. 2019a. New information on the Cretaceous sauropod dinosaurs of Zhejiang Province, China: impact on Laurasian titanosauriform phylogeny and biogeography. Royal Society Open Science 6:191057.

Mannion, P. D., P. Upchurch, O. Mateus, R. N. Barnes, and M. E. H. Jones. 2012. New information on the anatomy and systematic position of *Dinheirosaurus lourinhanensis* (Sauropoda: Diplodocoidea) from the Late Jurassic of Portugal, with a review of European diplodocoids. Journal of Systematic Palaeontology 10:521–551.

Mannion, P. D., P. Upchurch, D. Schwarz, and O. Wings. 2019b. Taxonomic affinities of the putative titanosaurs from the Late Jurassic Tendaguru Formation of Tanzania:

1817 phylogenetic and biogeographic implications for eusauropod dinosaur evolution.
1818 Zoological Journal of the Linnean Society 185:784–909.

1819 Marsh, O. C. 1878. Principal characters of American Jurassic dinosaurs: Part I. American
1820 Journal of Science 16 (series 3):411–416.

1821 Martínez, R., O. Giménez, J. Rodríguez, M. Luna, and M. C. Lamanna. 2004. An articulated
1822 specimen of the basal titanosaurian (Dinosauria: Sauropoda) *Epachthosaurus sciuttoi*
1823 from the early Late Cretaceous Bajo Barreal Formation of Chubut Province, Argentina.
1824 Journal of Vertebrate Paleontology 24:107–120.

1825 McIntosh, J. S. 1990. Sauropoda; pp. 345–401 *in* D. B. Weishampel, P. Dodson, and H.
1826 Osmólska (eds.), The Dinosauria. University of California Press, Berkeley.

1827 McLoughlin, S., A. N. Drinnan, and A. C. Rozefelds. 1995. A Cenomanian flora from the
1828 Winton Formation, Eromanga Basin, Queensland, Australia. Memoirs of the
1829 Queensland Museum 38:273–313.

1830 McLoughlin, S., C. Pott, and D. Elliott. 2010. The Winton Formation flora (Albian–
1831 Cenomanian, Eromanga Basin): implications for vascular plant diversification and
1832 decline in the Australian Cretaceous. Alcheringa 34:303–323.

1833 Mocho, P., A. Pérez-García, M. Martin Jiménez, and F. Ortega. 2019a. New remains from the
1834 Spanish Cenomanian shade light on the Gondwanan origin of European Early
1835 Cretaceous titanosaurs. Cretaceous Research 95:164–190.

1836 Mocho, P., R. Royo-Torres, and F. Ortega. 2019b. A new macronarian sauropod from the
1837 Upper Jurassic of Portugal. Journal of Vertebrate Paleontology 39:e1578782.

Molnar, R. E. 1991. Fossil reptiles in Australia; pp. 605–702 *in* P. Vickers-Rich, J. M. Monaghan, R. F. Baird, and T. H. Rich (eds.), Vertebrate Palaeontology of Australasia. Pioneer Design Studio, Melbourne.

Molnar, R. E. 2001. A reassessment of the phylogenetic position of Cretaceous sauropod dinosaurs from Queensland, Australia; pp. 139–144 *in* H. A. Leanza (ed.), VII International Symposium on Mesozoic Terrestrial Ecosystems: Asociacíon Paleontológica Argentina Publicación Especial No. 7. Asociacion Paleontologica Argentina, Buenos Aires.

Molnar, R. E. 2010. Taphonomic observations on eastern Australian Cretaceous sauropods. Alcheringa 34:421–429.

Molnar, R. E. 2011a. New morphological information about Cretaceous sauropod dinosaurs from the Eromanga Basin, Queensland, Australia. Alcheringa 35:329–339.

Molnar, R. E. 2011b. Sauropod (Saurischia: Dinosauria) material from the Early Cretaceous Griman Creek Formation of the Surat Basin, Queensland, Australia. Alcheringa 35:303–307.

Molnar, R. E., and S. W. Salisbury. 2005. Observations on Cretaceous sauropods from Australia; pp. 454–465 *in* V. Tidwell, and K. Carpenter (eds.), Thunder-lizards: The Sauropodomorph Dinosaurs. Indiana University Press, Bloomington & Indianapolis, IA.

Osborn, H. F. 1899. A skeleton of *Diplodocus*. Memoirs of the American Museum of Natural History 1:191–214.

Otero, A. 2010. The appendicular skeleton of *Neuquensaurus*, a Late Cretaceous saltasaurine sauropod from Patagonia, Argentina. Acta Palaeontologica Polonica 55:399–426.

Pentland, A. H., and S. F. Poropat. 2019. Reappraisal of *Mythunga camara* Molnar & Thulborn, 2007 (Pterosauria, Pterodactyloidea, Anhangueria) from the upper Albian Toolebuc Formation of Queensland, Australia. Cretaceous Research 93:151–169.

Pentland, A. H., S. F. Poropat, T. R. Tischler, T. Sloan, R. A. Elliott, H. A. Elliott, J. A. Elliott, and D. A. Elliott. 2019. *Ferrodraco lentoni* gen. et sp. nov., a new ornithocheirid pterosaur from the Winton Formation (Cenomanian–lower Turonian) of Queensland, Australia. Scientific Reports 9:13454.

Peters, M. D., and D. C. Christophel. 1978. *Austrosequoia wintonensis*, a new taxodiaceous cone from Queensland, Australia. Canadian Journal of Botany 56:3119–3128.

Poropat, S. F. 2013. Carl Wiman's sauropods: The Uppsala Museum of Evolution's collection. GFF 135:104–119.

Poropat, S. F., P. D. Mannion, P. Upchurch, S. A. Hocknull, B. P. Kear, and D. A. Elliott. 2015a. Reassessment of the non-titanosaurian somphospondylan *Wintonotitan wattsi* (Dinosauria: Sauropoda: Titanosauriformes) from the mid-Cretaceous Winton Formation, Queensland, Australia. Papers in Palaeontology 1:59–106.

Poropat, S. F., P. D. Mannion, P. Upchurch, S. A. Hocknull, B. P. Kear, M. Kundrát, T. R. Tischler, T. Sloan, G. H. K. Sinapius, J. A. Elliott, and D. A. Elliott. 2016. New Australian sauropods shed light on Cretaceous dinosaur palaeobiogeography. Scientific Reports 6:34467.

Poropat, S. F., S. K. Martin, A.-M. P. Tosolini, B. E. Wagstaff, L. B. Bean, B. P. Kear, P. Vickers-Rich, and T. H. Rich. 2018. Early Cretaceous polar biotas of Victoria, southeastern Australia—an overview of research to date. Alcheringa 42:157–229.

Poropat, S. F., J. P. Nair, C. E. Syme, P. D. Mannion, P. Upchurch, S. A. Hocknull, A. G. Cook, T. R. Tischler, and T. Holland. 2017. Reappraisal of *Austrosaurus mckillopi* Longman, 1933 from the Allaru Mudstone of Queensland, Australia's first named Cretaceous sauropod dinosaur. Alcheringa 41:543–580.

Poropat, S. F., P. Upchurch, P. D. Mannion, S. A. Hocknull, B. P. Kear, T. Sloan, G. H. K. Sinapius, and D. A. Elliott. 2015b. Revision of the sauropod dinosaur *Diamantinasaurus matildae* Hocknull et al. 2009 from the middle Cretaceous of Australia: implications for Gondwanan titanosauriform dispersal. Gondwana Research 27:995–1033.

Powell, J. E. 1992. Osteologia de *Saltasaurus loricatus* (Sauropoda–Titanosauridae) del Cretácico Superior del noroeste Argentino; pp. 165–230 *in* J. L. Sanz, and A. D. Buscalioni (eds.), Los Dinosaurios y Su Entorno Biótico: Actas del Segundo Curso de Paleontologia in Cuenca. Instituto "Juan de Valdés", Cuenca, Spain.

Powell, J. E. 2003. Revision of South American titanosaurid dinosaurs: palaeobiological, palaeobiogeographical and phylogenetic aspects. Records of the Queen Victoria Museum 111:1–173.

Romilio, A., and S. W. Salisbury. 2011. A reassessment of large theropod dinosaur tracks from the mid-Cretaceous (late Albian–Cenomanian) Winton Formation of Lark Quarry, central-western Queensland, Australia: A case for mistaken identity. Cretaceous Research 32:135–142.

Romilio, A., and S. W. Salisbury. 2014. Large dinosaurian tracks from the Upper Cretaceous (Cenomanian–Turonian) portion of the Winton Formation, Lark Quarry, central-western Queensland, Australia: 3D photogrammetric analysis renders the 'stampede trigger' scenario unlikely. Cretaceous Research 51:186–207.

Romilio, A., R. T. Tucker, and S. W. Salisbury. 2013. Reevaluation of the Lark Quarry dinosaur Tracksite (late Albian–Cenomanian Winton Formation, central-western Queensland, Australia): no longer a stampede? Journal of Vertebrate Paleontology 33:102–120.

Rose, P. J. 2007. A new titanosauriform sauropod (Dinosauria: Saurischia) from the Early Cretaceous of central Texas and its phylogenetic relationships. Palaeontologia Electronica 10:8A.

Royo-Torres, R., C. Fuentes, M. Meijide, F. Meijide-Fuentes, and M. Meijide-Fuentes. 2017. A new Brachiosauridae sauropod dinosaur from the lower Cretaceous of Europe (Soria Province, Spain). Cretaceous Research 80:38–55.

Salgado, L. 1993. Comments on *Chubutisaurus insignis* Del Corro (Saurischia, Sauropoda). Ameghiniana 30:265–270.

Salgado, L., S. Apesteguía, and S. E. Heredia. 2005. A new specimen of *Neuquensaurus australis*, a Late Cretaceous saltasaurine titanosaur from north Patagonia. Journal of Vertebrate Paleontology 25:623–634.

Salgado, L., and J. O. Calvo. 1993. Report of a sauropod with amphiplatyan mid-caudal vertebrae from the Late Cretaceous of Neuquen Province (Argentina). Ameghiniana 30:215–218.

Salgado, L., and I. d. S. Carvalho. 2008. *Uberabatitan ribeiroi*, a new titanosaur from the Marília Formation (Bauru Group, Upper Cretacous), Minas Gerais, Brazil. Palaeontology 51:881–901.

Salgado, L., R. A. Coria, and J. O. Calvo. 1997. Evolution of titanosaurid sauropods. I: Phylogenetic analysis based on the postcranial evidence. Ameghiniana 34:3–32.

Salgado, L., R. A. García, and J. D. Daza. 2006. Consideraciones sobre las laminas neurales de los dinosaurios saurópodos y su significado morfofuncional. Revista del Museo Argentino de Ciencias Naturales 8:69–79.

Salgado, L., and J. E. Powell. 2010. Reassessment of the vertebral laminae in some South American titanosaurian sauropods. Journal of Vertebrate Paleontology 30:1760–1772.

Salisbury, S., R. E. Molnar, E. Frey, and P. M. A. Willis. 2006. The origin of modern crocodyliforms: new evidence from the Cretaceous of Australia. Proceedings of the Royal Society B 273:2439–2448.

Salisbury, S. W., A. Romilio, M. C. Herne, R. T. Tucker, and J. P. Nair. 2017. The dinosaurian ichnofauna of the Lower Cretaceous (Valanginian–Barremian) Broome Sandstone of the Walmadany Area (James Price Point), Dampier Peninsula, Western Australia. Society of Vertebrate Paleontology Memoir 16:1–152.

Santucci, R. M., and A. C. Arruda-Campos. 2011. A new sauropod (Macronaria, Titanosauria) from the Adamantina Formation, Bauru Group, Upper Cretaceous of Brazil and the phylogenetic relationships of Aeolosaurini. Zootaxa 3085:1–33.

Santucci, R. M., and R. J. Bertini. 2006. A large sauropod titanosaur from Peirópolis, Bauru Group, Brazil. Neues Jahrbuch für Geologie und Paläontologie, Monatshefte 2006:344–360.

Sanz, J. L., J. E. Powell, J. Le Loeuff, R. Martínez, and X. Pereda Suberbiola. 1999. Sauropod remains from the Upper Cretaceous of Laño (northcentral Spain), titanosaur phylogenetic relationships. Estudios del Museo de Ciencias Naturales de Alava 14:235–255.

Scanlon, J. D., and S. A. Hocknull. 2008. A dolichosaurid lizard from the latest Albian (mid-Cretaceous) Winton Formation, Queensland, Australia; pp. 131–136 *in* M. J. Everhart (ed.), Proceedings of the Second Mosasaur Meeting. Fort Hays Studies, Special Issue 3. Fort Hays State University, Hays, Kansas.

Senior, B. R., and J. A. Mabbutt. 1979. A proposed method of defining deeply weathered rock units based on regional geological mapping in southwest Queensland. Journal of the Geological Society of Australia 26:237–254.

Silva Junior, J. C. G., T. S. Marinho, A. G. Martinelli, and M. C. Langer. 2019. Osteology and systematics of *Uberabatitan ribeiroi* (Dinosauria; Sauropoda): a Late Cretaceous titanosaur from Minas Gerais, Brazil. Zootaxa 4577:401–438.

Simón, E., L. Salgado, and J. O. Calvo. 2018. A new titanosaur sauropod from the Upper Cretaceous of Patagonia, Neuquén Province, Argentina. Ameghiniana 55:1–29.

Syme, C. E., and S. W. Salisbury. 2018. Taphonomy of *Isisfordia duncani* specimens from the Lower Cretaceous (upper Albian) portion of the Winton Formation, Isisford, central-west Queensland. Royal Society Open Science 5:171651.

Syme, C. E., K. J. Welsh, E. M. Roberts, and S. W. Salisbury. 2016. Depositional environment of the Lower Cretaceous (upper Albian) Winton Formation at Isisford, Central-West Queensland, Australia, inferred from sandstone concretions. Journal of Sedimentary Research 86:1067–1082.

Thulborn, R. A. 2013. Lark Quarry revisited: a critique of methods used to identify a large dinosaurian track-maker in the Winton Formation (Albian–Cenomanian), western Queensland, Australia. Alcheringa 37:312–330.

Thulborn, R. A., and M. Wade. 1979. Dinosaur stampede in the Cretaceous of Queensland. Lethaia 12:275–279.

Thulborn, R. A., and M. Wade. 1984. Dinosaur trackways in the Winton Formation (mid-Cretaceous) of Queensland. Memoirs of the Queensland Museum 21:413–517.

Thulborn, T. 2012. Impact of sauropod dinosaurs on lagoonal substrates in the Broome Sandstone (Lower Cretaceous), Western Australia. PLOS One 7:e36208.

Thulborn, T. 2017. Behaviour of dinosaurian track-makers in the Winton Formation (Cretaceous, Albian–Cenomanian) at Lark Quarry, western Queensland, Australia: running or swimming? Ichnos 24:1–18.

Thulborn, T., T. Hamley, and P. Foulkes. 1994. Preliminary report on sauropod dinosaur tracks in the Broome Sandstone (Lower Cretaceous) of Western Australia; pp. 85–94 *in* M. G. Lockley, V. F. Santos, C. A. Meyer, and A. P. Hunt (eds.), Aspects of Sauropod Paleobiology; Gaia, 10, Lisbon, Portugal.

Tschopp, E., and O. Mateus. 2013. Clavicles, interclavicles, gastralia, and sternal ribs in sauropod dinosaurs: new reports from Diplodocidae and their morphological, functional and evolutionary implications. Journal of Anatomy 222:321–340.

Tucker, R. T., E. M. Roberts, V. Darlington, and S. W. Salisbury. 2017. Investigating the stratigraphy and palaeoenvironments for a suite of newly discovered mid-Cretaceous vertebrate fossil-localities in the Winton Formation, Queensland, Australia. Sedimentary Geology 358:210–229.

Tucker, R. T., E. M. Roberts, Y. Hu, A. I. S. Kemp, and S. W. Salisbury. 2013. Detrital zircon age constraints for the Winton Formation, Queensland: contextualizing Australia's Late Cretaceous dinosaur faunas. Gondwana Research 24:767–779.

Turner, A. H., and A. C. Pritchard. 2015. The monophyly of Susisuchidae (Crocodyliformes) and its phylogenetic placement in Neosuchia. PeerJ 3:e759.

Upchurch, P. 1995. The evolutionary history of sauropod dinosaurs. Philosophical Transactions: Biological Sciences 349:365–390.

Upchurch, P. 1998. The phylogenetic relationships of sauropod dinosaurs. Zoological Journal of the Linnean Society 124:43–103.

Upchurch, P., P. M. Barrett, and P. Dodson. 2004. Sauropoda; pp. 259–322 *in* D. B. Weishampel, P. Dodson, and H. Osmólska (eds.), The Dinosauria: Second Edition. University of California Press, Berkeley.

Upchurch, P., P. D. Mannion, and M. P. Taylor. 2015. The anatomy and phylogenetic relationships of "*Pelorosaurus*" *becklesii* (Neosauropoda, Macronaria) from the Early Cretaceous of England. PLOS One 10:e0125819.

Vine, R. R. 1964. Mackunda, Queensland. 1:250 000 Geological Series Sheet SF54-11. Bureau of Mineral Resources, Geology and Geophysics, Canberra, Australia.

Vine, R. R., and D. J. Casey. 1967. Winton, Queensland. 1:250 000 geological series sheet SF54-12. Bureau of Mineral Resources, Geology and Geophysics, Canberra, Australia.

Vine, R. R., and R. W. Day. 1965. Nomenclature of the Rolling Downs Group, northern Eromanga Basin, Queensland. Queensland Government Mineral Journal 66:416–421.

Voegele, K. K., M. C. Lamanna, and K. J. Lacovara. 2017. Osteology of the dorsal vertebrae of the giant titanosaurian sauropod dinosaur *Dreadnoughtus schrani* from the Late Cretaceous of Argentina. Acta Palaeontologica Polonica 62:667–681.

Wedel, M. J. 2003. The evolution of vertebral pneumaticity in sauropod dinosaurs. Journal of Vertebrate Paleontology 23:344–357.

Wedel, M. J. 2009. Evidence for bird-like air sacs in saurischian dinosaurs. Journal of Experimental Zoology Part A: Ecological Genetics and Physiology 311A:611–628.

Wedel, M. J., and M. P. Taylor. 2013. Caudal pneumaticity and pneumatic hiatuses in the sauropod dinosaurs *Giraffatitan* and *Apatosaurus*. PLOS One 8:e78213.

White, M. A., P. R. Bell, A. G. Cook, S. F. Poropat, and D. A. Elliott. 2015. The dentary of *Australovenator wintonensis* (Theropoda, Megaraptoridae); implications for megaraptorid dentition. PeerJ 3:e1512.

White, M. A., R. B. J. Benson, T. R. Tischler, S. A. Hocknull, A. G. Cook, D. G. Barnes, S. F. Poropat, S. J. Wooldridge, T. Sloan, G. H. K. Sinapius, and D. A. Elliott. 2013. New *Australovenator* hind limb elements pertaining to the holotype reveal the most complete neovenatorid leg. PLOS One 8:e68649.

White, M. A., A. G. Cook, S. A. Hocknull, T. Sloan, G. H. K. Sinapius, and D. A. Elliott. 2012. New forearm elements discovered of holotype specimen *Australovenator wintonensis* from Winton, Queensland, Australia. PLOS One 7:e39364.

Whitehouse, F. W. 1954. The geology of the Queensland portion of the Great Australian Artesian Basin; pp. 1–20, Artesian Water Supplies in Queensland. Department of the Co-ordinator-General of Public Works, Brisbane, Australia.

Whitlock, J. A., M. D. D'Emic, and J. A. Wilson. 2011. Cretaceous diplodocids in Asia? Re-evaluating the phylogenetic affinities of a fragmentary specimen. Palaeontology 54:351–364.

Wilson, J. A. 1999. A nomenclature for vertebral laminae in sauropods and other saurischian dinosaurs. Journal of Vertebrate Paleontology 19:639–653.

Wilson, J. A. 2002. Sauropod dinosaur phylogeny: critique and cladistic analysis. Zoological Journal of the Linnean Society 136:217–276.

Wilson, J. A. 2012. New vertebral laminae and patterns of serial variation in vertebral laminae of sauropod dinosaurs. Contributions from the Museum of Paleontology, The University of Michigan 32:91–110.

Wilson, J. A., and M. T. Carrano. 1999. Titanosaurs and the origin of "wide-gauge" trackways: a biomechanical and systematic perspective on sauropod locomotion. Paleobiology 25:252–267.

Wilson, J. A., M. D. D'Emic, T. Ikejiri, E. M. Moacdieh, and J. A. Whitlock. 2011. A nomenclature for vertebral fossae in sauropods and other saurischian dinosaurs. PLOS One 6:e17114.

Wilson, J. A., and P. C. Sereno. 1998. Early evolution and higher-level phylogeny of sauropod dinosaurs. Society of Vertebrate Paleontology Memoir 5 (Journal of Vertebrate Paleontology Vol. 18, supplement to No. 2, June 1998):68 pp.

Wilson, J. A., and P. Upchurch. 2003. A revision of *Titanosaurus* Lydekker (Dinosauria – Sauropoda), the first dinosaur genus with a 'Gondwanan' distribution. Journal of Systematic Palaeontology 1:125–160.

Wilson, J. A., and P. Upchurch. 2009. Redescription and reassessment of *Euhelopus zdanskyi* (Dinosauria: Sauropoda) from the Early Cretaceous of China. Journal of Systematic Palaeontology 7:199–239.

Wiman, C. 1929. Die Kreide-Dinosaurier aus Shantung. Palaeontologia Sinica (Series C) 6:1–67.

Xu, X., X. Zhang, Q. Tan, X. Zhao, and L. Tan. 2006. A new titanosaurian sauropod from Late Cretaceous of Nei Mongol, China. Acta Geologica Sinica 80:20–26.

You, H.-l., D.-q. Li, L.-q. Zhou, and Q. Ji. 2008. *Daxiatitan binglingi*: a giant sauropod dinosaur from the Early Cretaceous of China. Gansu Geology 17:1–10.

Zhang, X., J. Lü, L. Xu, J. Li, L. Yang, W. Hu, S. Jia, Q. Ji, and C. Zhang. 2009. A new sauropod dinosaur from the Late Cretaceous Gaogou Formation of Nanyang, Henan Province. Acta Geologica Sinica 83:212–221.

Zurriaguz, V., and J. Powell. 2015. New contributions to the presacral osteology of *Saltasaurus loricatus* (Sauropoda, Titanosauria) from the Upper Cretaceous of northern Argentina. Cretaceous Research 54:283–300.

End section with: Submitted December 1, 2019; revisions received Month DD, YYYY; accepted Month DD, YYYY

FIGURE CAPTIONS

FIGURE 1. Locality maps for *Savannasaurus elliottorum* (modified from Poropat et al., 2016 and Pentland et al., 2019). **A**, Map of Australia showing the location of Queensland. **B**, Map of Queensland showing the distribution of Winton Formation outcrop. **C**, Map of the Winton area showing Winton Formation outcrop, the location of Belmont Station and other stations on which sauropod body fossils have been recovered from the Winton Formation, and museums in the region. This map incorporates geological information from Vine (1964) and Vine and Casey (1967) [© Commonwealth of Australia (Geoscience Australia) 2019. This product is released under the Creative Commons Attribution 4.0 International Licence. http://creativecommons.org/licenses/by/4.0/legalcode]. [INTENDED FOR FULL-PAGE WIDTH]

FIGURE 2. Stratigraphy of the Eromanga Basin, Queensland, with silhouettes representing known tetrapod taxa. WINTON FORMATION: *Australovenator wintonensis*; Ankylosauria indet.; Ornithopoda indet.; *Wintonotitan wattsi*; *Diamantinasaurus matildae*; *Savannasaurus elliottorum*; *Ferrodraco lentoni*; *Isisfordia duncani*; Varanoidea indet.; and Chelidae indet. MACKUNDA FORMATION: Ctenochasmatoidea indet.; *Muttaburrasaurus langdoni*; and Polycotylidae indet. ALLARU MUDSTONE (following faunal summary in Poropat et al. (2017)): *Kunbarrasaurus ieversi*; *Muttaburrasaurus* sp.; *Austrosaurus mckillopi*; Elasmosauridae indet.; Polycotylidae indet.; *Kronosaurus queenslandicus*; *Platypterygius australis*; and Chelonioidea indet. TOOLEBUC FORMATION (following faunal summary in Pentland and Poropat (2019)): *Mythunga camara*; *Aussiedraco molnari*; *Nanantius eos*; Ankylosauria indet.; Iguanodontia indet.; Titanosauriformes indet.; *Platypterygius australis*; *Eromangasaurus australis*; *Cratochelone berneyi*; *Kronosaurus queenslandicus*;

Bouliachelys suteri; *Notochelone costata*; and Polycotylidae indet. WALLUMBILLA FORMATION (DONCASTER MEMBER): *Platypterygius* sp.; Elasmosauridae indet.; Polycotylidae indet.; and *Kronosaurus queenslandicus*. [INTENDED FOR FULL-PAGE WIDTH]

FIGURE 3. *Savannasaurus elliottorum* holotype specimen. **A**, Skeletal reconstruction, based on the preserved elements, by Travis Tischler (modified from Poropat et al., 2016). **B–C**, 'Ho-Hum' Site (AODL 82) map in **B**, bird's-eye view (from Poropat et al., 2016) and **C**, sub-surface view. [INTENDED FOR TWO-THIRDS PAGE WIDTH]

FIGURE 4. *Savannasaurus elliottorum* posterior cervical vertebra in **A**, left lateral, **B**, dorsal (with anterior to top), **C**, posterior, and **D**, ventral (with anterior to bottom) views, and left cervical ribs in **E**, medial, **F**, lateral and **G**, ventral views. Scale bar equals 100 mm. [INTENDED FOR FULL-PAGE WIDTH]

FIGURE 5. *Savannasaurus elliottorum* dorsal vertebra III in **A**, anterior, **B**, left lateral, **C**, ventral, **D**, posterior, **E**, dorsal, and **F**, right lateral views. Scale bar equals 200 mm. [INTENDED FOR FULL-PAGE WIDTH]

FIGURE 6. *Savannasaurus elliottorum* dorsal vertebra IV in **A**, anterior, **B**, dorsal, **C**, left lateral, **D**, posterior, **E**, right lateral, and **F**, ventral views. Scale bar equals 200 mm. [INTENDED FOR FULL-PAGE WIDTH]

FIGURE 7. *Savannasaurus elliottorum* dorsal vertebra V in posterior view. Scale bar equals 200 mm. [INTENDED FOR SINGLE COLUMN WIDTH]

FIGURE 8. *Savannasaurus elliottorum* dorsal vertebra VI in **A**, anterior, **B**, left lateral, **C**, posterior, **D**, dorsal, **E**, right lateral, and **F**, ventral views. Scale bar equals 200 mm. [INTENDED FOR FULL-PAGE WIDTH]

FIGURE 9. *Savannasaurus elliottorum* dorsal vertebra VII in **A**, anterior, **B**, left lateral, **C**, ventral, **D**, posterior, **E**, dorsal, and **F**, right lateral views. Scale bar equals 200 mm. [INTENDED FOR FULL-PAGE WIDTH]

FIGURE 10. *Savannasaurus elliottorum* dorsal vertebra VIII in **A**, anterior, **B**, left lateral, **C**, posterior, **D**, dorsal, **E**, right lateral, and **F**, ventral views. Scale bar equals 200 mm. [INTENDED FOR FULL-PAGE WIDTH]

FIGURE 11. *Savannasaurus elliottorum* dorsal vertebra IX in **A**, anterior, **B**, left lateral, **C**, posterior, **D**, dorsal, **E**, right lateral, and **F**, ventral views. Scale bar equals 200 mm. [INTENDED FOR FULL-PAGE WIDTH]

FIGURE 12. *Savannasaurus elliottorum* dorsal vertebra X in **A**, posterior, **B**, right lateral, **C**, anterior, **D**, dorsal, **E**, left lateral, and **F**, ventral views. Scale bar equals 200 mm. [INTENDED FOR FULL-PAGE WIDTH]

FIGURE 13. *Savannasaurus elliottorum* dorsal rib head in **A**, posterior and **B**, anterior views. Scale bar equals 50 mm. [INTENDED FOR SINGLE COLUMN WIDTH]

FIGURE 14. *Savannasaurus elliottorum* sacrum in ventral view (posterior to the left, anterior to the right). Scale bar equals 200 mm. [INTENDED FOR SINGLE COLUMN WIDTH]

FIGURE 15. *Savannasaurus elliottorum* caudal vertebrae. Caudal vertebra A in **A**, anterior, **B**, dorsal, **C**, left lateral, and **D**, posterior views, and **E**, broken left neural arch in lateral view. Caudal vertebra B in **F**, anterior, **G**, dorsal, **H**, left lateral, **I**, posterior, and **J**, right lateral views. Caudal vertebra C in **K**, anterior, **L**, left lateral, **M**, dorsal, **N**, posterior, **O**, ventral, and **P**, right lateral views. Caudal vertebra D in **Q**, dorsal, **R**, right lateral, and **S**, anterior views. Scale bar for **A–D** and **F–S** equals 100 mm; scale bar for **E** equals 50 mm. [INTENDED FOR FULL-PAGE WIDTH]

FIGURE 16. *Savannasaurus elliottorum* left coracoid in **A**, lateral, **B**, posterior, **C**, dorsal, **D**, medial, **E**, ventral, and **F**, anterior views. Scale bar equals 100 mm. [INTENDED FOR FULL-PAGE WIDTH]

FIGURE 17. *Savannasaurus elliottorum* left sternal plate in **A**, ventral and **B**, dorsal views, with the anterior end towards the top of the page. The dashed line represents the division between the convex portion of the ventral surface (medial to the line) and the concave portion (lateral to the line). Scale bar equals 200 mm. [INTENDED FOR SINGLE COLUMN WIDTH]

FIGURE 18. *Savannasaurus elliottorum* right humerus in **A**, posterior, **B**, lateral, **C**, anterior, and **D**, medial views. Scale bar equals 200 mm. [INTENDED FOR FULL-PAGE WIDTH]

FIGURE 19. *Savannasaurus elliottorum* left radius in **A**, posterior, **B**, proximal and **C**, distal views. Scale bar equals 100 mm. [INTENDED FOR SINGLE COLUMN WIDTH]

FIGURE 20. *Savannasaurus elliottorum* manus. Articulated left metacarpals I–V in **A**, proximal and **B**, distal views. Left metacarpal I in **C**, anterior, **D**, distal, **E**, lateral, **F**, proximal, **G**, posterior, and **H**, medial views. Left metacarpal II in **I**, anterior, **J**, distal, **K**, lateral, **L**, proximal, **M**, posterior, and **N**, medial views. Left metacarpal III in **O**, anterior, **P**, distal, **Q**, lateral, **R**, proximal, **S**, posterior, and **T**, medial views. Left metacarpal IV in **U**, anterior, **V**, distal, **W**, lateral, **X**, proximal, **Y**, posterior, and **Z**, medial views. Left metacarpal V in **AA**, anterior, **AB**, distal, **AC**, lateral, **AD**, proximal, **AE**, posterior, and **AF**, medial views. Right metacarpal IV in **AG**, anterior, **AH**, medial, **AI**, proximal, **AJ**, posterior, and **AK**, lateral views. Left manual phalanx II-1 in **AL**, dorsal, **AM**, medial, **AN**, ventral, **AO**, distal, **AP**, lateral, and **AQ**, proximal views. Scale bar equals 100 mm. [INTENDED FOR FULL-PAGE WIDTH]

FIGURE 21. *Savannasaurus elliottorum* co-ossified left and right pubes and ischia in **A**, posterior, **B**, dorsal, **C**, right lateral, **D**, ventral (right pubis and ischium not included in this photograph), and **E**, anterior views. Scale bar equals 500 mm. [INTENDED FOR FULL-PAGE WIDTH]

FIGURE 22. *Savannasaurus elliottorum* tarsus and metatarsus. Left astragalus in **A**, proximal, **B**, posterior, **C**, medial, **D**, distal, **E**, anterior, and **F**, lateral views. Right metatarsal III in **G**, proximal, **H**, dorsal, **I**, lateral, **J**, distal, **K**, ventral, and **L**, medial views. Scale bar equals 100 mm. [INTENDED FOR FULL-PAGE WIDTH]

FIGURE 23. *Savannasaurus elliottorum* life restoration by Travis R. Tischler. [INTENDED FOR FULL-PAGE WIDTH]

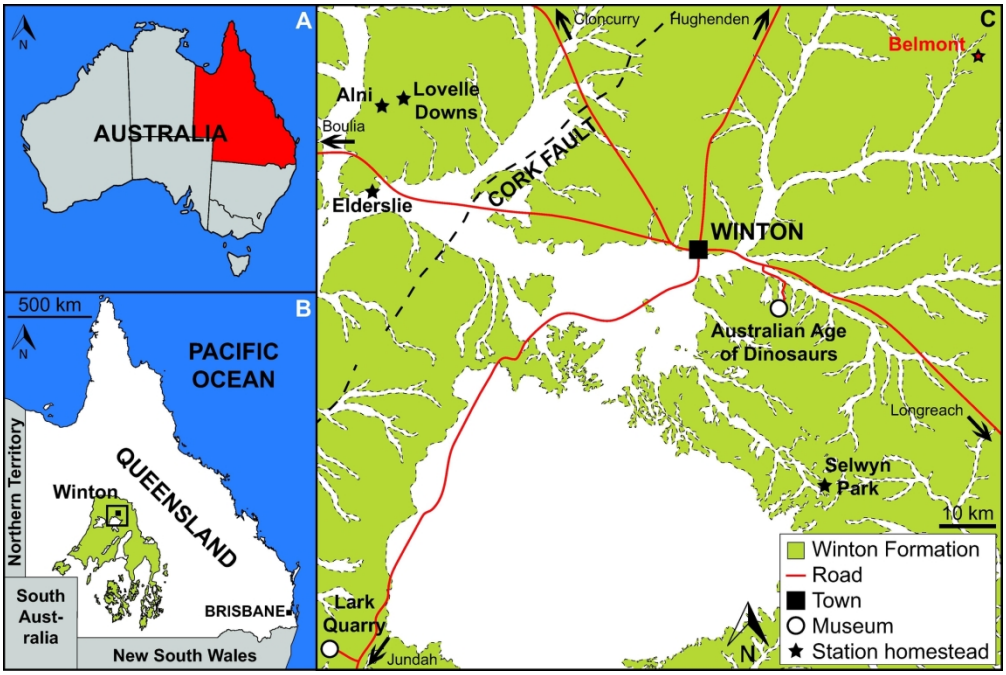

FIGURE 1. Locality maps for *Savannasaurus elliottorum* (modified from Poropat et al., 2016 and Pentland et al., 2019). **A**, Map of Australia showing the location of Queensland. **B**, Map of Queensland showing the distribution of Winton Formation outcrop. **C**, Map of the Winton area showing Winton Formation outcrop, the location of Belmont Station and other stations on which sauropod body fossils have been recovered from the Winton Formation, and museums in the region. This map incorporates geological information from Vine (1964) and Vine and Casey (1967) [© Commonwealth of Australia (Geoscience Australia) 2019. This product is released under the Creative Commons Attribution 4.0 International Licence. http://creativecommons.org/licenses/by/4.0/legalcode].

182x121mm (300 x 300 DPI)

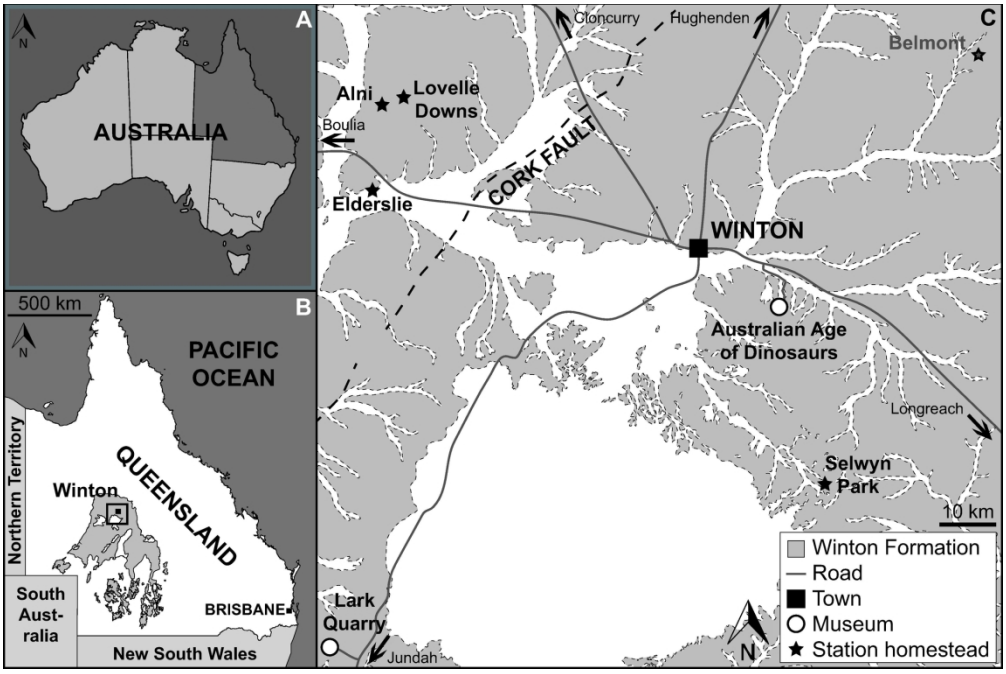

FIGURE 1. Locality maps for *Savannasaurus elliottorum* (modified from Poropat et al., 2016 and Pentland et al., 2019). **A**, Map of Australia showing the location of Queensland. **B**, Map of Queensland showing the distribution of Winton Formation outcrop. **C**, Map of the Winton area showing Winton Formation outcrop, the location of Belmont Station and other stations on which sauropod body fossils have been recovered from the Winton Formation, and museums in the region. This map incorporates geological information from Vine (1964) and Vine and Casey (1967) [© Commonwealth of Australia (Geoscience Australia) 2019. This product is released under the Creative Commons Attribution 4.0 International Licence. http://creativecommons.org/licenses/by/4.0/legalcode].

182x121mm (300 x 300 DPI)

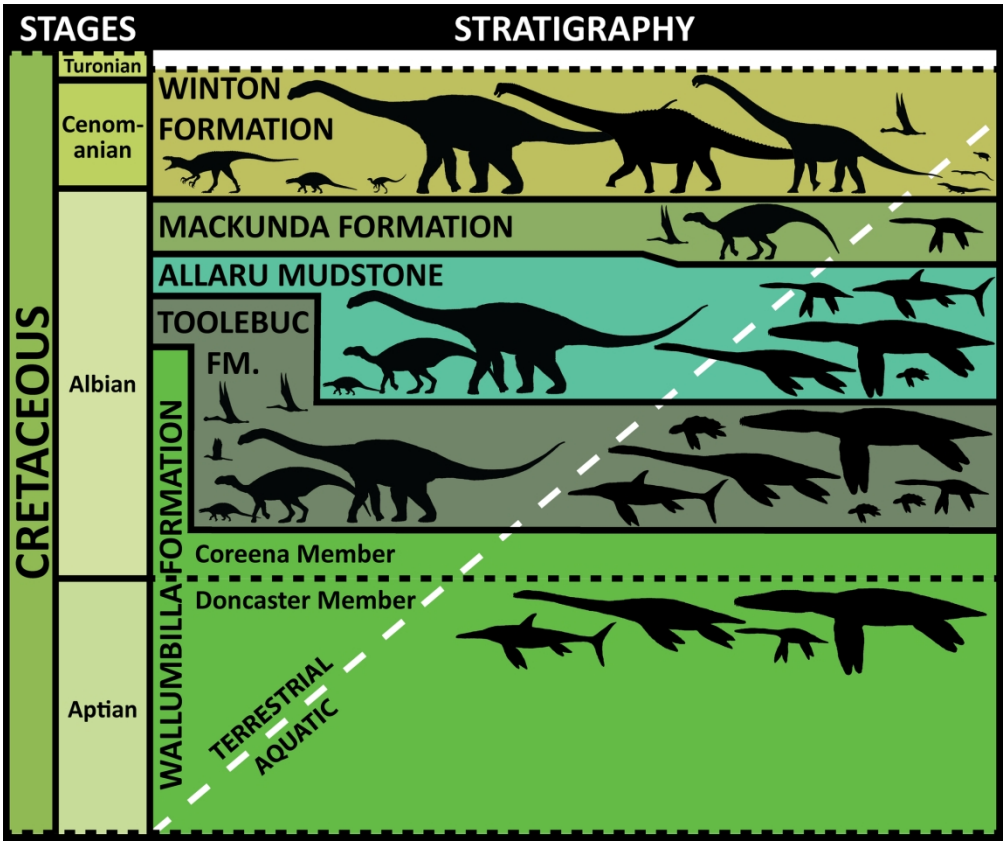

FIGURE 2. Stratigraphy of the Eromanga Basin, Queensland, with silhouettes representing known tetrapod taxa. WINTON FORMATION: *Australovenator wintonensis*; Ankylosauria indet.; Ornithopoda indet.; *Wintonotitan wattsi*; *Diamantinasaurus matildae*; *Savannasaurus elliottorum*; *Ferrodraco lentoni*; *Isisfordia duncani*; Varanoidea indet.; and Chelidae indet. MACKUNDA FORMATION: Ctenochasmatoidea indet.; *Muttaburrasaurus langdoni*; and Polycotylidae indet. ALLARU MUDSTONE (following faunal summary in Poropat et al. (2017)): *Kunbarrasaurus ieversi*; *Muttaburrasaurus* sp.; *Austrosaurus mckillopi*; Elasmosauridae indet.; Polycotylidae indet.; *Kronosaurus queenslandicus*; *Platypterygius australis*; and Chelonioidea indet. TOOLEBUC FORMATION (following faunal summary in Pentland and Poropat (2019)): *Mythunga camara*; *Aussiedraco molnari*; *Nanantius eos*; Ankylosauria indet.; Iguanodontia indet.; Titanosauriformes indet.; *Platypterygius australis*; *Eromangasaurus australis*; *Cratochelone berneyi*; *Kronosaurus queenslandicus*; *Bouliachelys suteri*; *Notochelone costata*; and Polycotylidae indet. WALLUMBILLA FORMATION (DONCASTER MEMBER): *Platypterygius* sp.; Elasmosauridae indet.; Polycotylidae indet.; and *Kronosaurus queenslandicus*.

182x153mm (300 x 300 DPI)

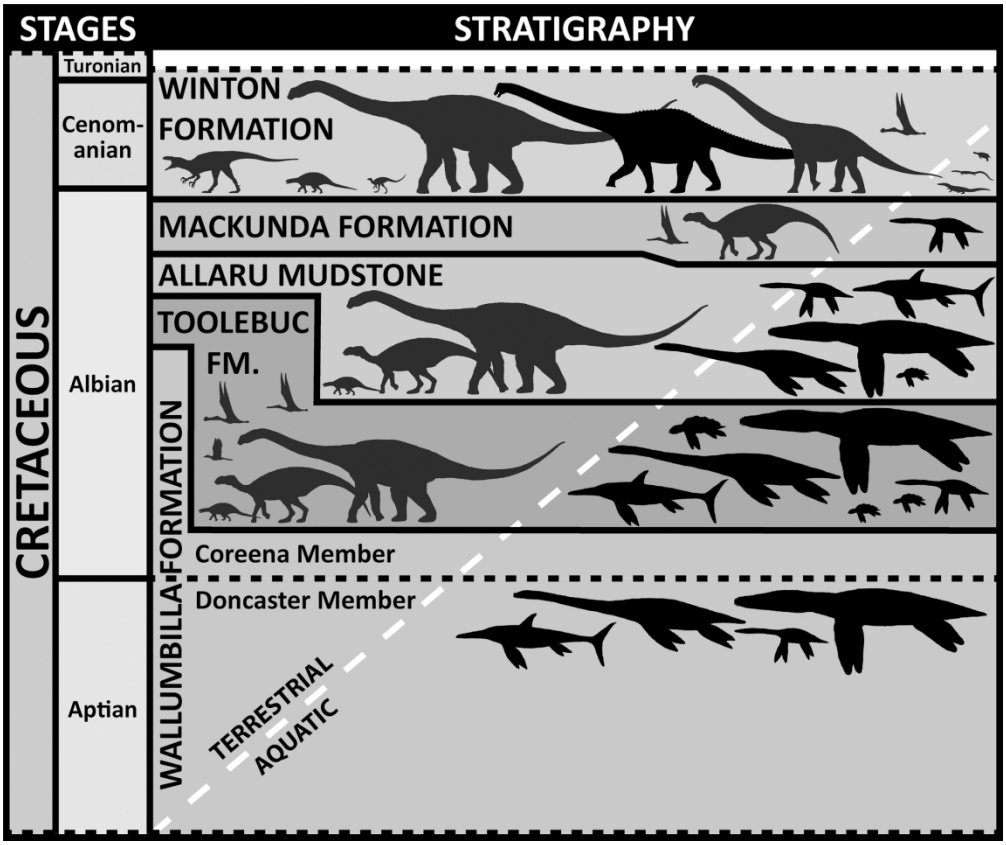

FIGURE 2. Stratigraphy of the Eromanga Basin, Queensland, with silhouettes representing known tetrapod taxa. WINTON FORMATION: *Australovenator wintonensis*; Ankylosauria indet.; Ornithopoda indet.; *Wintonotitan wattsi*; *Diamantinasaurus matildae*; *Savannasaurus elliottorum*; *Ferrodraco lentoni*; *Isisfordia duncani*; Varanoidea indet.; and Chelidae indet. MACKUNDA FORMATION: Ctenochasmatoidea indet.; *Muttaburrasaurus langdoni*; and Polycotylidae indet. ALLARU MUDSTONE (following faunal summary in Poropat et al. (2017)): *Kunbarrasaurus ieversi*; *Muttaburrasaurus* sp.; *Austrosaurus mckillopi*; Elasmosauridae indet.; Polycotylidae indet.; *Kronosaurus queenslandicus*; *Platypterygius australis*; and Chelonioidea indet. TOOLEBUC FORMATION (following faunal summary in Pentland and Poropat (2019)): *Mythunga camara*; *Aussiedraco molnari*; *Nanantius eos*; Ankylosauria indet.; Iguanodontia indet.; Titanosauriformes indet.; *Platypterygius australis*; *Eromangasaurus australis*; *Cratochelone berneyi*; *Kronosaurus queenslandicus*; *Bouliachelys suteri*; *Notochelone costata*; and Polycotylidae indet. WALLUMBILLA FORMATION (DONCASTER MEMBER): *Platypterygius* sp.; Elasmosauridae indet.; Polycotylidae indet.; and *Kronosaurus queenslandicus*.

182x153mm (300 x 300 DPI)

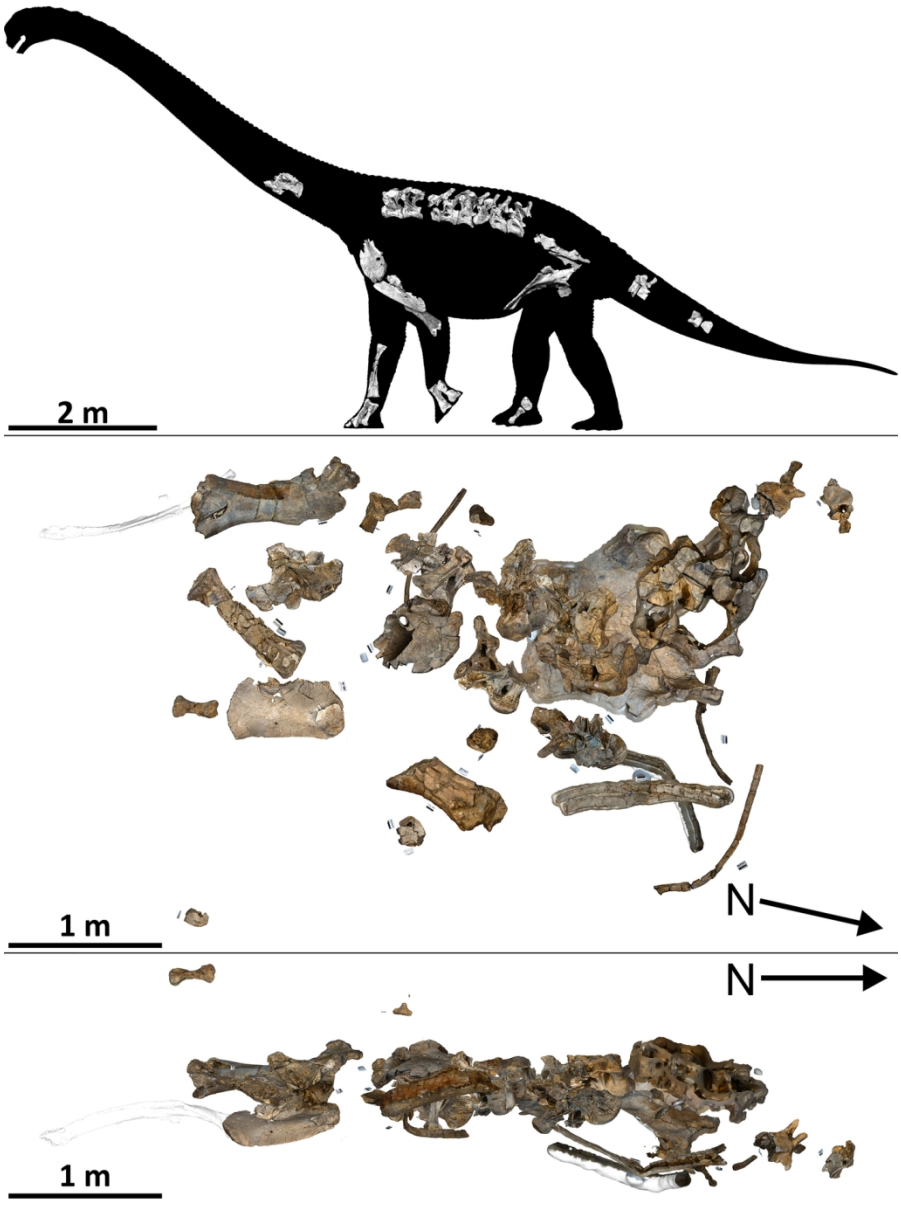

FIGURE 3. *Savannasaurus elliottorum* holotype specimen. **A**, Skeletal reconstruction, based on the preserved elements, by Travis Tischler (modified from Poropat et al., 2016). **B–C**, 'Ho-Hum' Site (AODL 82) map in **B**, bird's-eye view (from Poropat et al., 2016) and **C**, sub-surface view.

122x163mm (300 x 300 DPI)

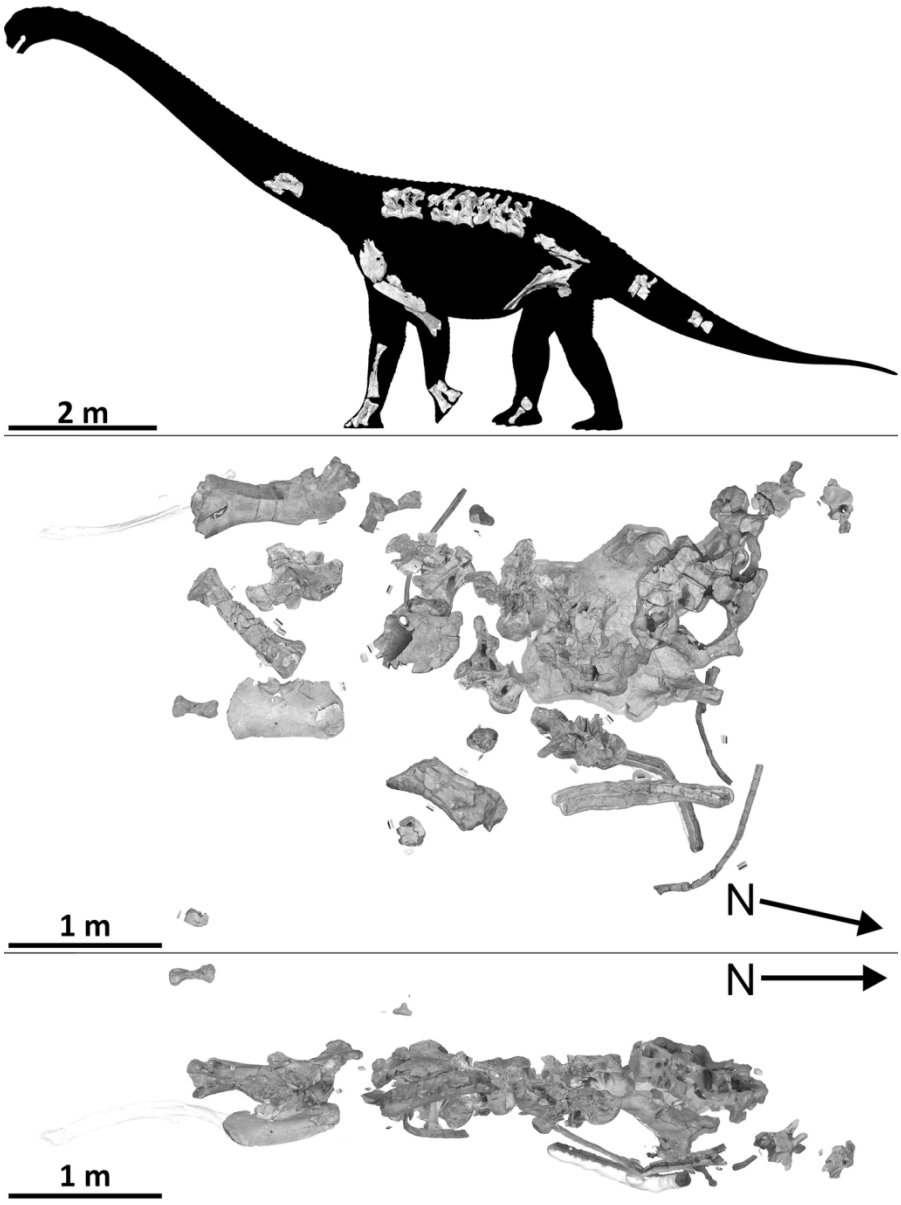

FIGURE 3. *Savannasaurus elliottorum* holotype specimen. **A**, Skeletal reconstruction, based on the preserved elements, by Travis Tischler (modified from Poropat et al., 2016). **B–C**, 'Ho-Hum' Site (AODL 82) map in **B**, bird's-eye view (from Poropat et al., 2016) and **C**, sub-surface view.

122x163mm (300 x 300 DPI)

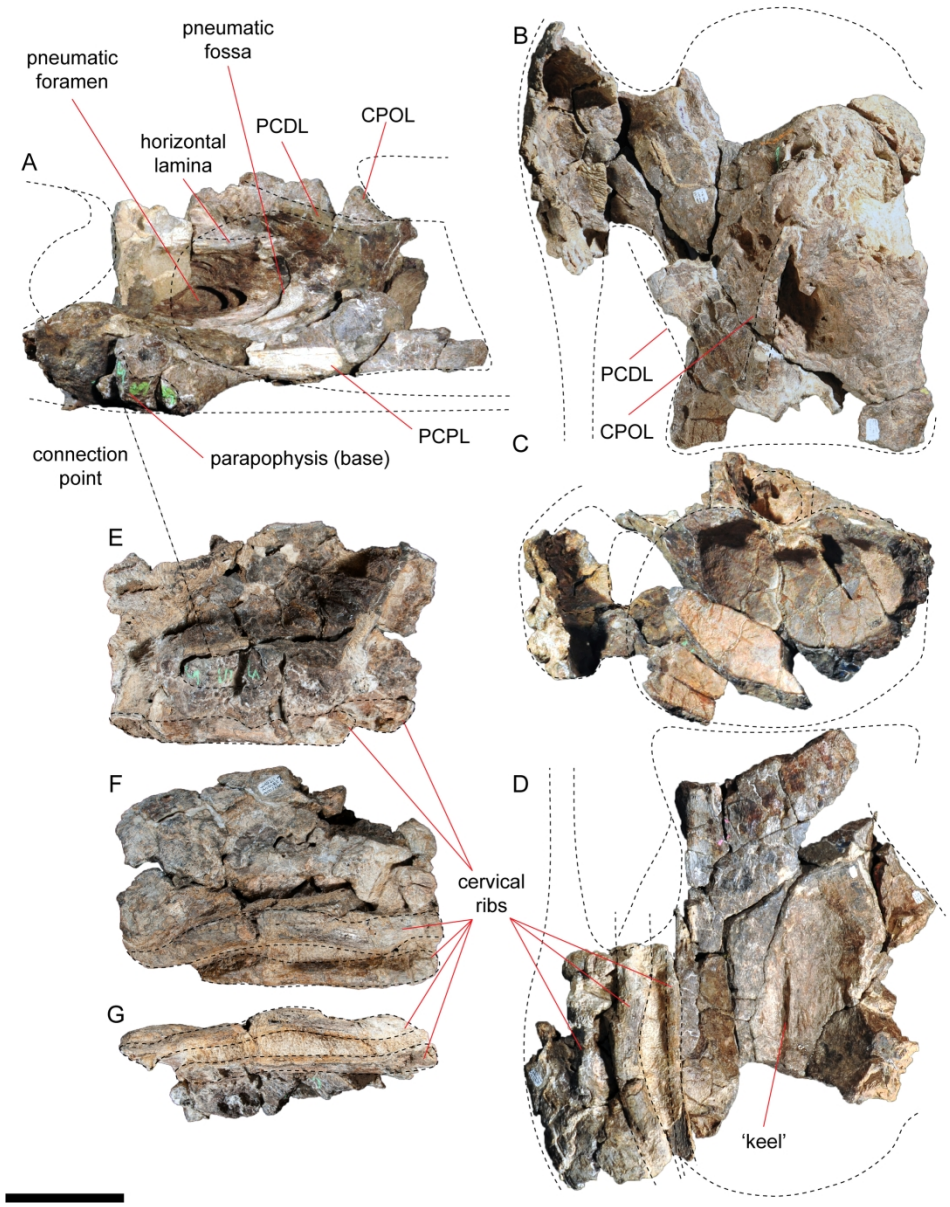

FIGURE 4. *Savannasaurus elliottorum* posterior cervical vertebra in **A**, left lateral, **B**, dorsal (with anterior to top), **C**, posterior, and **D**, ventral (with anterior to bottom) views, and left cervical ribs in **E**, medial, **F**, lateral and **G**, ventral views. Scale bar equals 100 mm.

182x232mm (300 x 300 DPI)

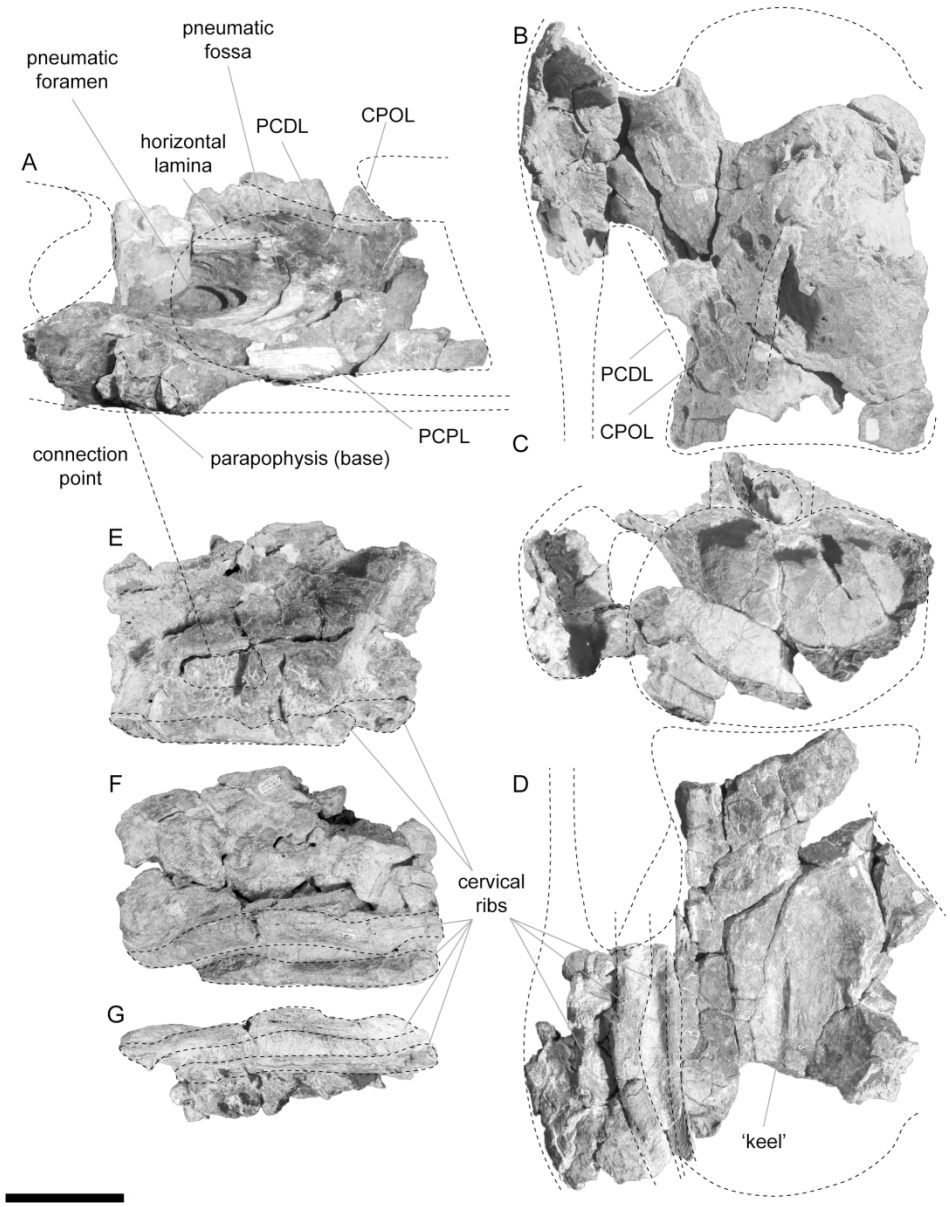

FIGURE 4. *Savannasaurus elliottorum* posterior cervical vertebra in **A**, left lateral, **B**, dorsal (with anterior to top), **C**, posterior, and **D**, ventral (with anterior to bottom) views, and left cervical ribs in **E**, medial, **F**, lateral and **G**, ventral views. Scale bar equals 100 mm.

182x232mm (300 x 300 DPI)

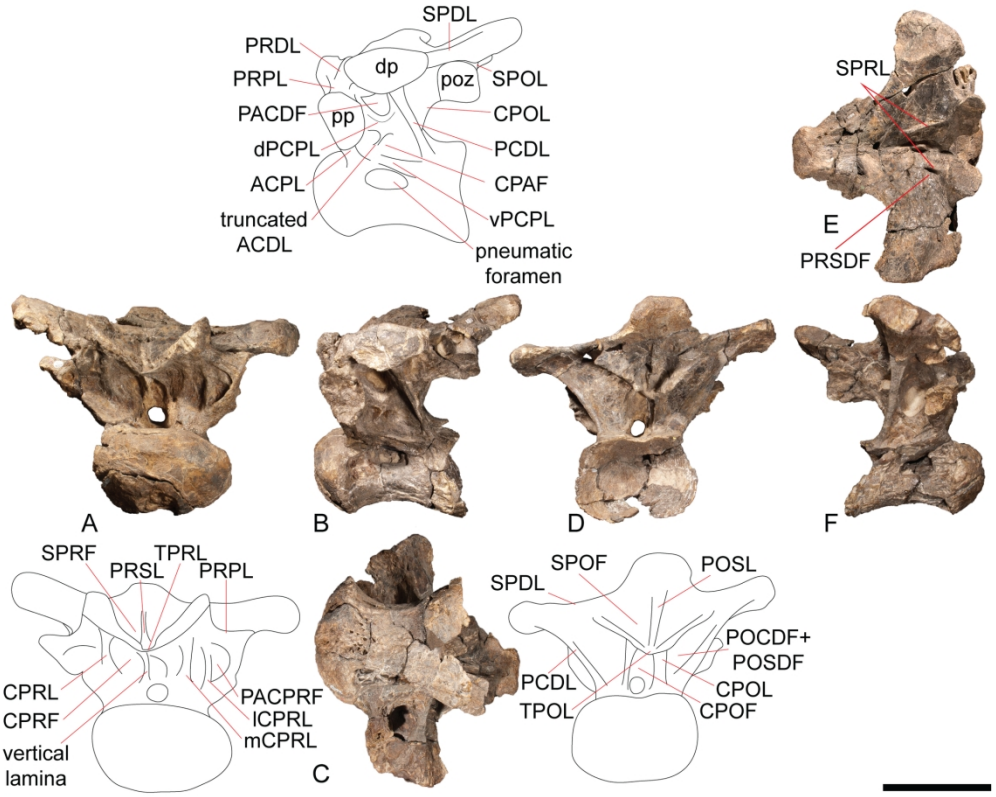

FIGURE 5. *Savannasaurus elliottorum* dorsal vertebra III in **A**, anterior, **B**, left lateral, **C**, ventral, **D**, posterior, **E**, dorsal, and **F**, right lateral views. Scale bar equals 200 mm.

182x146mm (300 x 300 DPI)

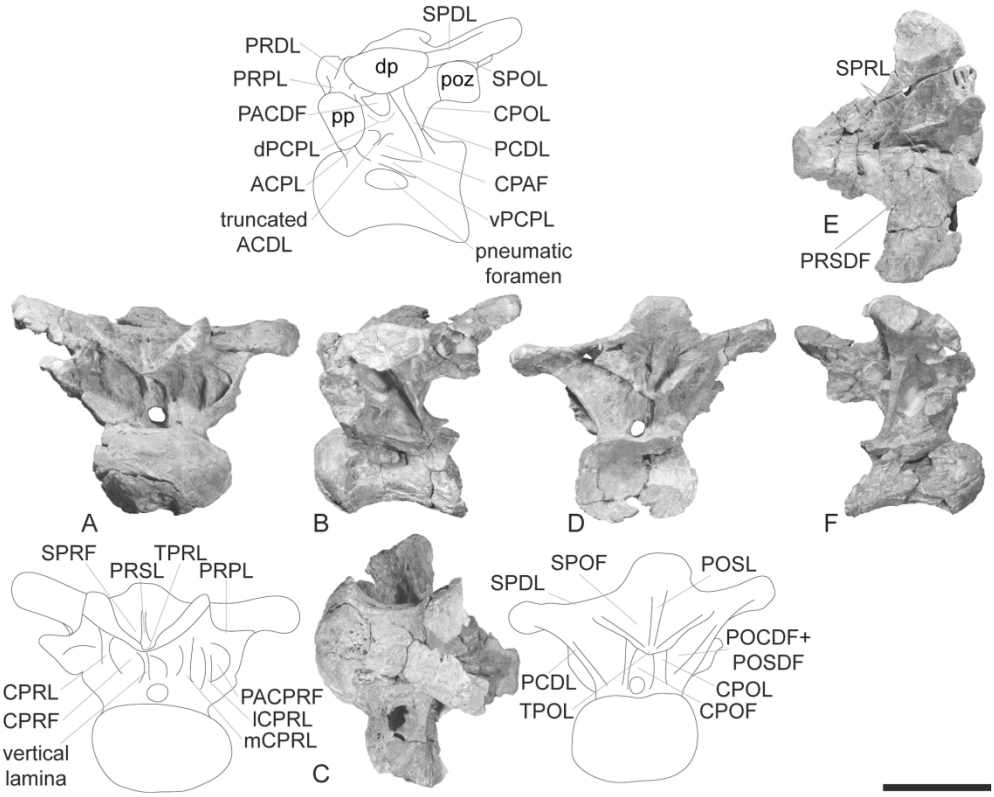

FIGURE 5. *Savannasaurus elliottorum* dorsal vertebra III in **A**, anterior, **B**, left lateral, **C**, ventral, **D**, posterior, **E**, dorsal, and **F**, right lateral views. Scale bar equals 200 mm.

182x146mm (300 x 300 DPI)

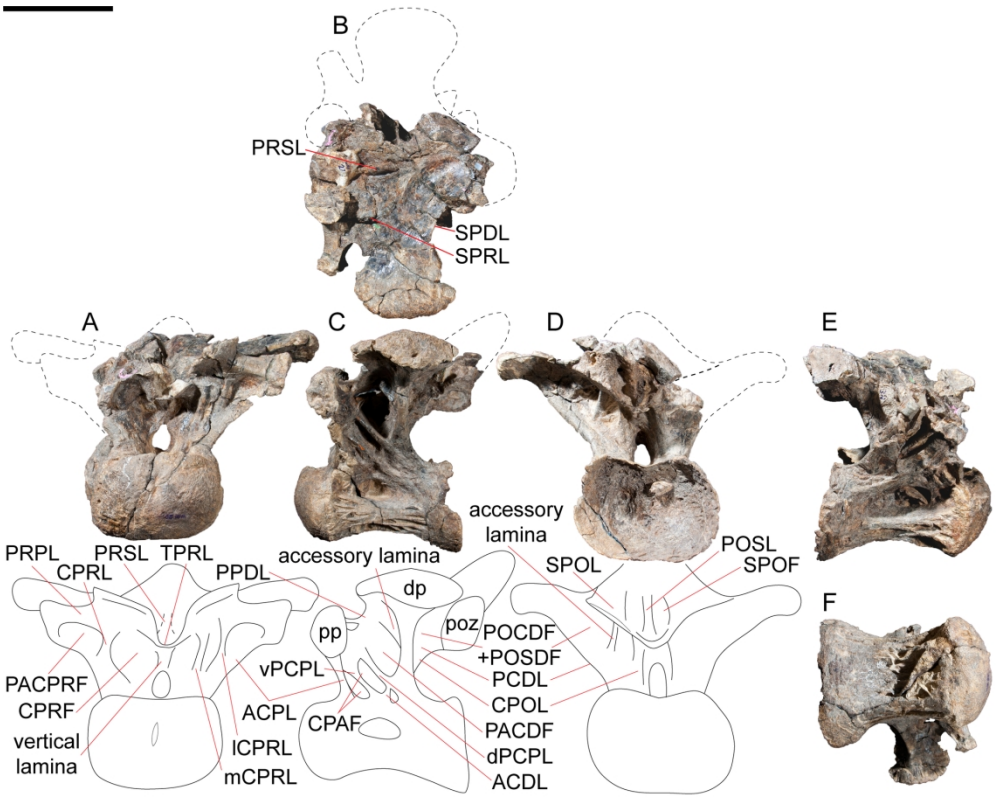

FIGURE 6. *Savannasaurus elliottorum* dorsal vertebra IV in **A**, anterior, **B**, dorsal, **C**, left lateral, **D**, posterior, **E**, right lateral, and **F**, ventral views. Scale bar equals 200 mm.

182x144mm (300 x 300 DPI)

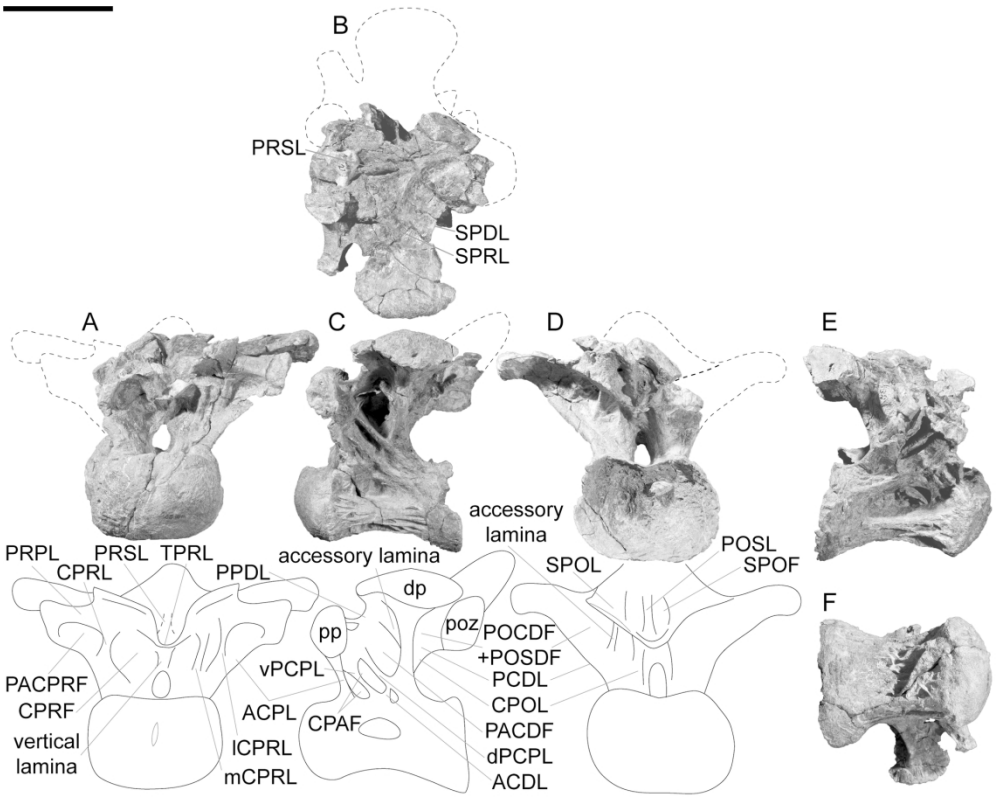

FIGURE 6. *Savannasaurus elliottorum* dorsal vertebra IV in **A**, anterior, **B**, dorsal, **C**, left lateral, **D**, posterior, **E**, right lateral, and **F**, ventral views. Scale bar equals 200 mm.

182x144mm (300 x 300 DPI)

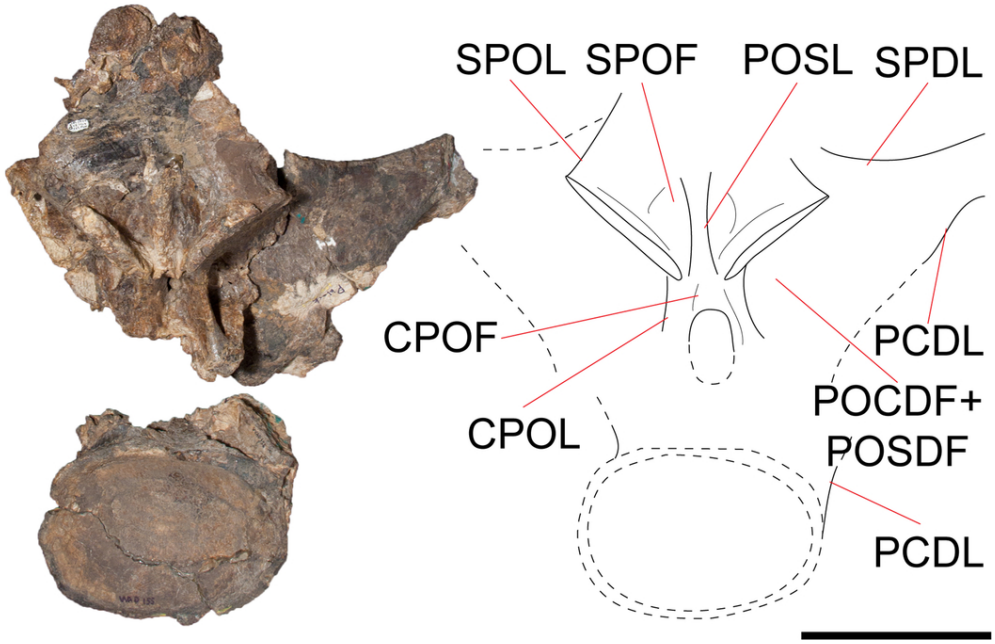

FIGURE 7. *Savannasaurus elliottorum* dorsal vertebra V in posterior view. Scale bar equals 200 mm.

90x57mm (300 x 300 DPI)

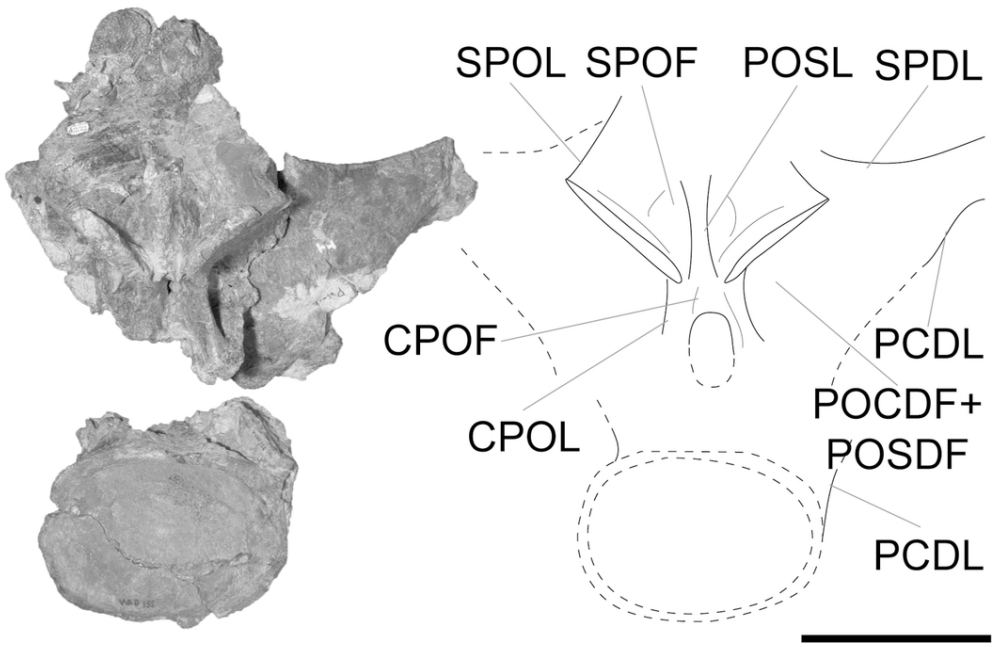

FIGURE 7. *Savannasaurus elliottorum* dorsal vertebra V in posterior view. Scale bar equals 200 mm.

90x57mm (300 x 300 DPI)

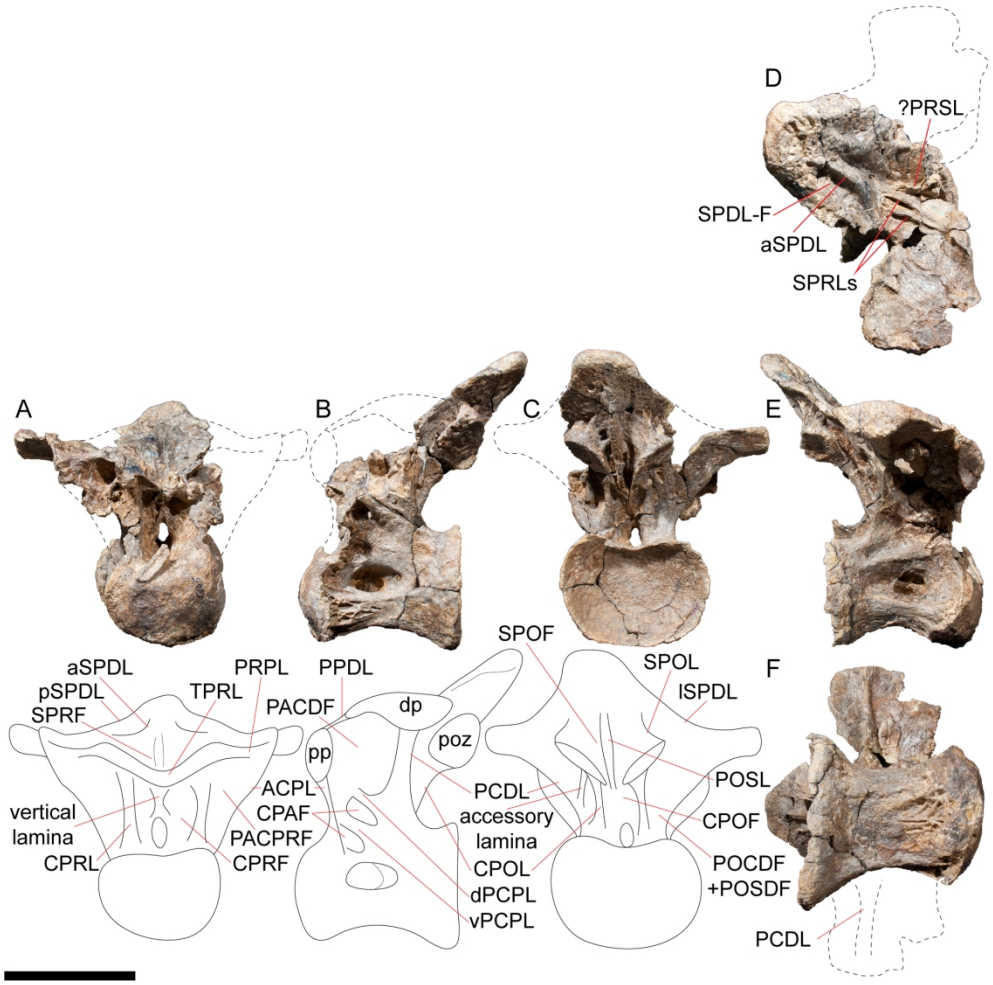

FIGURE 8. *Savannasaurus elliottorum* dorsal vertebra VI in **A**, anterior, **B**, left lateral, **C**, posterior, **D**, dorsal, **E**, right lateral, and **F**, ventral views. Scale bar equals 200 mm.

182x178mm (300 x 300 DPI)

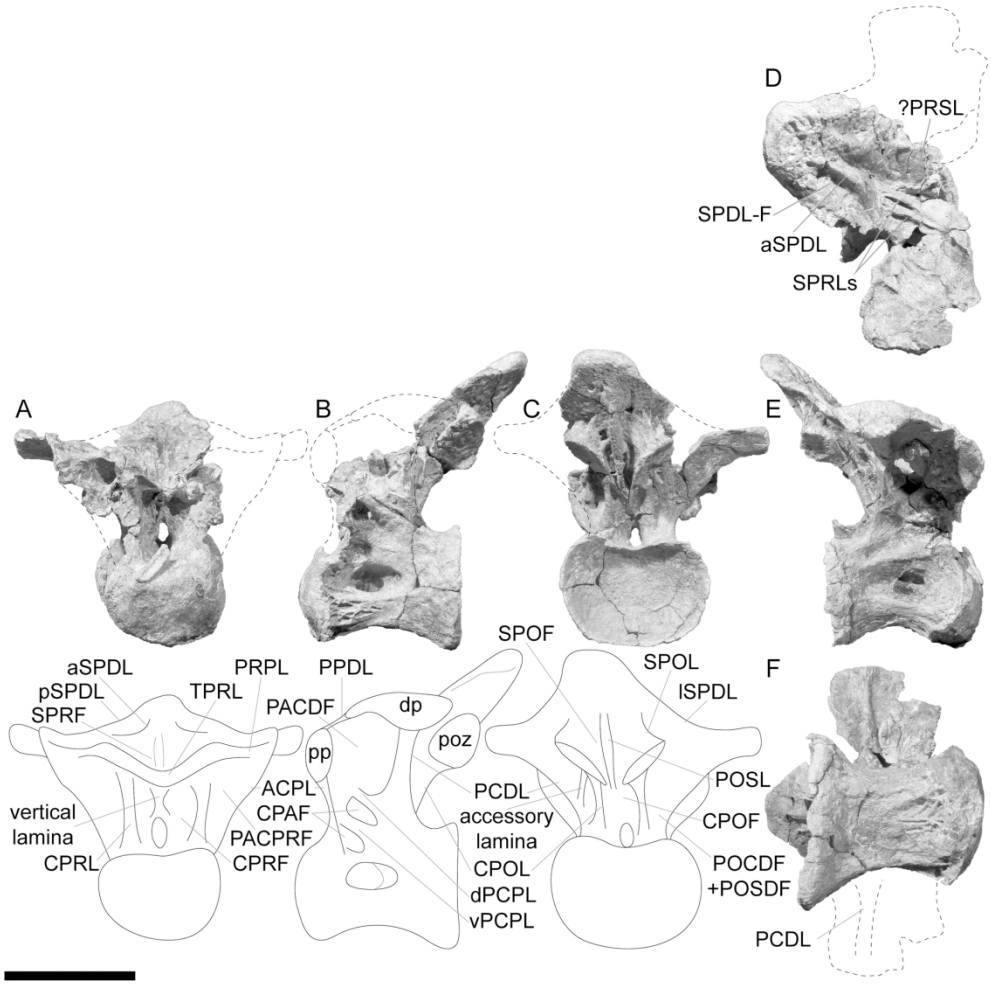

FIGURE 8. *Savannasaurus elliottorum* dorsal vertebra VI in **A**, anterior, **B**, left lateral, **C**, posterior, **D**, dorsal, **E**, right lateral, and **F**, ventral views. Scale bar equals 200 mm.

182x178mm (300 x 300 DPI)

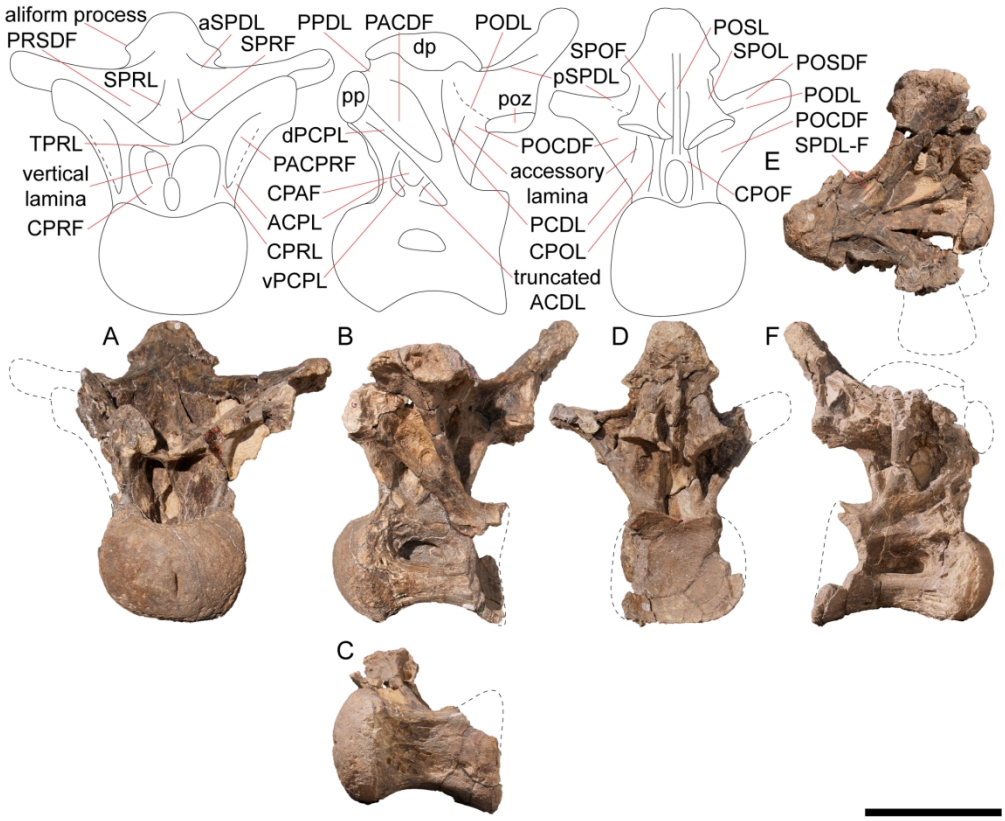

FIGURE 9. *Savannasaurus elliottorum* dorsal vertebra VII in **A**, anterior, **B**, left lateral, **C**, ventral, **D**, posterior, **E**, dorsal, and **F**, right lateral views. Scale bar equals 200 mm.

182x149mm (300 x 300 DPI)

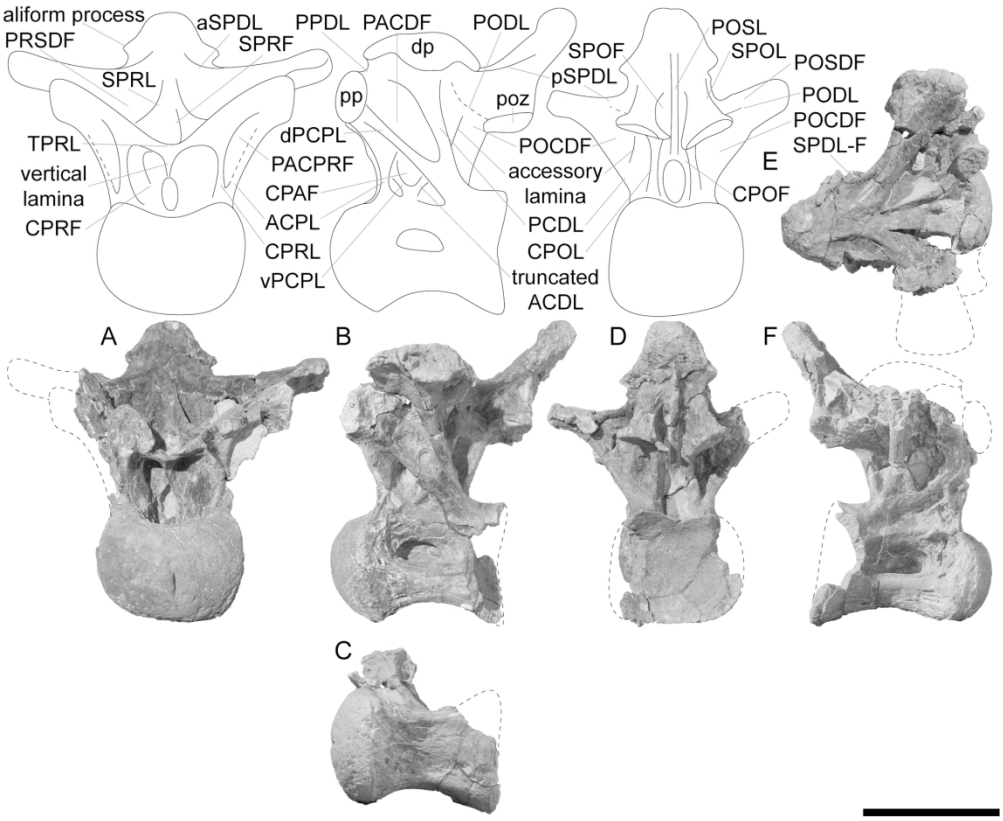

FIGURE 9. *Savannasaurus elliottorum* dorsal vertebra VII in **A**, anterior, **B**, left lateral, **C**, ventral, **D**, posterior, **E**, dorsal, and **F**, right lateral views. Scale bar equals 200 mm.

182x149mm (300 x 300 DPI)

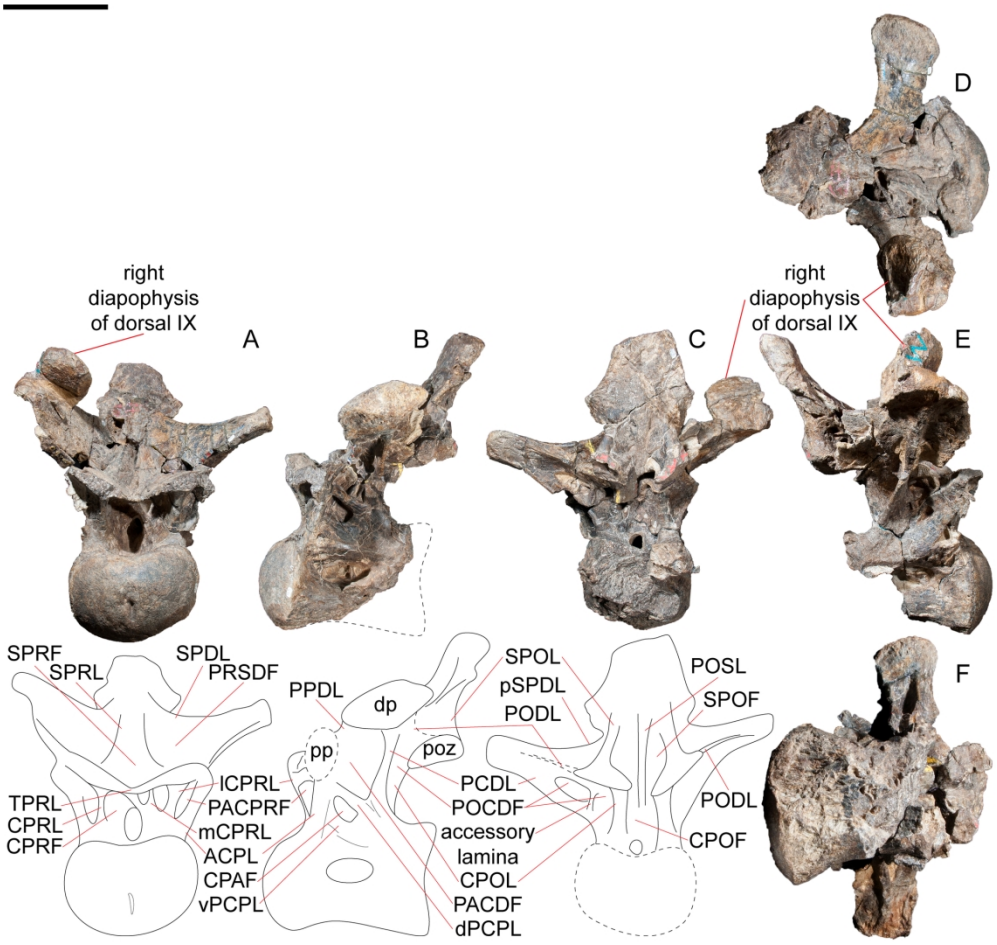

FIGURE 10. *Savannasaurus elliottorum* dorsal vertebra VIII in **A**, anterior, **B**, left lateral, **C**, posterior, **D**, dorsal, **E**, right lateral, and **F**, ventral views. Scale bar equals 200 mm.

182x172mm (300 x 300 DPI)

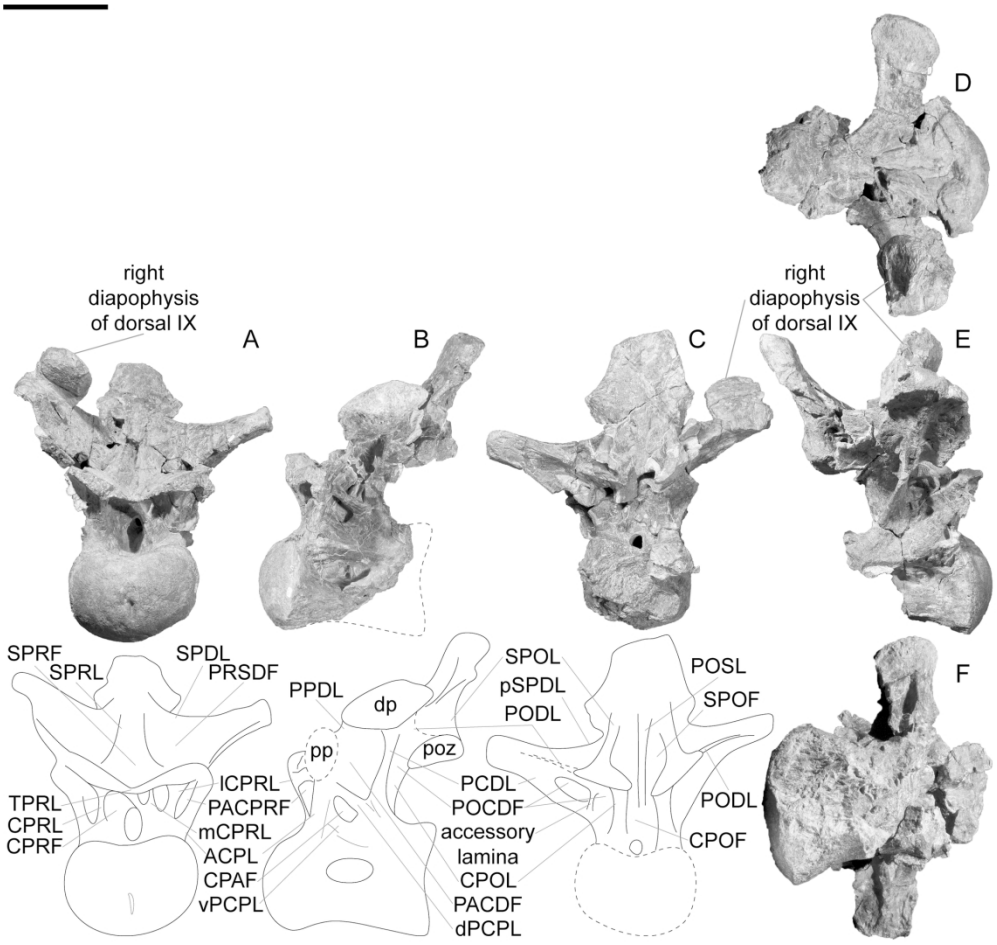

FIGURE 10. *Savannasaurus elliottorum* dorsal vertebra VIII in **A**, anterior, **B**, left lateral, **C**, posterior, **D**, dorsal, **E**, right lateral, and **F**, ventral views. Scale bar equals 200 mm.

182x172mm (300 x 300 DPI)

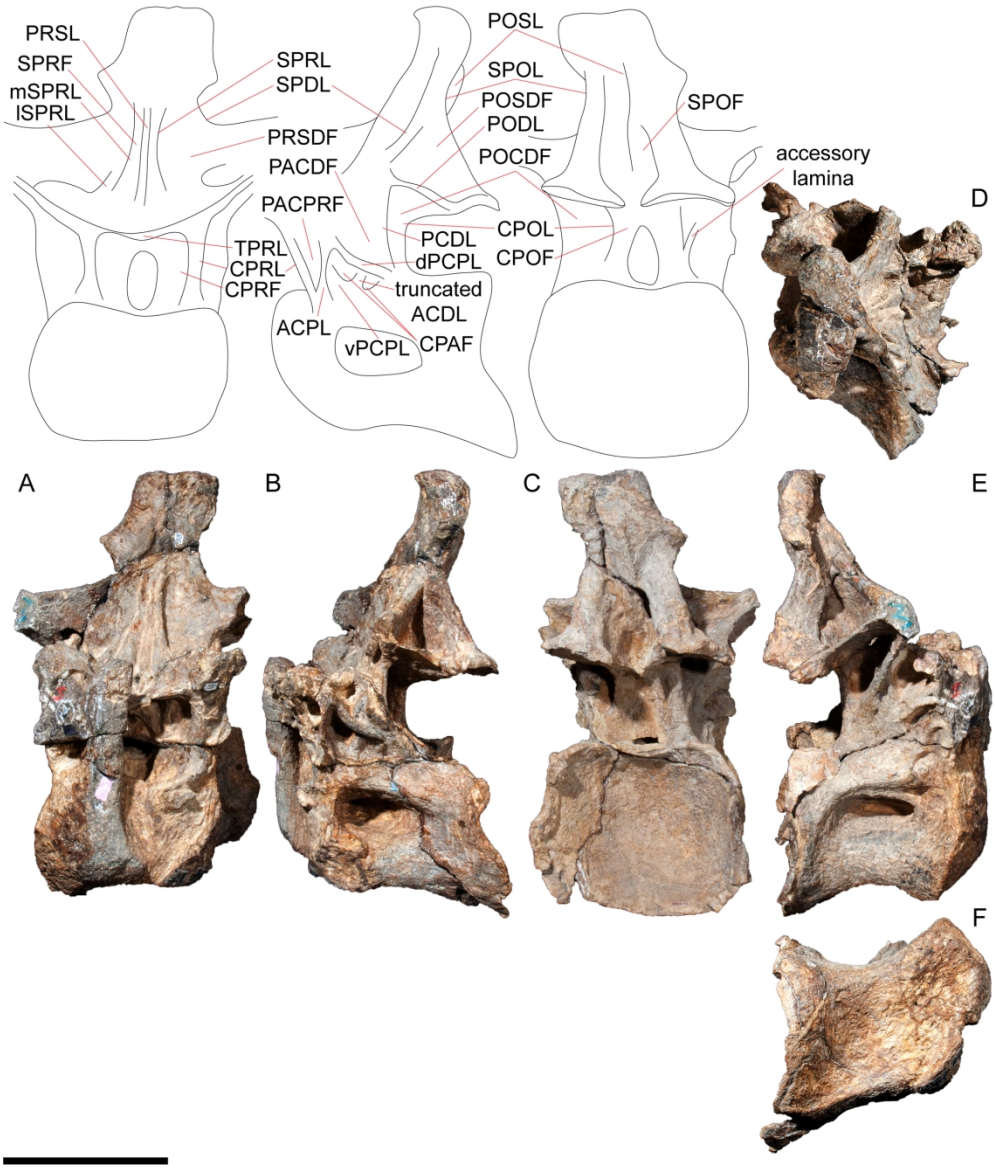

FIGURE 11. *Savannasaurus elliottorum* dorsal vertebra IX in **A**, anterior, **B**, left lateral, **C**, posterior, **D**, dorsal, **E**, right lateral, and **F**, ventral views. Scale bar equals 200 mm.

182x213mm (300 x 300 DPI)

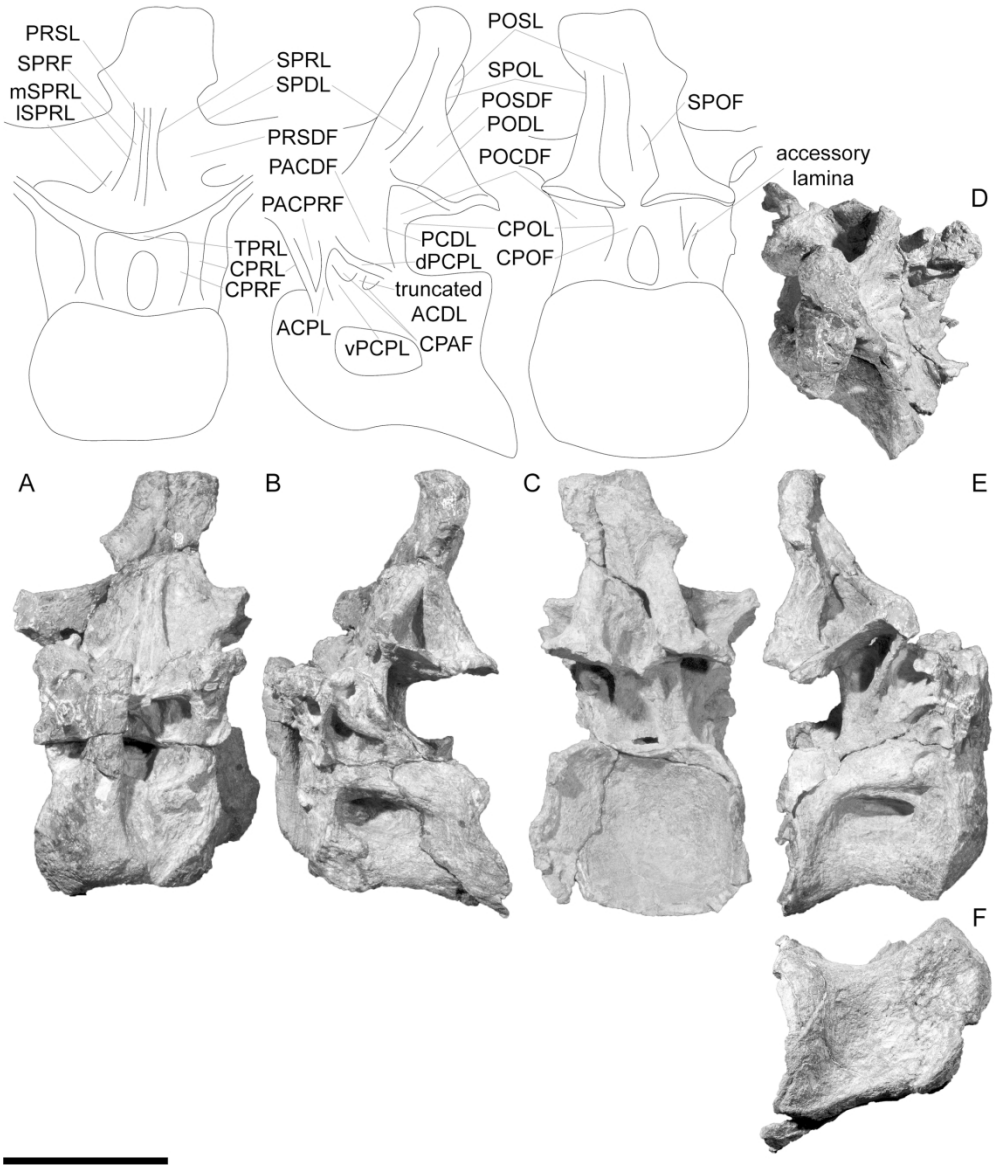

FIGURE 11. *Savannasaurus elliottorum* dorsal vertebra IX in **A**, anterior, **B**, left lateral, **C**, posterior, **D**, dorsal, **E**, right lateral, and **F**, ventral views. Scale bar equals 200 mm.

182x213mm (300 x 300 DPI)

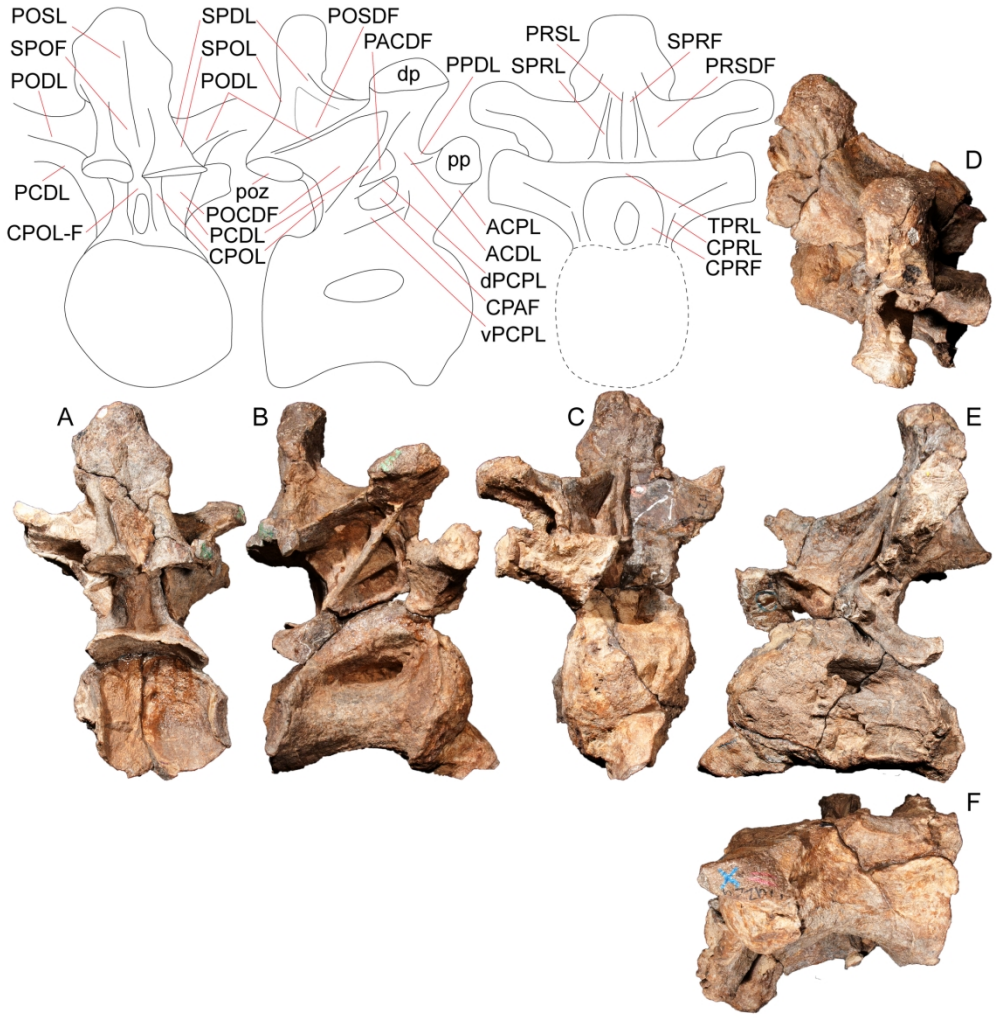

FIGURE 12. *Savannasaurus elliottorum* dorsal vertebra X in **A**, posterior, **B**, right lateral, **C**, anterior, **D**, dorsal, **E**, left lateral, and **F**, ventral views. Scale bar equals 200 mm.

182x188mm (300 x 300 DPI)

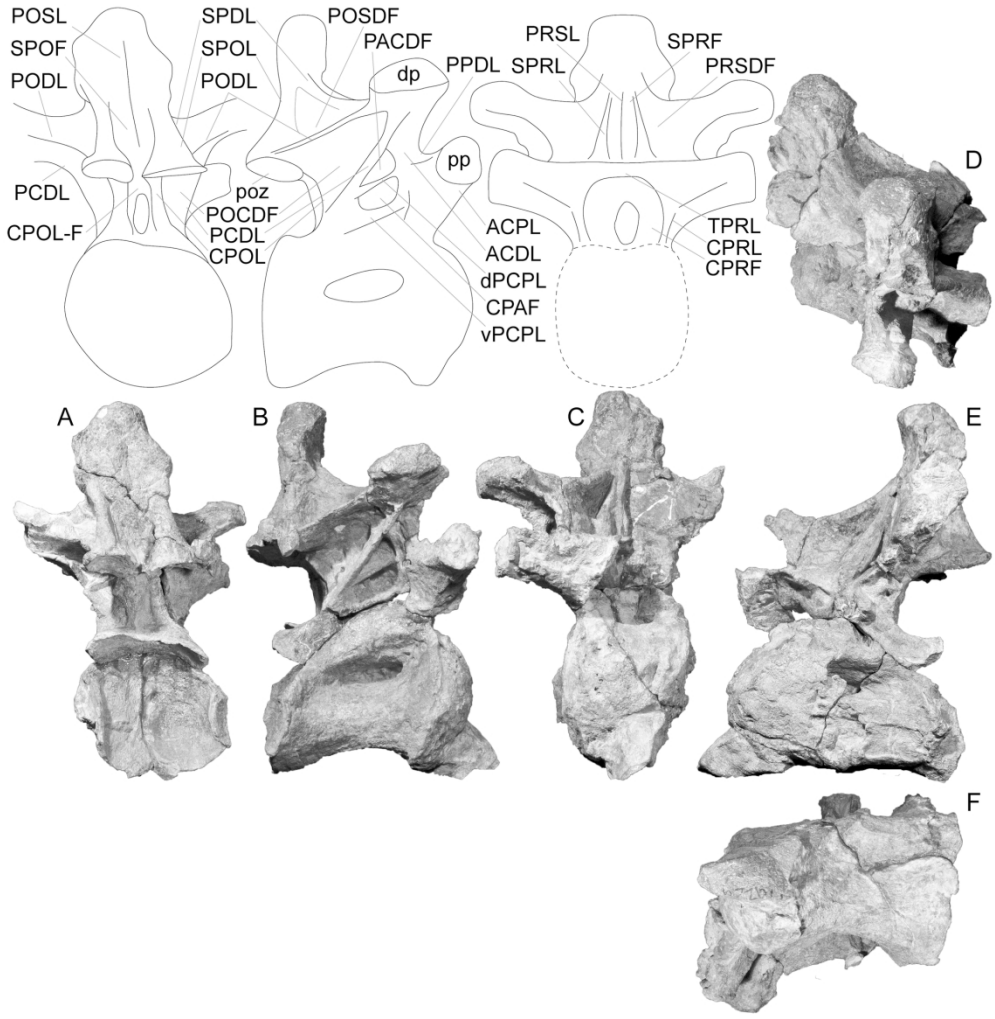

FIGURE 12. *Savannasaurus elliottorum* dorsal vertebra X in **A**, posterior, **B**, right lateral, **C**, anterior, **D**, dorsal, **E**, left lateral, and **F**, ventral views. Scale bar equals 200 mm.

182x188mm (300 x 300 DPI)

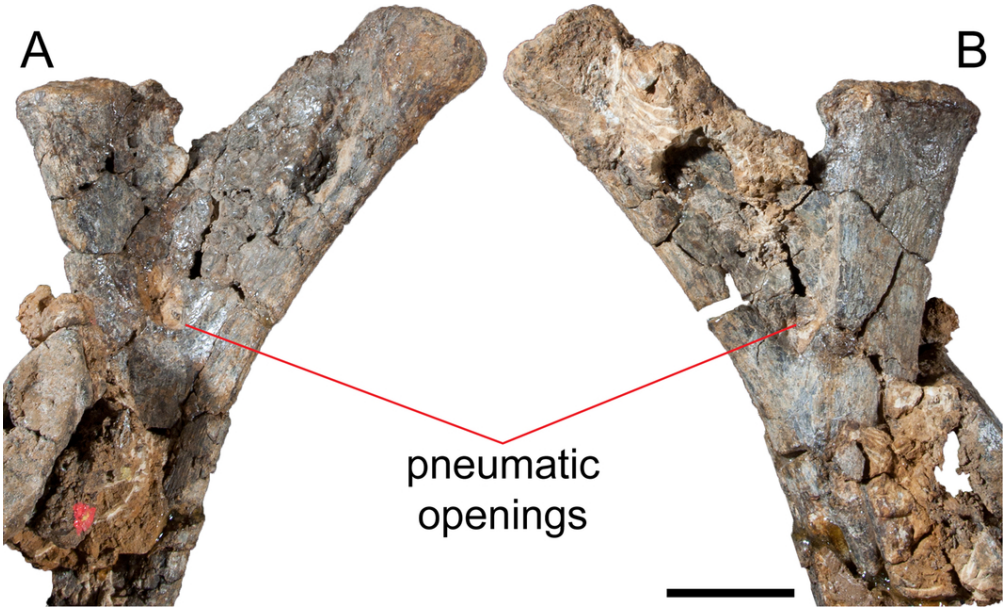

FIGURE 13. *Savannasaurus elliottorum* dorsal rib head in **A**, posterior and **B**, anterior views. Scale bar equals 50 mm.

90x54mm (300 x 300 DPI)

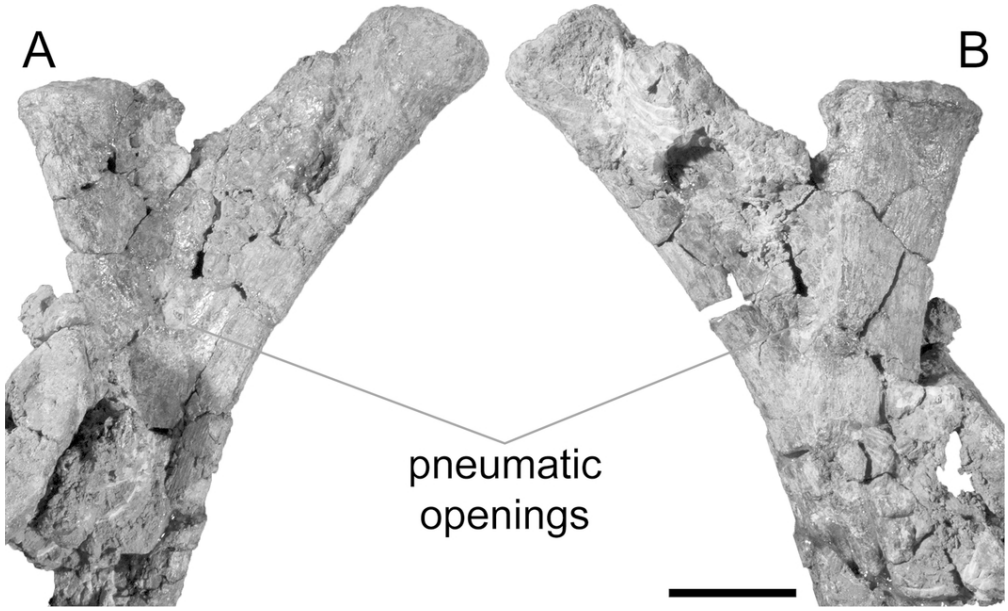

FIGURE 13. *Savannasaurus elliottorum* dorsal rib head in **A**, posterior and **B**, anterior views. Scale bar equals 50 mm.

90x54mm (300 x 300 DPI)

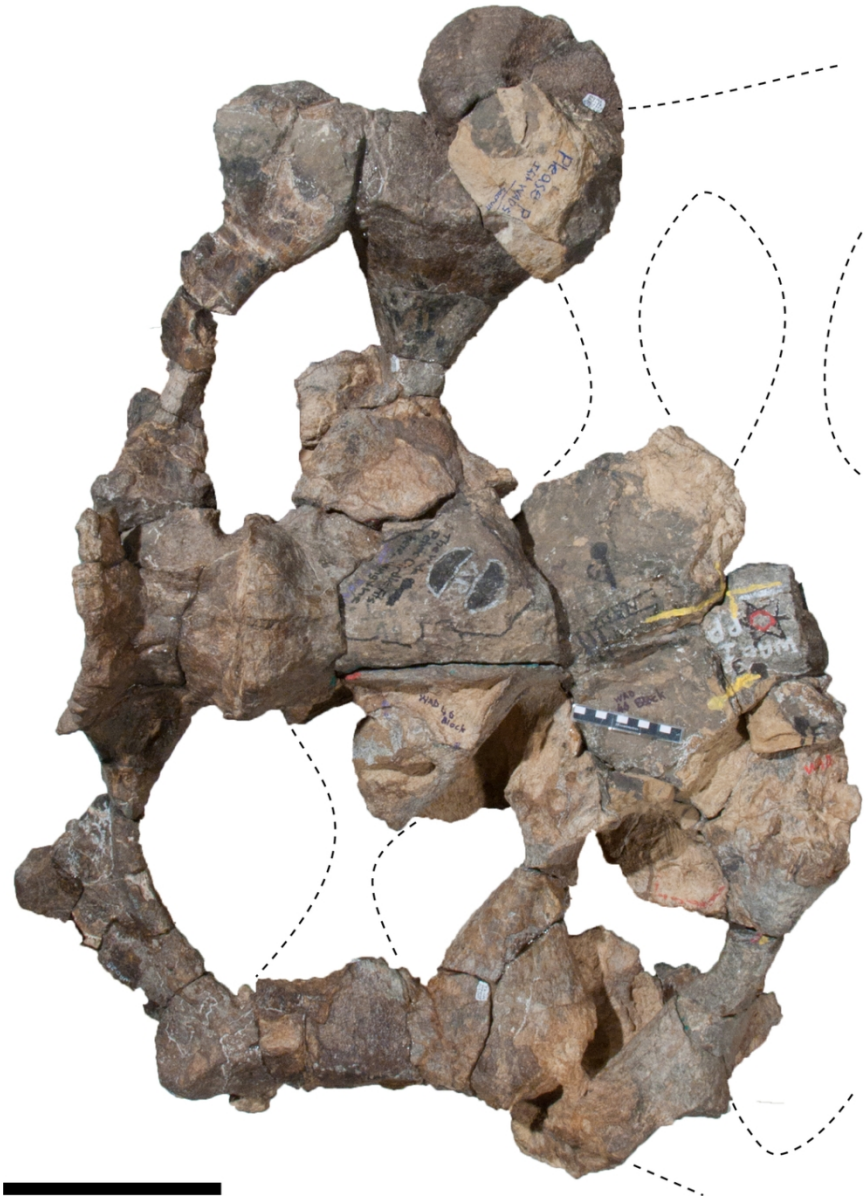

FIGURE 14. *Savannasaurus elliottorum* sacrum in ventral view (posterior to the left, anterior to the right). Scale bar equals 200 mm.

90x123mm (300 x 300 DPI)

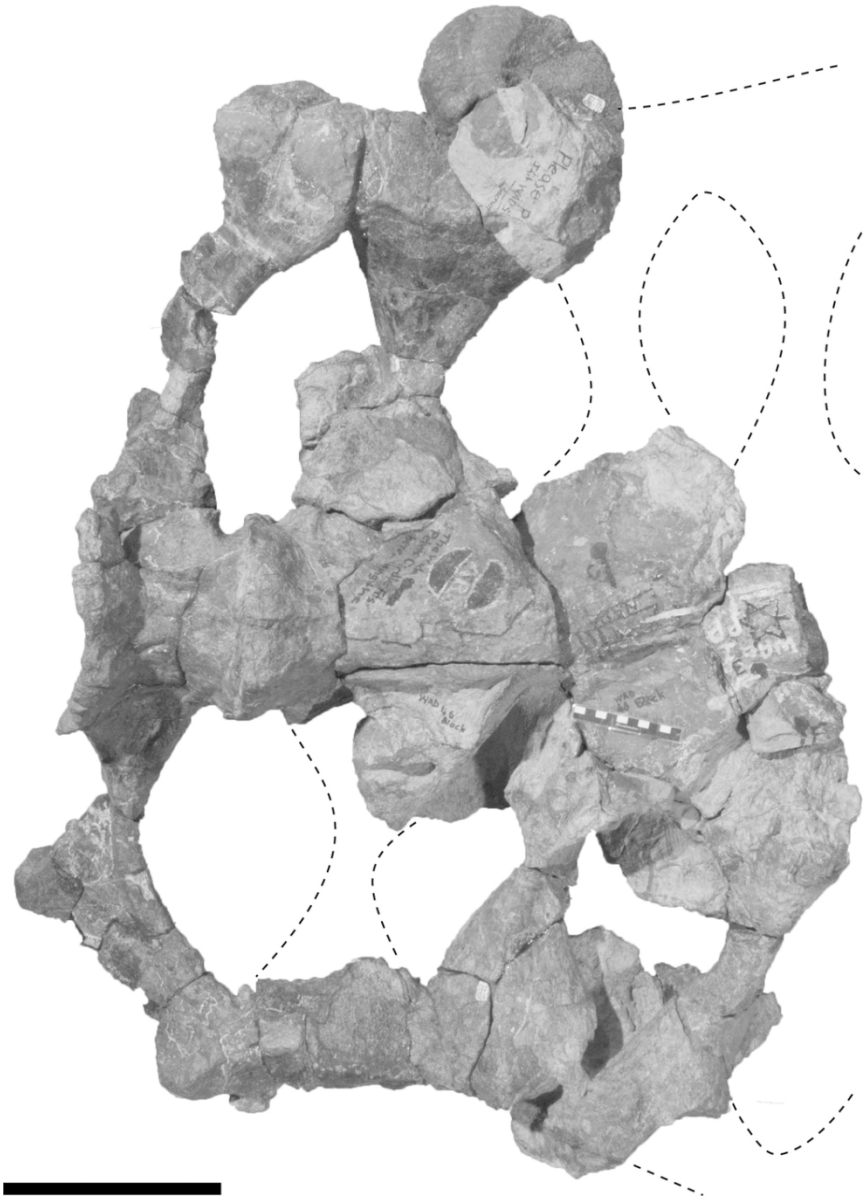

FIGURE 14. *Savannasaurus elliottorum* sacrum in ventral view (posterior to the left, anterior to the right). Scale bar equals 200 mm.

90x123mm (300 x 300 DPI)

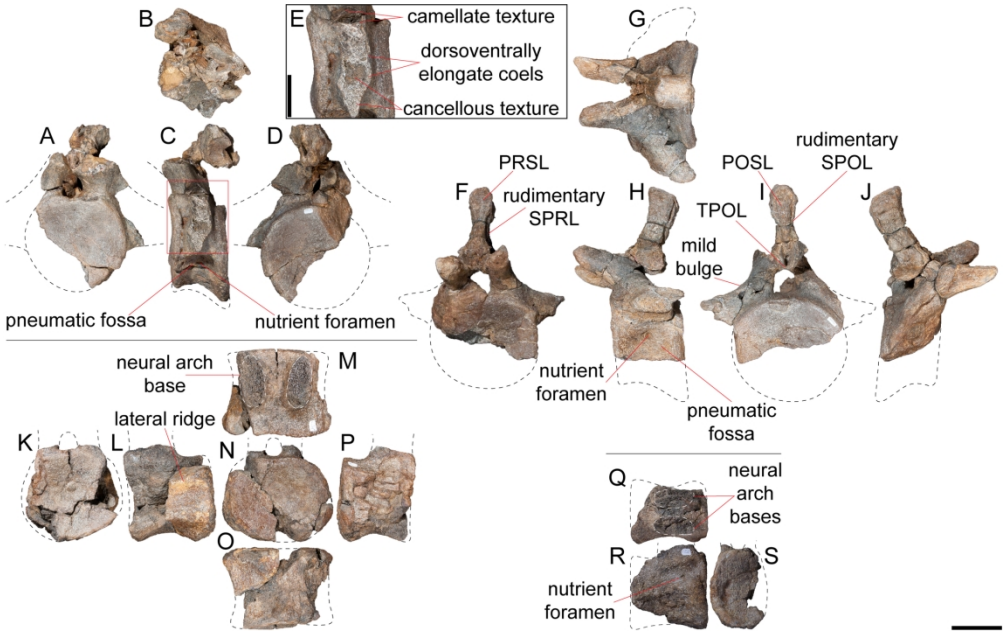

FIGURE 15. *Savannasaurus elliottorum* caudal vertebrae. Caudal vertebra A in **A**, anterior, **B**, dorsal, **C**, left lateral, and **D**, posterior views, and **E**, broken left neural arch in lateral view. Caudal vertebra B in **F**, anterior, **G**, dorsal, **H**, left lateral, **I**, posterior, and **J**, right lateral views. Caudal vertebra C in **K**, anterior, **L**, left lateral, **M**, dorsal, **N**, posterior, **O**, ventral, and **P**, right lateral views. Caudal vertebra D in **Q**, dorsal, **R**, right lateral, and **S**, anterior views. Scale bar for **A–D** and **F–S** equals 100 mm; scale bar for **E** equals 50 mm.

182x114mm (300 x 300 DPI)

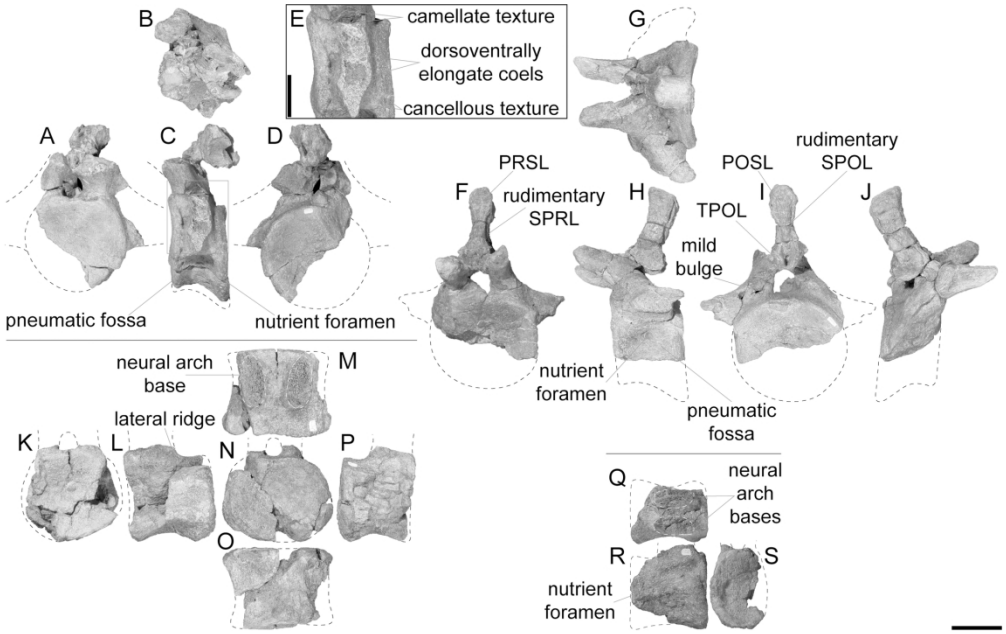

FIGURE 15. *Savannasaurus elliottorum* caudal vertebrae. Caudal vertebra A in **A**, anterior, **B**, dorsal, **C**, left lateral, and **D**, posterior views, and **E**, broken left neural arch in lateral view. Caudal vertebra B in **F**, anterior, **G**, dorsal, **H**, left lateral, **I**, posterior, and **J**, right lateral views. Caudal vertebra C in **K**, anterior, **L**, left lateral, **M**, dorsal, **N**, posterior, **O**, ventral, and **P**, right lateral views. Caudal vertebra D in **Q**, dorsal, **R**, right lateral, and **S**, anterior views. Scale bar for **A–D** and **F–S** equals 100 mm; scale bar for **E** equals 50 mm.

182x114mm (300 x 300 DPI)

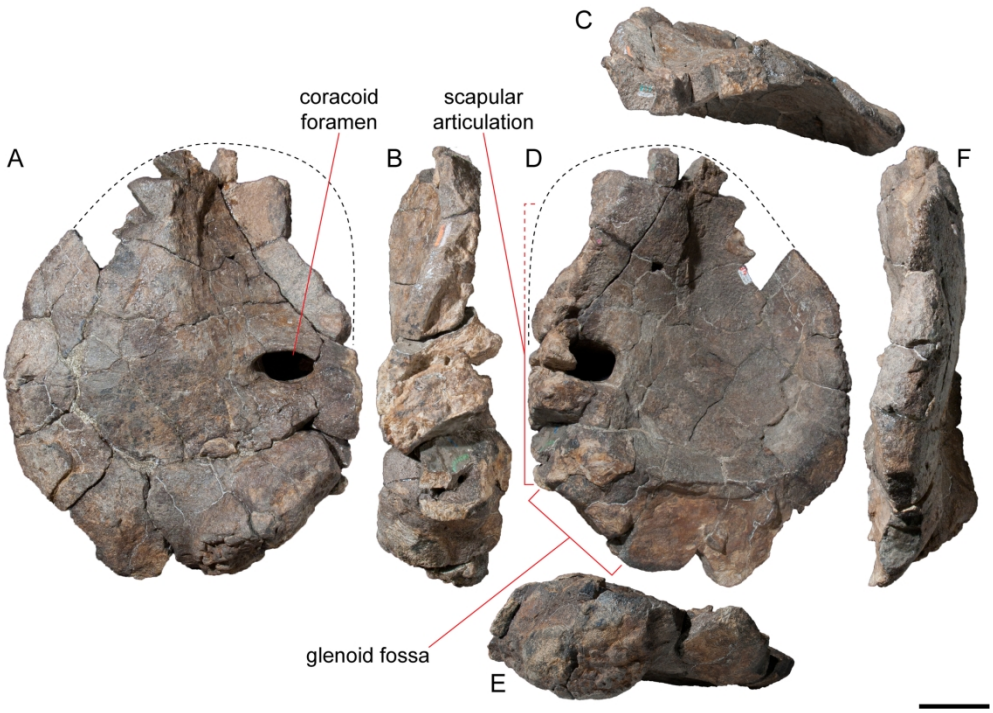

FIGURE 16. *Savannasaurus elliottorum* left coracoid in **A**, lateral, **B**, posterior, **C**, dorsal, **D**, medial, **E**, ventral, and **F**, anterior views. Scale bar equals 100 mm.

182x129mm (300 x 300 DPI)

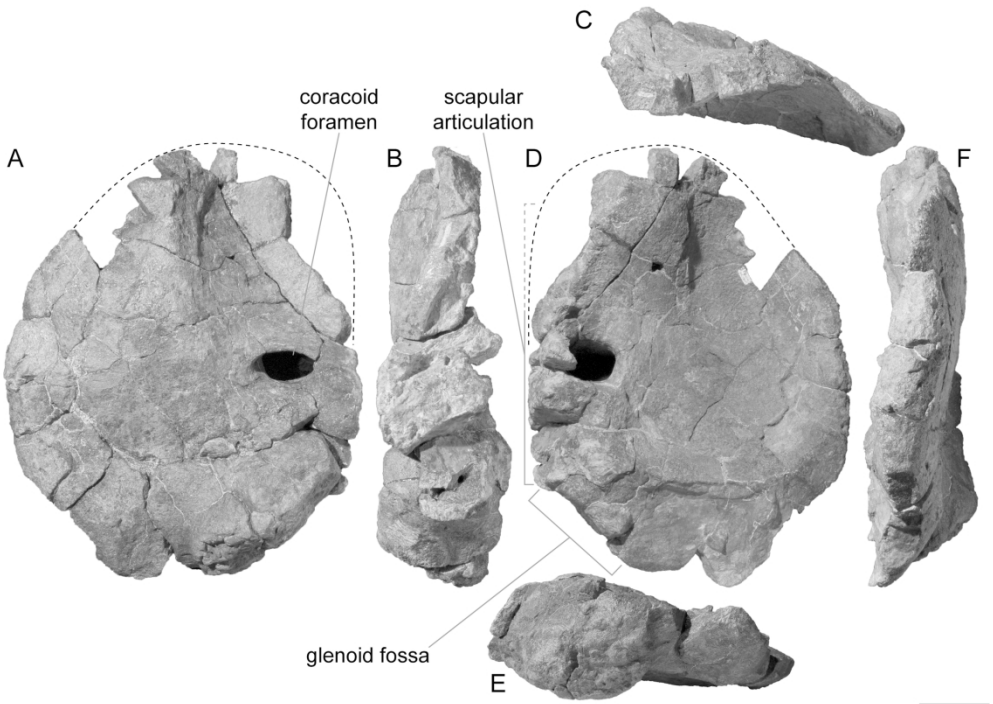

FIGURE 16. *Savannasaurus elliottorum* left coracoid in **A**, lateral, **B**, posterior, **C**, dorsal, **D**, medial, **E**, ventral, and **F**, anterior views. Scale bar equals 100 mm.

182x129mm (300 x 300 DPI)

FIGURE 17. *Savannasaurus elliottorum* left sternal plate in **A**, ventral and **B**, dorsal views, with the anterior end towards the top of the page. The dashed line represents the division between the convex portion of the ventral surface (medial to the line) and the concave portion (lateral to the line). Scale bar equals 200 mm.

90x73mm (300 x 300 DPI)

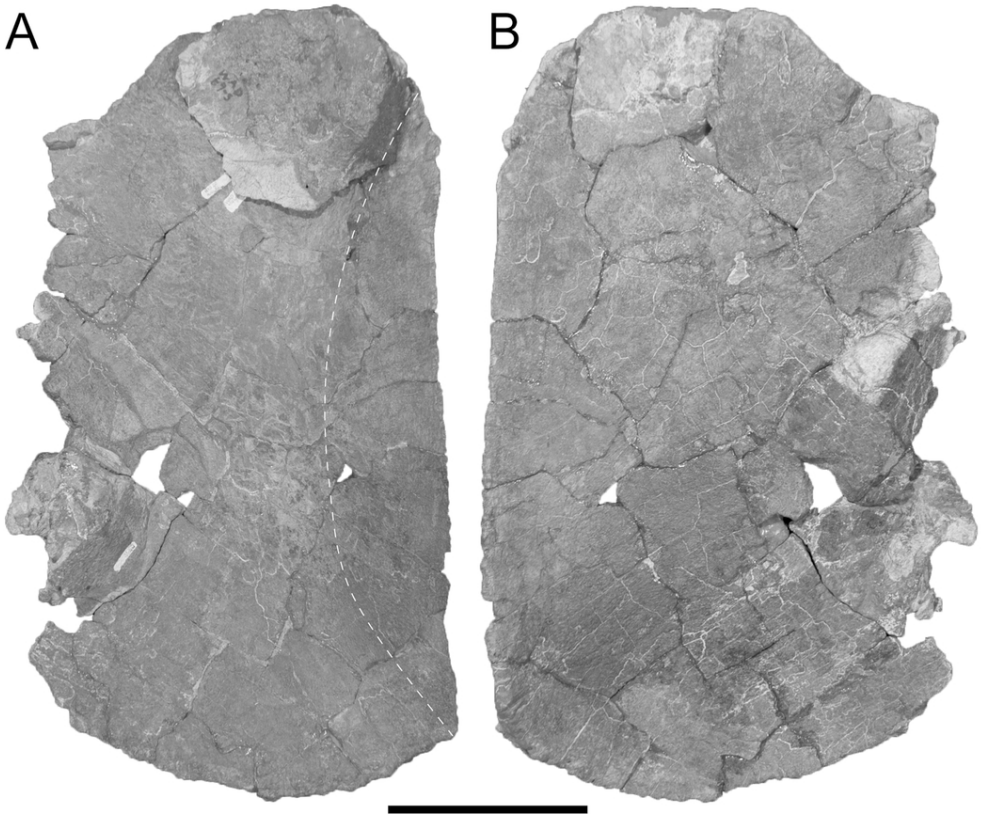

FIGURE 17. *Savannasaurus elliottorum* left sternal plate in **A**, ventral and **B**, dorsal views, with the anterior end towards the top of the page. The dashed line represents the division between the convex portion of the ventral surface (medial to the line) and the concave portion (lateral to the line). Scale bar equals 200 mm.

90x73mm (300 x 300 DPI)

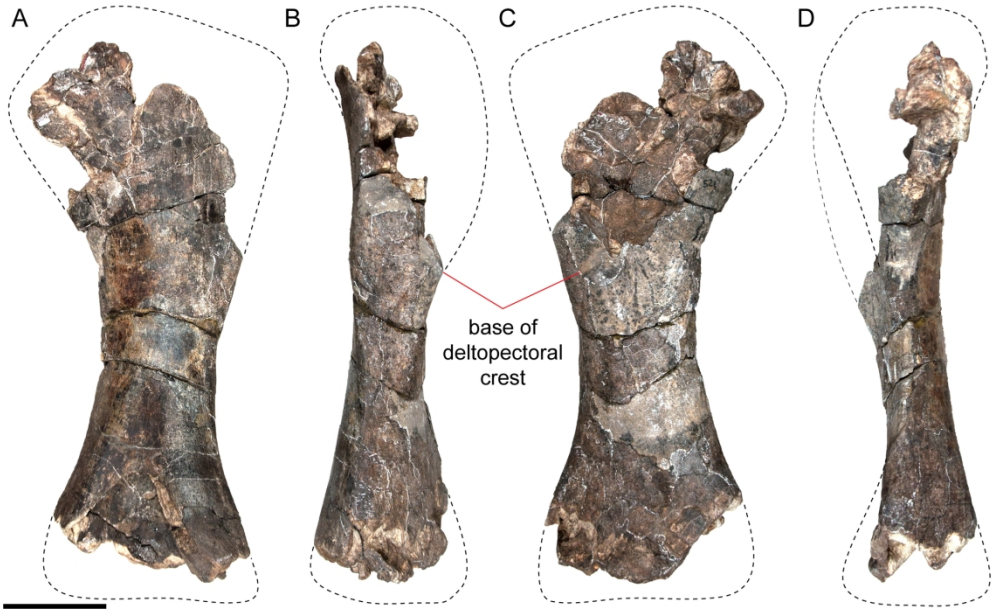

FIGURE 18. *Savannasaurus elliottorum* right humerus in **A**, posterior, **B**, lateral, **C**, anterior, and **D**, medial views. Scale bar equals 200 mm.

182x110mm (300 x 300 DPI)

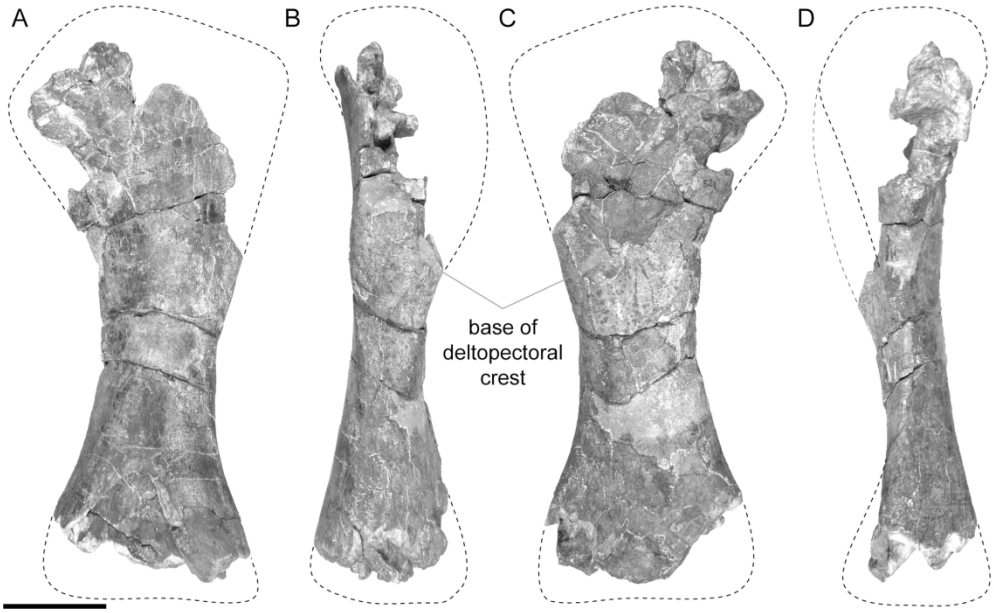

FIGURE 18. *Savannasaurus elliottorum* right humerus in **A**, posterior, **B**, lateral, **C**, anterior, and **D**, medial views. Scale bar equals 200 mm.

182x110mm (300 x 300 DPI)

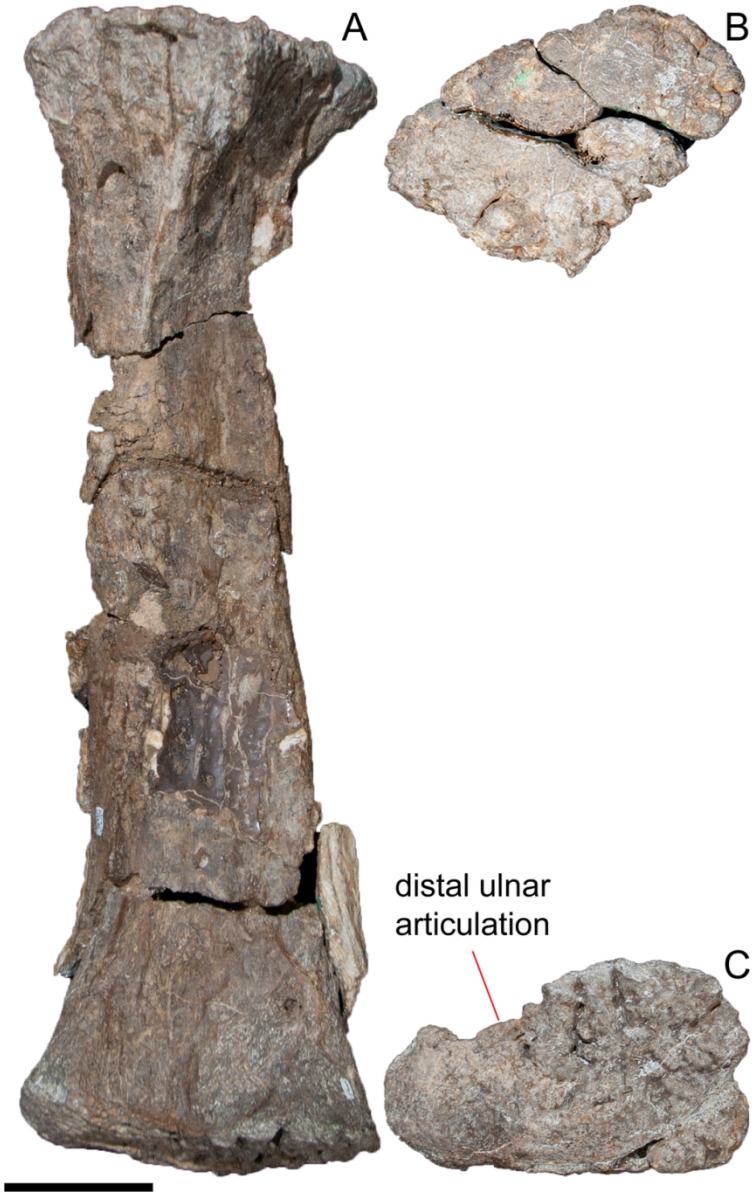

FIGURE 19. *Savannasaurus elliottorum* left radius in **A**, posterior, **B**, proximal and **C**, distal views. Scale bar equals 100 mm.

90x140mm (300 x 300 DPI)

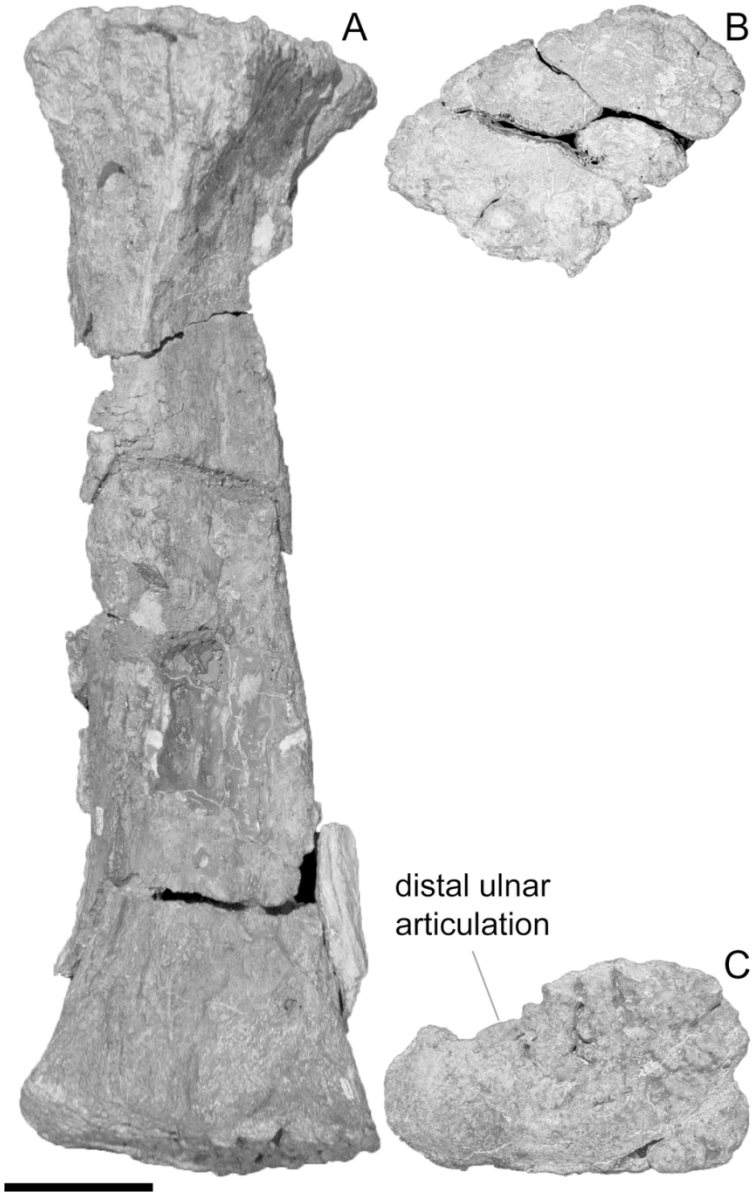

FIGURE 19. *Savannasaurus elliottorum* left radius in **A**, posterior, **B**, proximal and **C**, distal views. Scale bar equals 100 mm.

90x140mm (300 x 300 DPI)

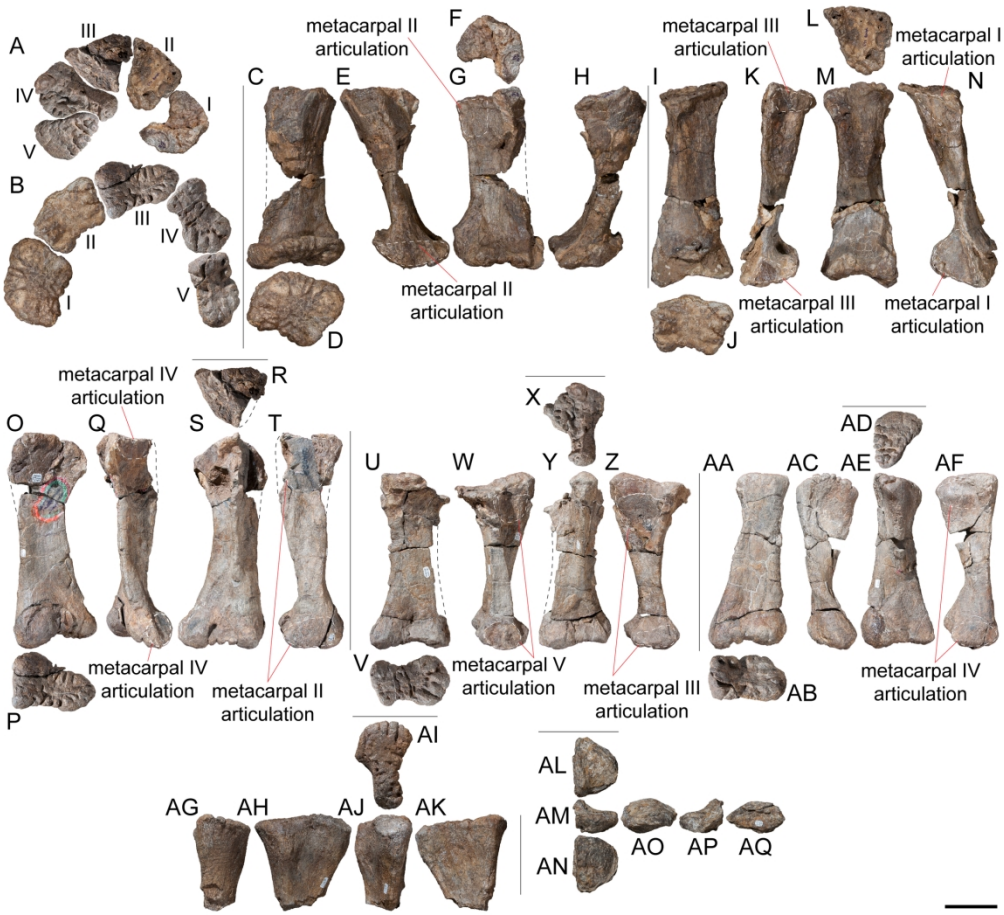

FIGURE 20. *Savannasaurus elliottorum* manus. Articulated left metacarpals I–V in **A**, proximal and **B**, distal views. Left metacarpal I in **C**, anterior, **D**, distal, **E**, lateral, **F**, proximal, **G**, posterior, and **H**, medial views. Left metacarpal II in **I**, anterior, **J**, distal, **K**, lateral, **L**, proximal, **M**, posterior, and **N**, medial views. Left metacarpal III in **O**, anterior, **P**, distal, **Q**, lateral, **R**, proximal, **S**, posterior, and **T**, medial views. Left metacarpal IV in **U**, anterior, **V**, distal, **W**, lateral, **X**, proximal, **Y**, posterior, and **Z**, medial views. Left metacarpal V in **AA**, anterior, **AB**, distal, **AC**, lateral, **AD**, proximal, **AE**, posterior, and **AF**, medial views. Right metacarpal IV in **AG**, anterior, **AH**, medial, **AI**, proximal, **AJ**, posterior, and **AK**, lateral views. Left manual phalanx II-1 in **AL**, dorsal, **AM**, medial, **AN**, ventral, **AO**, distal, **AP**, lateral, and **AQ**, proximal views. Scale bar equals 100 mm.

182x167mm (300 x 300 DPI)

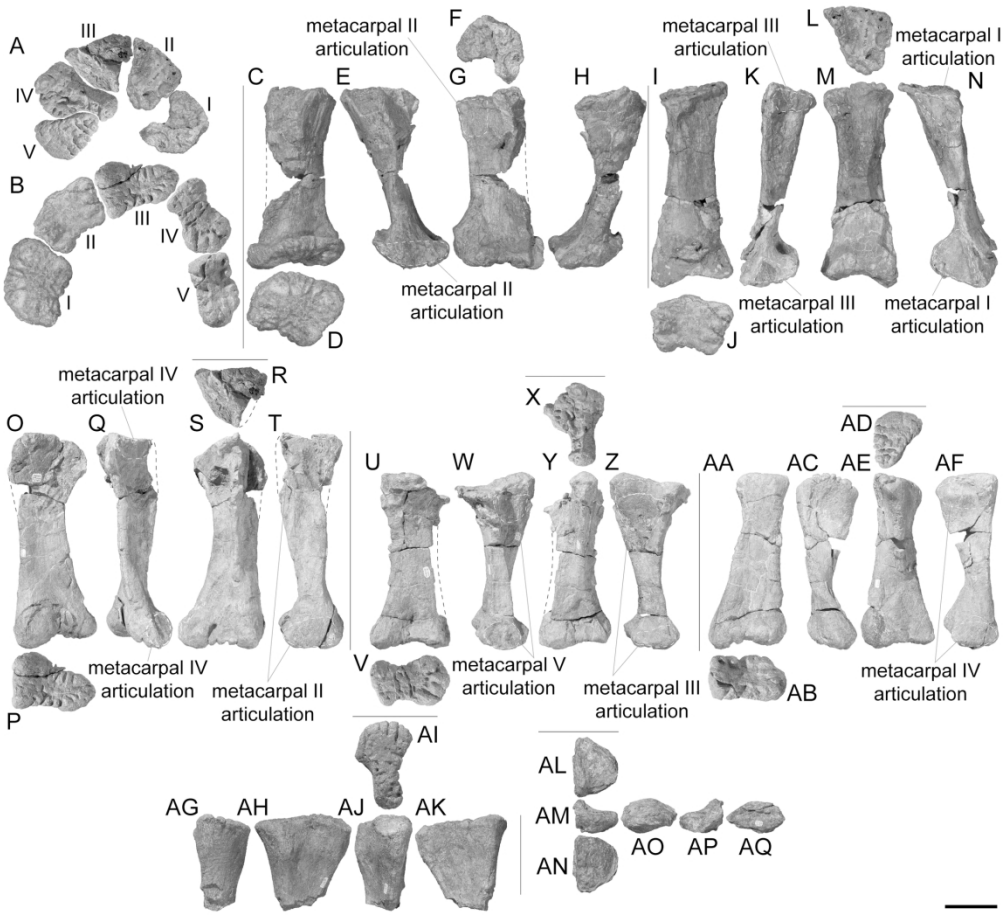

FIGURE 20. *Savannasaurus elliottorum* manus. Articulated left metacarpals I–V in **A**, proximal and **B**, distal views. Left metacarpal I in **C**, anterior, **D**, distal, **E**, lateral, **F**, proximal, **G**, posterior, and **H**, medial views. Left metacarpal II in **I**, anterior, **J**, distal, **K**, lateral, **L**, proximal, **M**, posterior, and **N**, medial views. Left metacarpal III in **O**, anterior, **P**, distal, **Q**, lateral, **R**, proximal, **S**, posterior, and **T**, medial views. Left metacarpal IV in **U**, anterior, **V**, distal, **W**, lateral, **X**, proximal, **Y**, posterior, and **Z**, medial views. Left metacarpal V in **AA**, anterior, **AB**, distal, **AC**, lateral, **AD**, proximal, **AE**, posterior, and **AF**, medial views. Right metacarpal IV in **AG**, anterior, **AH**, medial, **AI**, proximal, **AJ**, posterior, and **AK**, lateral views. Left manual phalanx II-1 in **AL**, dorsal, **AM**, medial, **AN**, ventral, **AO**, distal, **AP**, lateral, and **AQ**, proximal views. Scale bar equals 100 mm.

182x167mm (300 x 300 DPI)

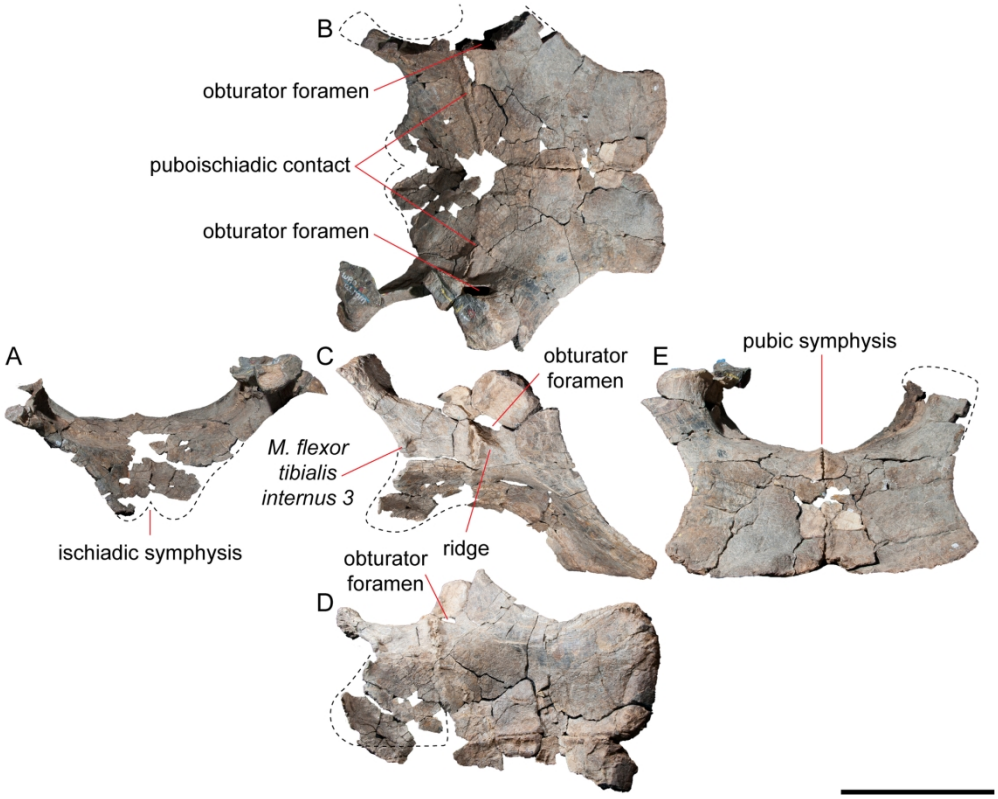

FIGURE 21. *Savannasaurus elliottorum* co-ossified left and right pubes and ischia in **A**, posterior, **B**, dorsal, **C**, right lateral, **D**, ventral (right pubis and ischium not included in this photograph), and **E**, anterior views. Scale bar equals 500 mm.

182x145mm (300 x 300 DPI)

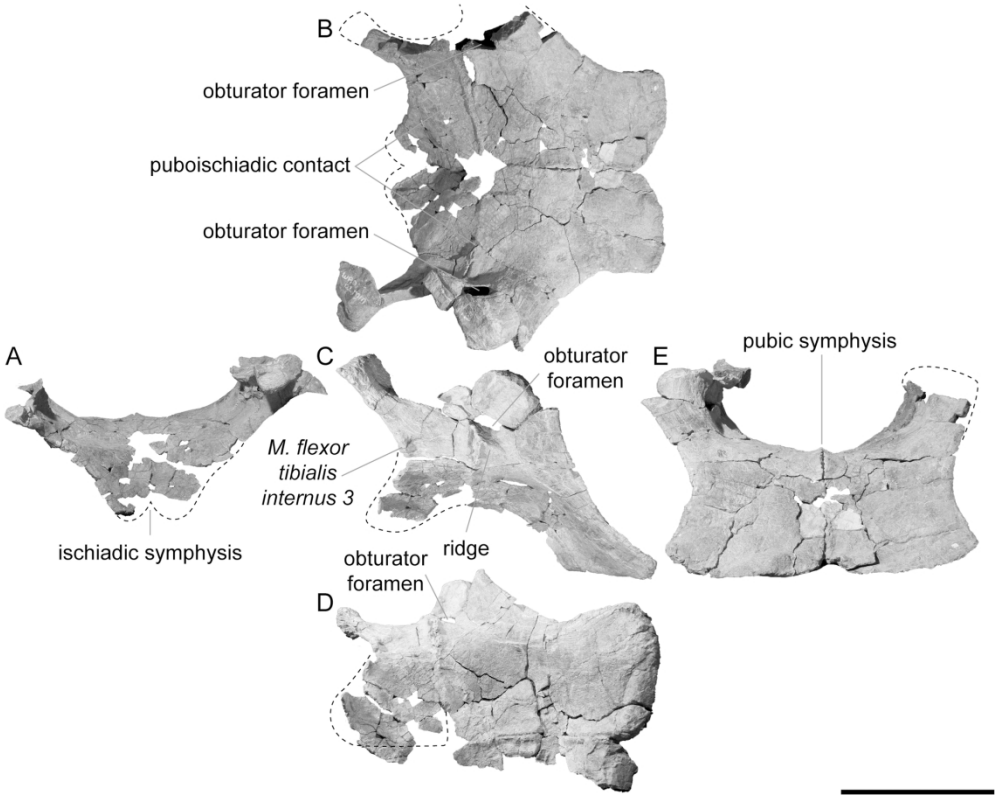

FIGURE 21. *Savannasaurus elliottorum* co-ossified left and right pubes and ischia in **A**, posterior, **B**, dorsal, **C**, right lateral, **D**, ventral (right pubis and ischium not included in this photograph), and **E**, anterior views. Scale bar equals 500 mm.

182x145mm (300 x 300 DPI)

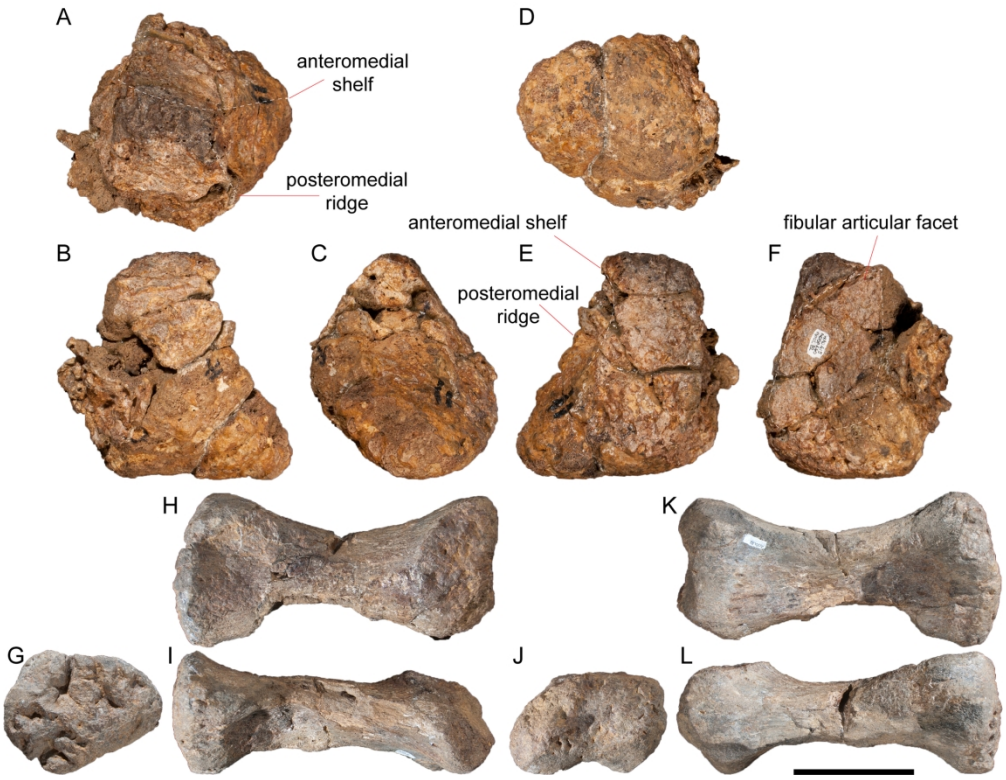

FIGURE 22. *Savannasaurus elliottorum* tarsus and metatarsus. Left astragalus in **A**, proximal, **B**, posterior, **C**, medial, **D**, distal, **E**, anterior, and **F**, lateral views. Right metatarsal III in **G**, proximal, **H**, dorsal, **I**, lateral, **J**, distal, **K**, ventral, and **L**, medial views. Scale bar equals 100 mm.

182x141mm (300 x 300 DPI)

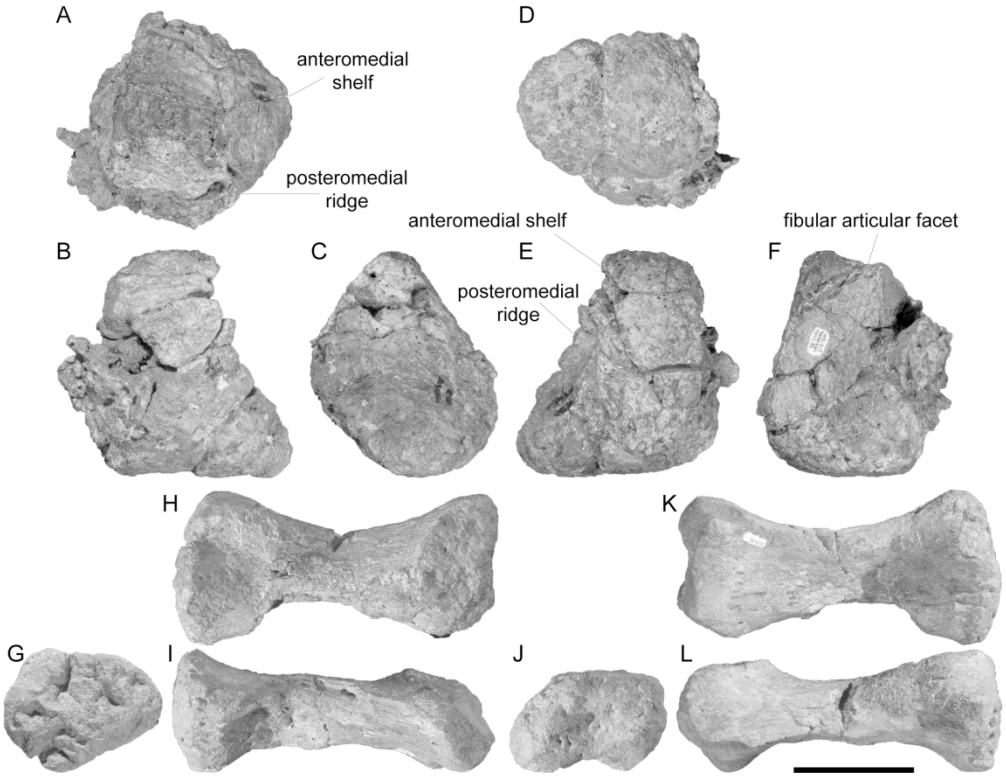

FIGURE 22. *Savannasaurus elliottorum* tarsus and metatarsus. Left astragalus in **A**, proximal, **B**, posterior, **C**, medial, **D**, distal, **E**, anterior, and **F**, lateral views. Right metatarsal III in **G**, proximal, **H**, dorsal, **I**, lateral, **J**, distal, **K**, ventral, and **L**, medial views. Scale bar equals 100 mm.

182x141mm (300 x 300 DPI)

FIGURE 23. *Savannasaurus elliottorum* life restoration by Travis R. Tischler.

182x129mm (300 x 300 DPI)

FIGURE 23. *Savannasaurus elliottorum* life restoration by Travis R. Tischler.

182x129mm (300 x 300 DPI)